Title
The Deformation, Yielding, and Fracture of Ultra-High Molecular Weight Polyethylene for Use in Total Joint Replacements

Author
Malito, Louis Gregory

Publication Date
2018

Peer reviewed|Thesis/dissertation

The Deformation, Yielding, and Fracture of Ultra-High Molecular Weight Polyethylene for Use in Total Joint Replacements

By

Louis Gregory Malito

A dissertation submitted in partial satisfaction of the

requirements for the degree of

Doctor of Philosophy

in

Engineering – Mechanical Engineering

in the

Graduate Division

of the

University of California, Berkeley

Committee in charge:

Professor Lisa A. Pruitt, Chair
Professor Robert O. Ritchie
Professor Ronald Gronsky

Spring 2018

The Deformation, Yielding, and Fracture of Ultra-High Molecular Weight Polyethylene for Use in Total Joint Replacements

By Louis Gregory Malito

Abstract

The Deformation, Yielding, and Fracture of Ultra-High Molecular Weight Polyethylene for Use in Total Joint Replacements

by

Louis Gregory Malito

Doctor of Philosophy in Engineering – Mechanical Engineering

University of California, Berkeley

Each year close to one millions patients within the United States, receive a total joint replacement (TJR) to alleviate pain from severe debilitating osteoarthritis. TJRs can comprise hip, knee, shoulder, and even elbow and ankle replacements. Though these implants differ in anatomical function they have a consistent theme, a hard-on-soft bearing couple consisting of hard cobalt chrome (CoCr) and soft ultra-high molecular weight polyethylene (UHMWPE). UHMWPE is a semi-crystalline polymer with 2-6 million g/mol where long molecular chains create high entanglements and help give the material high energetic toughness. These molecular characteristics also provide a low coefficient of friction desirable for TJRs. This coupling pair has been the standard of care for nearly sixty years however not without some complications. TJRs primarily fail from wear debris that is liberated from the UHMWPE bearing surface. This wear debris is caused by successive plastic deformation from implant loading leading to crack initiation below the implant surface. Crack initiation leads to fatigue crack growth with the eventual liberation of debris. As a result of this detriment, there have been several changes to the formulations that make up UHMWPE. These changes primarily include radiation cross-linking to improve wear resistance. Increased wear resistance comes with concomitant trade-offs to the mechanical properties of the material.

Radiation cross-linking through gamma irradiation, introduces free radicals to the material. Free-radical need to be eliminated otherwise they will react with the body and cause the polymer to oxidize in an *in vivo* environment. To alleviate these free-radicals post processing is performed. This post processing usually consists of thermal annealing treatments either above or below the melt temperature of UHMWPE. More recently, UHMWPE materials have moved away from post irradiation annealing in favor of antioxidant additions to the material. These antioxidants, such as vitamin E, are added to stabilize the material after irradiation and to prevent any possibility of oxidative embrittlement during *in vivo* operation. All of these unique additions to UHMWPE pose the important question of how the material's fundamental mechanical properties are affected. There is a plethora of research data on the mechanical properties of UHMWPE and some of its material formulations, however when one dives into the procedural methods of these studies there are significant inconsistencies.

These inconsistencies are rooted in the procedures used to analyze and create material mechanical properties. Unlike metallic materials where methods for analyzing mechanical properties are very well understood, polymeric materials offer a more complex challenge when interpreting their constitutive behavior. This is extremely important when polymeric materials, such as UHMWPE are used in safety critical applications such as TJRs. These challenges increase when UHMWPE is tailored through combinations of resin type, radiation cross-linking, and antioxidant additions. As a result there is a need to answer from a methodological perspective how the mechanical properties of UHMWPE change with different material formulations under different loading scenarios.

This dissertation provides a comprehensive and thorough assessment of the mechanical properties of UHMWPE across 12 different material formulations focusing on how the methods used to analyze mechanical behavior can be extremely important. First, a comprehensive microstructural analysis is performed through differential scanning calorimetry (DSC) and small angle x-ray scattering (SAXS) to gather microstructure data for its potential effect on mechanical properties. Then tensile deformation in UHMWPE and its various material formulations are investigated. Engineering versus true tensile stress-strain data is looked at to elucidate the differences between analysis methods for determining elastic properties, yield, post yield, and ultimate behavior. Tensile constitutive properties are then compared to properties determined from compression and nanoindentation in an effort to understand material deformation trends across measurement methods. Then microstructure and tensile analysis are applied in the determination of the elastic-plastic fracture, or *J*-integral, toughness behavior of UHMWPE. Finally, this study concludes with a mechanistic analysis of the crack growth mechanisms to validate fracture toughness methods.

To Rimshot and Grandma. I miss you both dearly.

Acknowledgments

This is an amazing and yet bittersweet feeling now that my time as a graduate student at the University of California, Berkeley is coming to a close. There are a number of people who have touched my life in many ways and given me the immense support and encouragement to achieve this insane goal. First and foremost I want to thank my doctoral advisor Lisa Pruitt. You are an amazing human being and I am so happy you saw a potential in me to do great things here at Berkeley. I was able to teach four incredible semesters with you, and present at research conferences in far away and exotic places. You have helped me hone my scientific and engineering prowess over these last few years and for that I am incredibly grateful. You and the Medical Polymer Group (MPG) will also have a special place in my heart. I hope that I can continue making you feel proud with the future endeavors that I embark on.

To Professor Robert Ritchie, like Lisa, you also took a gamble on me. You are not a particular fan of the mechanical behavior/fracture mechanics of polymeric materials. In fact on more than one occasion you have said to me, "why can't you just work on metals?" However over the last year and a half, it's been beyond belief to see how excited you've become with my *J*-integral fracture project even to the point where I have become your go to *J*-integral person. I am indebted to you for all of your mentorship and guidance. I am grateful that you accepted me with open arms into the Ritchie group even becoming a co-advisor to me. I look forward to an enduring friendship as I depart Berkeley.

To Dr. Bernd Gludovatz, thank you for pushing me to pursue *J*-integral fracture of UHMWPE. I will never forget what you told me in lab. "Do you see my hand shaking? This will add experimental error. Many things will add error to the experiment. This is why we have statistics. On that note, just pre-crack your darn specimens and get this thing going!" Your straight forward candor was the motivation I needed to get through my fracture project. I look forward to continuing a lifelong friendship with you. Also, I am not doing fatigue on these materials ☺.

To Adam Kozak and Stephen Spiegelberg at Cambridge Polymer Group, thank you for all of your testing help. You were an invaluable resource and sounding board for all my thoughts deciphering methodologies for reporting mechanical properties of UHMWPE.

To Anuj Bellare, thank you for all of your help gather microstructure data and being an invaluable UHMWPE resource.

To Jessica, thank you for being my partner in crime with fracture testing of UHMWPE. I know you may have had some reservations at the start (you know the meeting with Rob and Bernd I am talking about ;)) and wondered if this would actually work, but I am glad you stuck around. Please keep in touch wherever you end up for work or grad school.

To all the members of the Ritchie group, Ryan, Keli, Jon, and Amy, your comradery and candor helped me survive my fracture project.

To all the members of MPG past and present, Farzana, Noah, Audrey, and Sofia thank you for listening, thank you for keeping me company in lab. Thank you for all the advice and help with

prelims, quals, and the lot. I will sorely miss ORS, Hawai'i, and other far away international conference trips with all of you.

To Dennis Liu and Jacob Gallego in the Etcheverry machine shop, thank you guys so much! You literally made every single test specimen I used for my PhD. If it weren't for the two of you I would not been able to complete my dissertation.

To Dr. Scott Robertson, thank you for giving me the motivation to receive my PhD. Eight years ago when you were my supervisor at NDC, you took the time to nurture my curiosity about nitinol and the whole world of the mechanical behavior of engineering materials. You were the person responsible for introducing me to Lisa and Rob. You even wrote my letter of recommendation for Berkeley! I would have not been able to embark on this crazy journey if it wasn't for your motivation and belief that I could excel in a PhD environment. I am forever grateful.

To Dr. Devinder Grewal, thank you for exposing me to the world of engineering consulting and leading me down the path to Exponent. All those long conversations over beers at Fathom were amazing!

Finally to my mother and father Olga and Louis Malito, the two of you are responsible for all of my successes in life. You pushed me past my comfort zone and allowed me to view the immense possibilities that I could achieve in this world. You lifted me up when I needed it, you brought me back to earth when I got too high. This PhD is for both of you. May you now sit back and feel joy of what you helped your only son accomplish.

Table of Contents

List of Figures

List of Tables

Chapter 1 – Motivation

Ultra-high molecular weight polyethylene (UHMWPE) has been the premier biopolymer used in orthopedic implants for over sixty years. Dr. John Charnley, the father of the modern total joint replacement (TJR), first used UHMWPE in 1962 after previous failures using polytetrafluorethylene as a lubricous counter bearing in his hip replacement design. Since then, UHMWPE has found uses in knee, shoulder, elbow and ankle replacements to name a few. Over the years there have been many improvements to the material such as cross-linking to prevent wear resistance and antioxidant addition to prevent *in vivo* embrittlement. Despite its long history, use, and improvements, when sifting through the literature, understanding UHMWPE's basic mechanical behavior can be somewhat of a mystery. One would think given UHMWPE's extensive track record it would be easy to find values for properties such as Young's modulus, Poisson's ratio, yield, and fracture toughness. Given the complex mechanical nature that semi-crystalline polymers exhibit, there are a wide array of procedures researchers have used to report mechanical properties.

Mechanical properties exist within the literature and handbooks however depending on the source can vary quite significantly, even by an order of magnitude. There are two main procedural choices researchers have to report constitutive properties in polymers, true or engineering. There are complexities and subtleties even within defining procedures on these two categories. As a result there exists a great need to systematically analyze the mechanical behavior of UHMWPE as it can provide a basis for the mechanical analysis of other semi-crystalline engineering polymers. Not understanding proper constitutive properties can lead to failure and in the case of orthopedic implants, pain and even worse, revision surgery for the patient. Basic tensile constitutive behavior can have a cascade effect when performing a mechanical analysis since tensile properties are directly linked to fracture toughness behavior.

It is the aim of this dissertation to provide an extensive mechanical and microstructural analysis of UHMWPE as a basis for defining proper analysis methodologies while attempting to understand structure property relationships.

Chapter 2 – The deformation and yielding of ultra-high molecular weight polyethylene

Abstract

This is the first study to simultaneously measure material properties in tension, compression, nanoindentation as well as microstructure (crystallinity and lamellar level properties) across a wide variety of clinically relevant ultra-high molecular weight polyethylene (UHMWPE) formulations. Methodologies for the measurement of UHMWPE mechanical properties—namely elastic modulus, yield stress, yield strain, ultimate strength, energetic toughness, Poisson's ratio, hardness and constitutive variables—are evaluated. Engineering stress-strain behavior is compared to true stress-strain behavior for UHMWPE across a range of cross-linking and antioxidant chemistry. The tensile mechanical properties and constitutive behavior of UHMWPE are affected by resin type, antioxidant source and degree of cross-linking. Poisson's ratio is shown to be affected by resin type, antioxidant addition, and cross-linking dosage. Relationships between bulk mechanical properties from different measurement methodologies as well as microstructure are analyzed across all material formulations using Spearman rank correlation coefficients. Modulus and yield strength correlate in both tension and compression. Similarly, tensile and compressive properties including modulus and yield strength correlate strongly with crystallinity (X_c) and lamellar thickness (D). This work has broad application and provides a basis for interpreting the mechanical behavior of UHMWPE used in orthopedic implants.

2.1 Introduction

For nearly sixty years, medical grade ultra-high molecular weight polyethylene (UHMWPE) has been the longstanding material of choice for use as a bearing surface in total joint arthroplasty (Kurtz 2015). In its tenure as an orthopedic biomaterial, UHMWPE has undergone numerous iterations in its processing in order to address ongoing clinical challenges faced in total joint replacements (TJRs) including wear-debris induced osteolysis (Bozic et al., 2009; Muratoglu et al., 1999), oxidation embrittlement (Costa et al., 1998; Edidin et al., 2000; Premnath et al., 1996) and fracture associated with high cyclic contact stresses (Baker et al., 2003; Furmanski et al., 2009; Gencur et al., 2006). Contemporary formulations of UHMWPE are owed to decades of research that have addressed challenges of wear, oxidation, and fatigue fracture of this polymer in both laboratory as well as clinical settings (Atwood et al., 2011; Kurtz, 2015).

UHMWPE is a semicrystalline polymer with approximately half of its structure in an ordered crystalline lamellae domain (Atwood et al., 2011; Bistolfi et al., 2009; Turell & Bellare, 2004). The polymer has a very high molecular weight (2-6 million g/mol) that facilitates high entanglement density in its amorphous phase and superior energetic toughness as compared to other homopolymers (Kurtz, 2009; Pruitt, 2005). Despite its excellent energetic toughness and inherent biocompatibility, the polymer in its untailored form is susceptible to wear when articulating against the hard bearings typically used in TJRs (Kurtz, 2015; Kurtz, 2009). Cross-linking through energetic schemes improves wear resistance but comes with a concomitant reduction in mechanical properties (Atwood et al., 2011; Crowninshield & Muratoglu, 2008; Gencur et al., 2006; Rimnac & Pruitt, 2008) as well as susceptibility to oxidation (Costa et al., 1998; Kurtz et al., 1999b; Premnath et al., 1996). Initial improvements to oxidation resistance in cross-linked formulations of UHMWPE utilized thermal annealing methods yet such treatments either failed to fully eliminate free radicals or altered the microstructure in a way that compromised fatigue resistance (Sara A Atwood et al., 2011; Morrison and Jani, 2009; Pruitt, 2005). Antioxidants such as vitamin E have been recently added to UHMWPE in order to improve oxidation resistance without detriment to mechanical properties but are known to limit the extent of cross-linking in the polymer (Furmanski & Pruitt, 2007; Oral et al., 2006). With so many options available to tailor medical grades of UHMWPE, it is necessary to understand how these alterations affect structural properties and performance in orthopedic bearing applications.

The purpose of this study was to evaluate the microstructure and mechanical properties of twelve clinically relevant blends of UHMWPE that provided unique combinations of resin type, cross-linking dosage, and antioxidants. We evaluated the microstructure using differential scanning calorimetry (DSC) and small angle x-ray scattering (SAXS). In parallel, we conducted a comprehensive analysis of constitutive behavior and assessment of mechanical properties in both tension and compression. Surface mechanical properties were determined using nanoindentation. Correlations between structure and mechanical properties were then assessed for all material groups. Our study is, to our knowledge, the first unified body of work to provide a comprehensive analysis of microstructure, constitutive behavior in tension and compression, as well as nanomechanical properties across a spectrum of clinical formulations of UHMWPE. Our methods and analysis provide a basis for engineers and designers to better understand and grasp the mechanical performance of UHMWPE used in orthopedic implants.

2.2 Materials and Methods

2.2.1 Materials

For this study, twelve clinical formulations of UHMWPE were investigated (**Table 2.1**). Material was sourced from three different UHMWPE consolidators: Orthoplastics (Lancashire, UK), DePuy (Warsaw, IN), and Quadrant EPP (Fort Wayne, IN). Variations to two base resins, GUR 1020 and GUR 1050, were investigated across a range of cross-link density and antioxidant chemistry. The antioxidants were comprised of 0.1 wt% Vitamin E (VE) and COVERNOX™ (AO) (medical grade version of Irganox™ 1010) which were blended into GUR 1020 resin before consolidation. Lastly, irradiation cross-linking dosages at 75kGy in base resin materials were re-melted (RM) to alleviate free radicals and served as cross-linked samples without antioxidants. Four distinct material categories (**Table 2.1**) were explored: 1020 resin (0 kGy, 35 kGy, 75 kGy RM); 1020 resin with AO antioxidant (AO 0kGy, AO 80 kGy); 1020 resin with 0.1 wt% vitamin E (VE 0 kGy, VE 55 kGy, VE 75 kGy, VE 100 kGy, VE 125 kGy); and 1050 resin (0 kGy, 75 kGy RM). All UHMWPE materials were compression molded except for GUR 1050 75kGy RM which was ram extruded.

Table 2. 1 – UHMWPE material formulations and consolidators. Darker colors at the top of the table denote base formulations in that group. The following lighter colors denote irradiation cross-link treatments to that material formulation group.

UHMWPE Material Formulation and Manufacturer			
GUR 1020 (Orthoplastics)	GUR 1020 AO (Depuy)	GUR 1020 VE (Orthoplastics)	GUR 1050 (Orthoplastics)
GUR 1020 35kGy (Orthoplastics)	GUR 1020 AO 80kGy (Depuy)	GUR 1020 VE 50 kGy (Orthoplastics)	GUR 1050 75kGy RM (Quadrant)
GUR 1020 75kGy RM (Orthoplastics)		GUR 1020 VE 75kGy (Orthoplastics)	
		GUR 1020 VE 100 kGy (Orthoplastics)	
		GUR 1020 VE 125kGy (Orthoplastics)	

2.3.2 Methods

2.3.2.1 Microstructure

The degree of crystallinity in each of the UHMWPE formulations was determined using differential scanning calorimetry (DSC) analysis. DSC measurements were obtained according to ASTM F2625-10 (2016) using a TA Instruments Q2000 DSC (New Castle, DE). The test specimens were cut with a clean razor blade from un-tested tensile specimens into 4.9-5.8 mg pieces and crimped between a standard DSC aluminum pan and lid. DSC specimens were subjected to a heating rate of 10 °C/min up to a temperature of 200 °C. The percent crystallinity was determined using the following relationship:

$$\%X = \frac{\Delta H_s}{\Delta H_f} \times 100\% \quad (1)$$

where ΔH_s is the heat of fusion of the sample in J/g and ΔH_f is the heat of fusion of a 100% crystalline sample (289.3 J/g for polyethylene as per ASTM F2625).

Small angle x-ray scattering (SAXS) was utilized to determine lamellar size distribution across the UHMWPE groups. SAXS data was collected using a laboratory CuKα rotating anode SAXSLAB instrument. The collimated beam had a diameter of approximately 0.4 mm at the sample position. The SAXS scattering intensity was collected by a DECTRIS PILATUS 300K detector placed at a distance that corresponds to an angular scattering range of $\boldsymbol{q}_{min}$ = 0.032 [nm^{-1}] and $\boldsymbol{q}_{max}$=2.5 [nm^{-1}], and the scattering vector, q, was defined as

$$q = (4\pi/\lambda)\sin\theta \quad (2)$$

where λ is the wavelength of the x-ray used (0.154 nm) and θ is half the scattering angle. The x-ray source was operated at 45kV and 30mA. Based on beam diameter and sample thickness, the sampling volume associated with each x-ray measurement was estimated to be 0.06 mm^3. All SAXS samples were 4.5mm x 10mm x 1mm (thickness).

2.3.2.2 Tension Testing and Constitutive Modeling

Tension testing was utilized to determine the engineering stress-strain and true stress-strain behavior across the UHMWPE formulations. The tensile elastic modulus, yield stress, yield strain, non-linear hardening coefficients, engineering ultimate stress, true ultimate stress, true ultimate strain, and energetic toughness was determined per ASTM D638. Type IV tensile bar specimens, approximately 3.2 mm thick and 6mm in width, were CNC machined from stock material with n=5 specimens per UHMWPE material group. The specimens were machined such that the gauge length was parallel to the long axis of the stock material. Specimens were conditioned at 25 °C and 50% relative humidity in a Caron 6010 environmental chamber (Marietta, OH) for at least 40 hours prior to testing. Tension testing was performed on a Shimadzu AGS-X electromechanical load frame (Kyoto, Japan) with a 1kN load cell at 50 mm/min with test temperature maintained at 23 ± 2 °C.

Material deformation was measured by a non-contact dual video extensometer (based on a Point Grey FL3-U3-88S2C-C camera) validated to the criteria outlined in ASTM E83 for a class B-2 extensometer. Custom developed software tracked optical targets on the sample to measure true axial, transverse strain, and instantaneous cross-sectional area at the gauge length through the

deformation process. The video extensometer was calibrated before use to an Edmund Optics 0.5mm pitch optical calibration grid, correcting for perspective and non-linear distortion. A gauge length of approximately 26mm was used for used for axial strain measurements. In additiona, crosshead displacement was also tracked during testing to record engineering tensile properties. Finally, the data was analyzed using a custom MATLAB script (Natick, MA).

Elastic modulus was determined by a linear least squares regression from 0.0005 strain to 0.009 strain on the true stress-strain curve. Regression analysis was also performed to other upper strain limits (0.02 and 0.04) in an effort to understand elastic modulus as a metric for relative comparison between material formulations. Engineering and true properties were calculated based on their respective curves taking engineering yield stress as the local maximum on the engineering curve while true yield stress and strain were calculated using a 0.002 offset line from the elastic region on the true curve per the established method of Kurtz and co-workers (Kurtz et al., 2002; Kurtz et al., 1998; Kurtz et al., 2006). It has also been found that a two-segment elastic-plastic material model closely represents the true stress-strain behavior of UHMWPE in tension (as well as compression) when a 0.002 offset line is used to predict yielding. The two segment elastic-plastic material model is given by:

$$\sigma = \begin{cases} E\varepsilon, & \varepsilon \leq \varepsilon_y \\ \alpha + \beta \exp(\gamma\varepsilon), & \varepsilon_y < \varepsilon \leq 0.12 \end{cases} \quad (3)$$

where σ (MPa) is the true stress, E (MPa) is the elastic modulus, ε is the true axial strain, ε_y is the true yield strain, α (MPa) is the asymptotic true stress at infinite strains, β (MPa) is the rate at which the stress approaches the asymptotic limit and γ represents the curvature of the true stress-strain curve (Kurtz et al., 1998). Non-linear coefficients, β and γ, for the plastic model were found using a least squares regression from true offset yield strain to 0.12 true strain which in previous studies was found as the maximum equivalent strain of an UHMWPE tibial component (Bartel et al., 1995; Kurtz et al., 1998). The parameter α was eliminated by making the two segment elastic plastic model intersect at the yield point producing the following equation:

$$\alpha = E\varepsilon_y - \beta\exp(\gamma\varepsilon_y) \quad (4)$$

In addition to the true ultimate stress, engineering ultimate stress was computed as it has been found that the latter property best represents the flow stress when constructing the blunting line for J-integral based fracture toughness of UHMWPE (Pascaud et al., 1997a; Pascaud et al., 1997b; Rimnac et al., 1988). Energetic toughness was found as the area under the true stress-strain curve integrated through the failure strain.

2.3.2.3 Poisson's ratio

Poisson's ratio was determined from uniaxial tension experiments per ASTM D638, Appendix A3. Type IV tensile bar specimens, approximately 3.2 mm thick and 6mm in width, were CNC machined from stock material with n=5 specimens per UHMWPE material group. Specimen conditioning and testing temperature and relative humidity were identical to the method described above for the tension specimens. Poisson's ratio testing was performed using a MTS Mini-Bionix II load frame (Eden Prairie, MN) using a 5 kN load cell. A preload of 2.5 N was applied at 0.1mm/min to mitigate presence of a toe region during testing. Poisson's ratio testing was then conducted at 5 mm/min per the ASTM standard. UHMWPE deformation was measured by the same non-contact video extensometer setup as employed for the tension samples (described

above). A gauge length of approximately 5mm was used for axial and transverse strain measurements.

The Poisson's ratio was determined based on measured true axial and transverse strain as defined by ASTM D638 appendix A3:

$$\nu = \frac{\frac{d\varepsilon_t}{dP}}{\frac{d\varepsilon_a}{dP}} \tag{5}$$

where $d\varepsilon_t$ is the absolute change in transverse strain, $d\varepsilon_a$ is the absolute change in axial strain, and dP is the change in the applied load. The slopes of $d\varepsilon_t/dP$ and $d\varepsilon_a/dP$ were found from a linear regression of the data from 0.0005 true axial strain to the true offset yield strain determined from the aforementioned tension experiments. The data was analyzed using a custom MATLAB script.

2.3.2.4 Compression Testing

Compression testing was utilized for the determination of elastic modulus, true yield stress and true yield strain was performed per the established method of Kurtz and co-workers for compression analysis of UHMWPE based on ASTM D695 (Kurtz et al., 2002; Kurtz et al., 1998). Cylindrical test specimens were CNC machined from stock material with a 10 mm diameter, 15 mm height, and a minimum of n = 5 specimens per material group. Specimens were machined such that the height of the sample was parallel to the long axis of the stock material to match the orientation of the tensile samples. Testing was performed on an Instron 8871 load frame (Norton, MA) with a 5 kN load cell. Samples were loaded in compression between two parallel polished platens at a rate of 18 mm/min (0.02/s) and a temperature of 25 C. Engineering stress was determined as

$$\sigma_0 = \frac{|P|}{A_0} \tag{6}$$

where P is the load and A_0 is the initial cross sectional area of the sample. Platen displacement was checked for accuracy using a compressometer and found to be in agreement for the displacements necessary for our tests and subsequent analysis. According to Kurtz, homogeneous compression without barreling can occur up to 0.12 strain therefore assuming constancy of volume up to that point (Kurtz et al., 1998). As a result true strain could be calculated straight from the platen displacement not exceeding 0.12 strain (Kurtz et al., 2002). As a result true strain, ε, was measured according to

$$\varepsilon = \frac{|\delta|}{l_0} \tag{7}$$

where δ is the platen displacement and l_0 is the starting platen separation. Engineering stress was converted to true stress by combining the following equations

$$\varepsilon = -\ln(1 - e) \tag{8}$$

$$\sigma = \sigma_0(1 - e) \tag{9}$$

where e, is the engineering strain, and solving for true stress, σ, in terms of true strain to produce

$$\sigma = \sigma_0 \exp(-\varepsilon) \quad (10).$$

Finally, the data was analyzed using a custom MATLAB script.

Elastic modulus was determined by a least squares regression from 0.0005 to 0.009 strain. Yield stress and strain were calculated from a 0.002 offset line from the elastic region. Analysis was performed in this manner based on previous compression work and for direct comparison with the true tensile data (Kurtz et al., 2002; Kurtz et al., 1998; Kurtz et al., 2006).

2.3.2.5 Nanoindentation Testing

Nanoindentation was utilized to determine the surface hardness and reduced elastic modulus across the UHMWPE formulations (Oliver and Pharr 1992, Pruitt and Rondinone, 1996; Klapperich et al., 2001). Samples were fabricated into 4 mm cubes and then microtomed with a glass blade to obtain optically smooth surfaces. The tip-area function during indentation is described by the following equation:

$$A_c(h_c) = C_0 h_c^2 + C_1 h_c + C_2 h_c^{1/2} + C_3 h_c^{1/4} \quad (11)$$

where A_c is the contact area, h_c is the contact depth, and C_0, C_1, C_2 and C_3 are calibration coefficients obtained using a polycarbonate standard (Pruitt and Rondinone, 1996; Klapperich et al., 2001).

A TI 900 Hysitron TriboIndenter (Minneapolis, MN) was used to perform indentations at ambient temperature using a conospherical diamond tip with a nominal 20 μm radius. The indentations were load-controlled with a rate of 30 μN/s. A trapezoidal loading-unloading function was used with a ten-second hold at each maximum load to minimize creep effects (Klapperich et al., 2001; Pruitt et al., 1996). Each sample group (n=5 specimens per material group) comprised 15 indentations with a prescribed maximum load of 150-650 uN in equally spaced intervals (Klapperich et al., 2001). A custom MATLAB script was created to calculate elastic modulus and contact hardness based on the following equations:

$$S = \frac{dP}{dh} = \frac{2\sqrt{A_c}}{\sqrt{\pi}} E_r \quad (12)$$

$$\frac{1}{E_r} = \frac{1-\upsilon^2}{E} + \frac{1-\upsilon^2}{E_i} \quad (13)$$

$$H_c = \frac{P_{max}}{A_c} \quad (14)$$

where S is the stiffness and $\frac{dP}{dh}$ is the slope of the initial unloading portion of the indentation load versus displacement curve, E_r is the reduced elastic modulus, and H_c is the hardness. For calculations of reduced elastic modulus a Poisson's ratio of 0.46 was utilized (Kurtz 2009). Experimental Poisson's ratio from our tests was not utilized in the calculations of nanomechanical properties since a full investigation of anisotropic effects was not performed.

2.3.2.6 Statistical Analysis

Determination of relationships between bulk mechanical properties analyzed from different methods as well as relationships between microstructure and mechanical properties was performed using a nonparametric Spearman rank correlation coefficient (MATLAB) (Atwood et al., 2011). Median values of mechanical properties were used for correlations.

2.4 Results

2.4.1 Microstructure

Crystallinity determined from DSC scans was found to range from 52.4 – 61.2%. A summary of crystallinity and microstructure for all material groups is summarized in **Table 2**. Lamellar architecture was determined from SAXS scattering functions. Paired distance distribution functions *p(r)* were determined using the relationship

$$p(r) = \frac{1}{{r_e}^2}\frac{1}{2\pi^2}\int_0^\infty q^2 I(q)\cos(qr)\,dq \tag{15}$$

where, r_e is the classical radius of an electron (2.81794E^{-13} cm), *I(q)* is the experimental scattering function, q is the scattering vector, and r is the radial distance perpendicular to lamellar surfaces (Iijima and Strobl, 2000; Turell and Bellare, 2004). The inter-lamellar spacing (L) was measured from first maximum on p(r) as shown in **Figure 1**. The scattering function was also used to measure specific internal surfaces (O_{ac}), which depicts area per unit volume of the interface separating the crystalline and amorphous regions (Turell and Bellare, 2004). O_{ac} was determined as:

$$O_{ac} = \frac{-2dP/dr}{\Delta\rho_e^2} \tag{16}$$

where dP/dr presents the slope of linear fit to the self-correlation portion of the *p(r)* function and $\Delta\rho_e$ is the difference in electron density between the crystalline and the amorphous regions of UHMWPE.

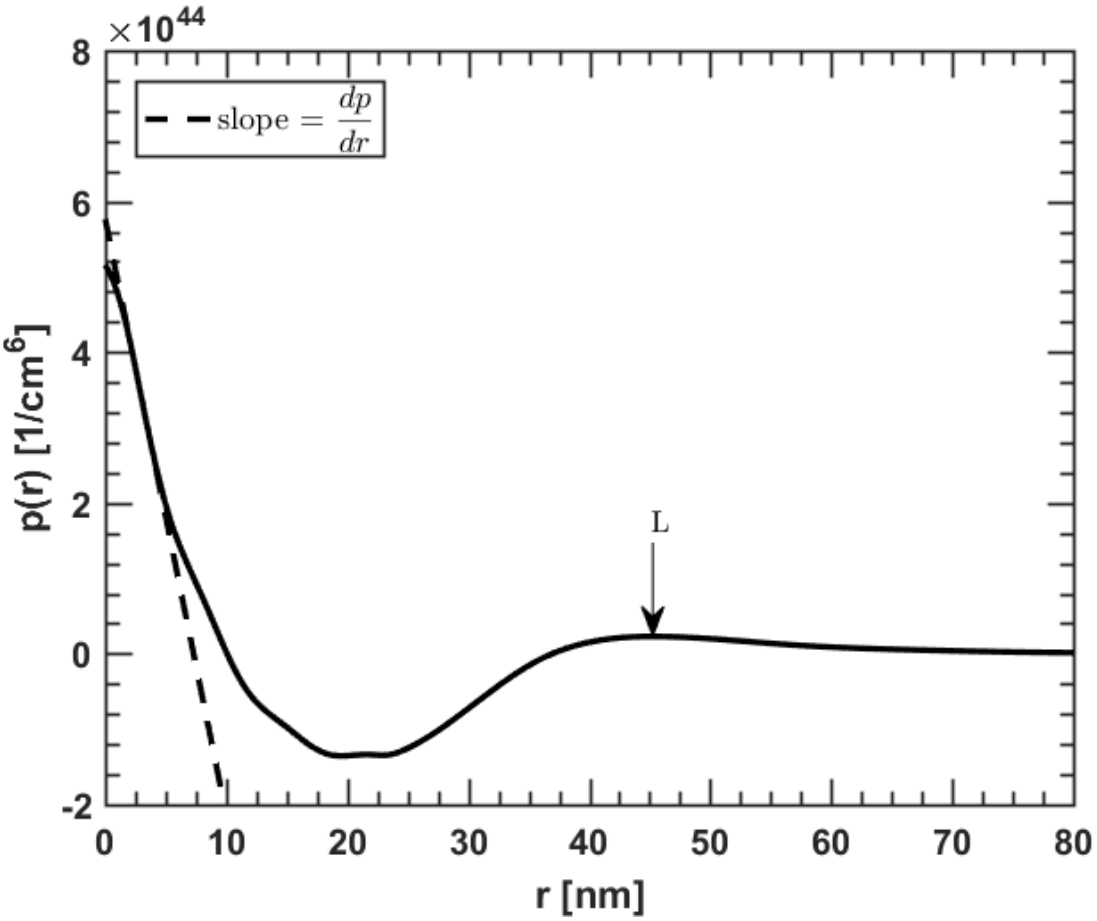

Figure 2. 1 – One-dimensional correlation function and associated parameters for GUR 1020.

The electron densities of the crystalline and amorphous regions were determined from:

$$\rho = \frac{[\sum_1^n z_i]\rho_m Av}{M} \tag{17}$$

where z_i is the number of electrons per atomic species, ρ_m is the density of the crystalline or amorphous regions of UHMWPE (g/cm^3), Av is Avogadro's number (mol^{-1}), and M is the molecular weight (g/mol) of the species. Densities for the crystalline and amorphous regions of UHMWPE were determined form

$$\rho_c = \frac{1}{0.994+2.614\times10^{-4}T+4.43\times10^{-7}T^2} \tag{18}$$

$$\rho_a = \frac{1}{1.152+8.8\times10^{-4}T} \tag{19}$$

where T is temperature in degrees Celsius (Tanabe et al., 1986). A temperature of 23 °C was chosen to calculate the crystalline and amorphous densities of UHMWPE.
Finally, lamellar thickness (*D*) was calculated based on the following equation:

$$D = X_C L \tag{20}$$

where X_c is the crystallinity determined from DSC. The thickness of the amorphous region (*A*) was calculated from the difference between interlamellar thickness (*L)* and lamellar thickness *D*. These microstructural features have been summarized in **Table 2.2**.

Table 2. 2 – Summary of microstructural properties for the different UHMWPE materials. The table follows the color format for the different material formulations established in **Table 2.1**.

UHMMPE Material Formulation	Xc [%]	L [nm]	D [nm]	A [nm]	Oac [1/cm]
GUR 1020	57.7	45.5	26.3	19.2	6.20E+05
GUR 1020 35kGy	57.8	45.2	26.1	19.1	6.37E+05
GUR 1020 75kGy RM	52.4	43.9	23.0	20.9	7.82E+05
GUR 1020 AO	57.5	46.3	26.6	19.7	6.41E+05
GUR 1020 AO 80kGy	61.2	49.7	30.4	19.3	6.92E+05
GUR 1020 VE	60.0	48.9	29.3	19.6	7.59E+05
GUR 1020 VE 50kGy	56.5	45.8	25.9	19.9	7.26E+05
GUR 1020 VE 75kGy	60.7	48.4	29.3	19.0	6.41E+05
GUR 1020 VE 100kGy	60.7	44.5	27.0	17.5	6.73E+05
GUR 1020 VE 125kGy	60.8	46.3	28.1	18.1	8.53E+05
GUR 1050	55.8	50.2	28.0	22.2	5.72E+05
GUR 1050 75kGy RM	55.8	49.7	27.7	21.9	6.88E+05

2.4.2 Tension Properties and Constitutive Behavior

The tensile mechanical properties and constitutive behavior of UHMWPE were affected by resin type, antioxidant source and degree of cross-linking (**Table 2.3**). The elastic modulus ranged from 655-1077 MPa with the highest elastic modulus observed in GUR 1020 AO 80kGy and the lowest in GUR 1020 75kGy RM. The regression analysis from 0.0005 to 0.009 strain produced the highest R^2 values (0.95-0.99) compared to the other regression strain limits investigated. Also a strain limit of 0.009 produced the same relative standard deviation for calculating elastic modulus as the other strain limits while producing the greatest difference in modulus values between material formulations. This helped justify our decision for choosing 0.009 as the strain limit in determining the elastic properties of UHMWPE for relative comparison between formulations. The UHMWPE materials without antioxidants exhibited a decrease in elastic modulus with increasing cross-linking; whereas formulations with antioxidants exhibited

an increase in elastic modulus with radiation dosage 75-80kGy followed by a decline with further irradiation. Overall due to the viscoelastic nature of UHMWPE, elastic modulus will depend on deformation rate and not exhibit a clear elastic region. Therefore defining a single value as the elastic modulus can be somewhat misleading. Its chief value is as a straightforward comparison tool as long as the procedure for calculating elastic modulus is clearly defined such as in the case of our study.

The engineering yield stress in the UHMWPE formulations ranged from 21.7 to 26.2 MPa while the true 0.002 offset yield stress ranged from 10.2 - 15.3 MPa and the true 0.002 offset yield strain spanned 0.015 to 0.018. As with modulus, GUR 1020 AO 80kGy had the highest yield strength for engineering and true values while GUR 1020 75kGy RM exhibited the lowest. The non-linear plastic model parameters β and γ ranged between -20.5 to -18.0 MPa and -34.9 to -27.6 respectively with $R^2 > 0.99$ across all test samples. Representative elastic-plastic material models are provided in **Figure 2.2**. Material groups that had higher moduli and true offset yield stress values, exhibited higher plastic hardening curves as shown in **Figure 2.2B** with GUR 1020 AO 80kGy compared to GUR 1020 75kGy RM.

The engineering ultimate stress ranged from 39.7 to 52.9 MPa while true ultimate stress ranged between 127.9 to 229.1 MPa. From the experimental data, the engineering ultimate stress severely underestimates the true material behavior since it does not account for the stable necking UHMWPE undergoes during the deformation process. The true ultimate strain and energetic toughness decreased with increasing radiation cross-linking dosages across all materials **Figure 2.3**. GUR 1020 VE exhibited the highest engineering ultimate stress, true ultimate stress, true ultimate strain, and energetic toughness while GUR 1050 75kGy RM had the lowest values in these material properties excluding engineering ultimate stress.

Representative engineering and true stress-strain curves for the four base materials (GUR 1050, GUR1020 VE, GUR 1020, and GUR 1020 AO) are provided in **Figure 2.4**. Note that a local maximum is present on the engineering stress-strain curve while no such point is observed on the true stress-strain curves.

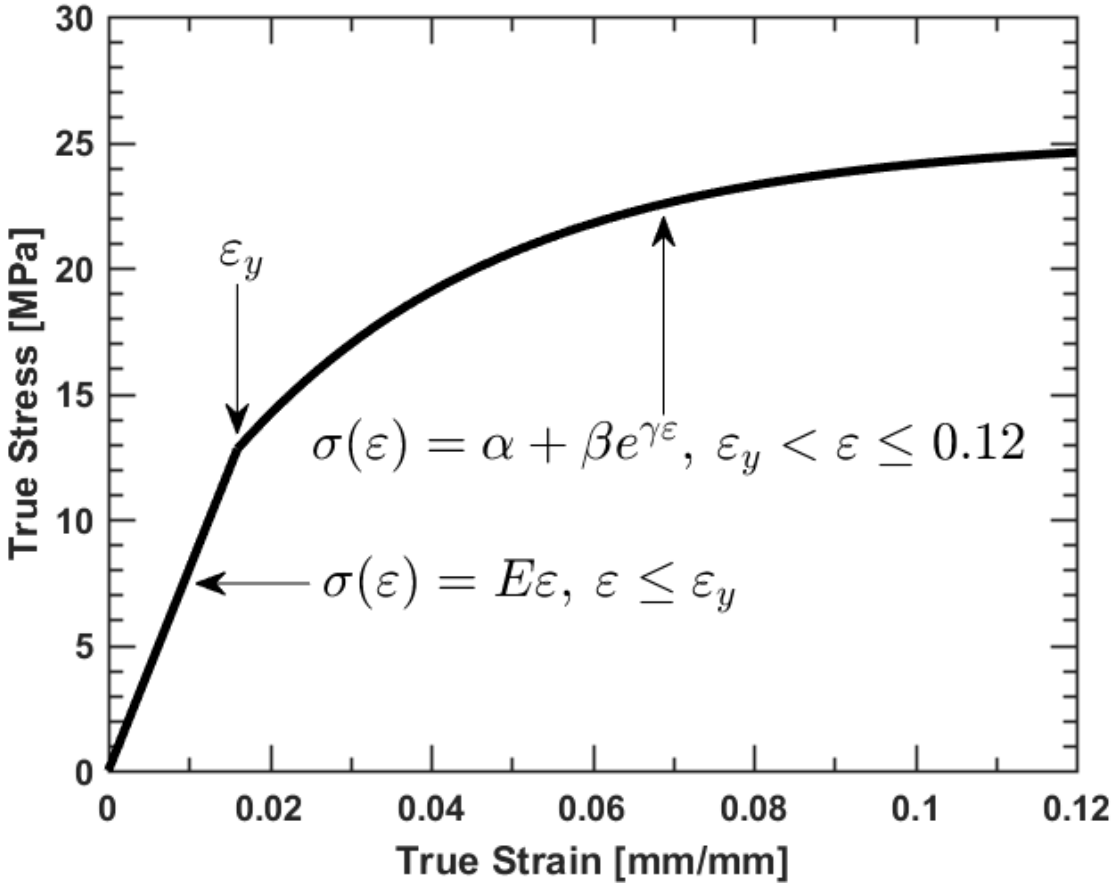
True Stress [MPa]
True Strain [mm/mm]
0
5
10
15
20
25
30
0
0.02
0.04
0.06
0.08
0.1
0.12
ε_y
$\sigma(\varepsilon) = \alpha + \beta e^{\gamma\varepsilon},\ \varepsilon_y < \varepsilon \leq 0.12$
$\sigma(\varepsilon) = E\varepsilon,\ \varepsilon \leq \varepsilon_y$

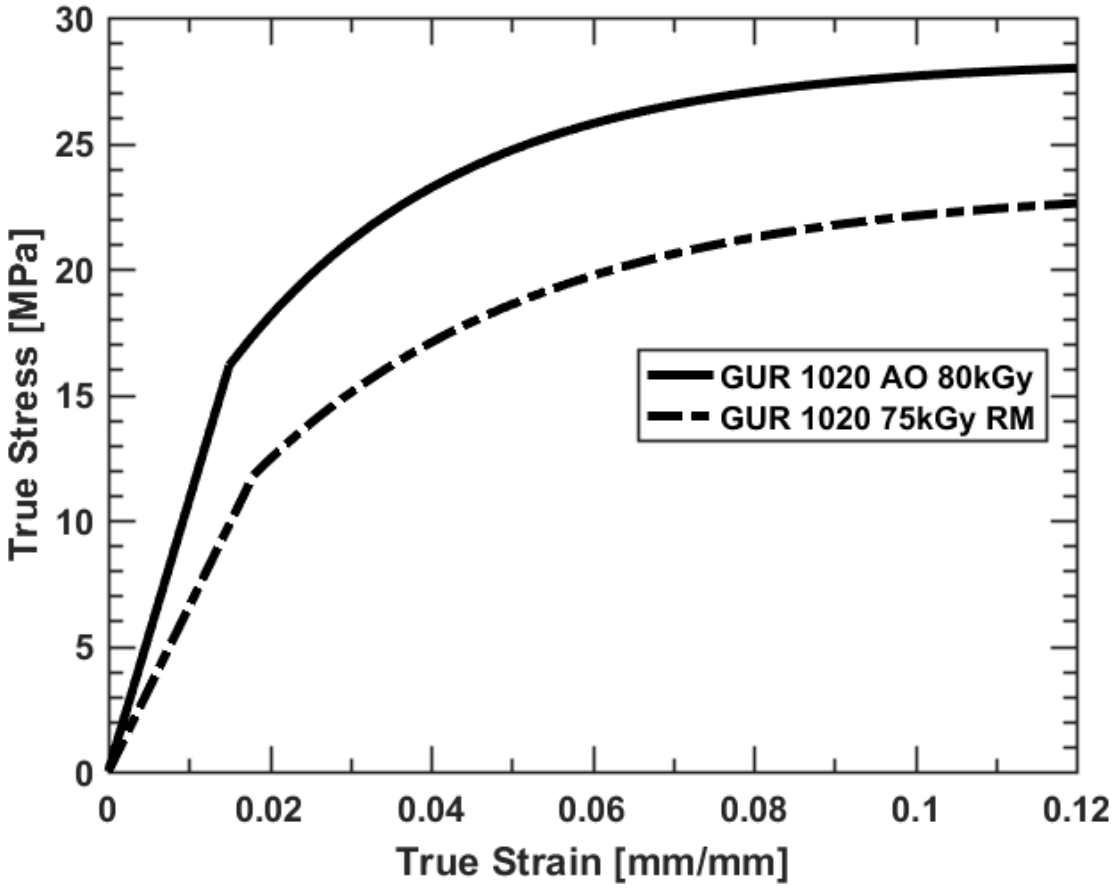

Figure 2. 2 – (A**)** Representative two segment elastic-plastic material model for UHMWPE using average values gathered from GUR 1020. **(**B**)** Representative two segment elastic-plastic material model highlighting the differences for materials GUR 1020 AO 80kGy and GUR 1020 75kGy RM. These two materials exhibited the highest and lowest modulus and yield strength values respectively.

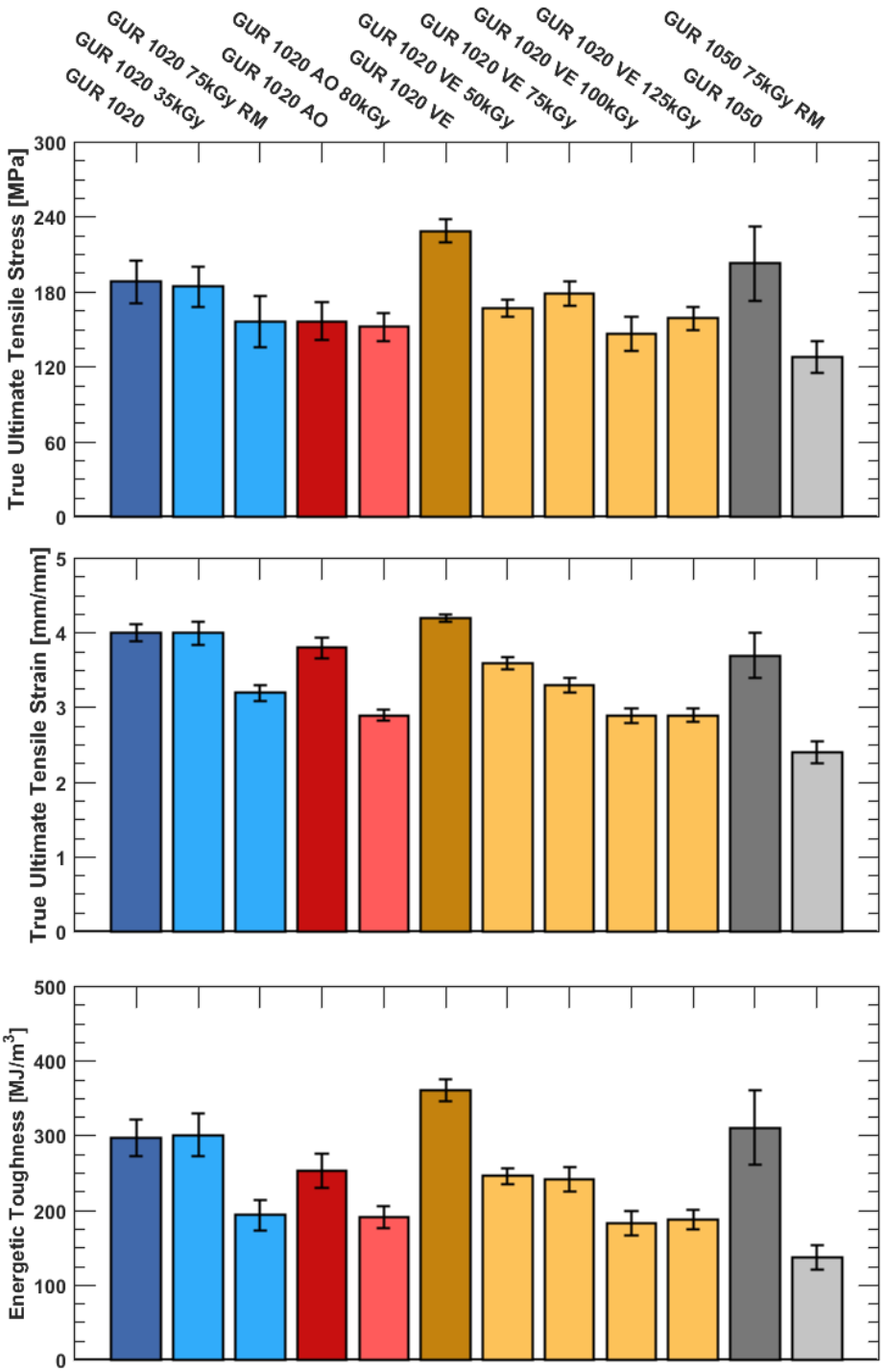

Figure 2. 3 – Bar charts showing the True Ultimate Tensile Stress, True Ultimate Tensile Strain, and Energetic Toughness across all material formulations (mean ± standard deviation). The bar charts follow the color format for the different material formulations established in **Table 2.1**.

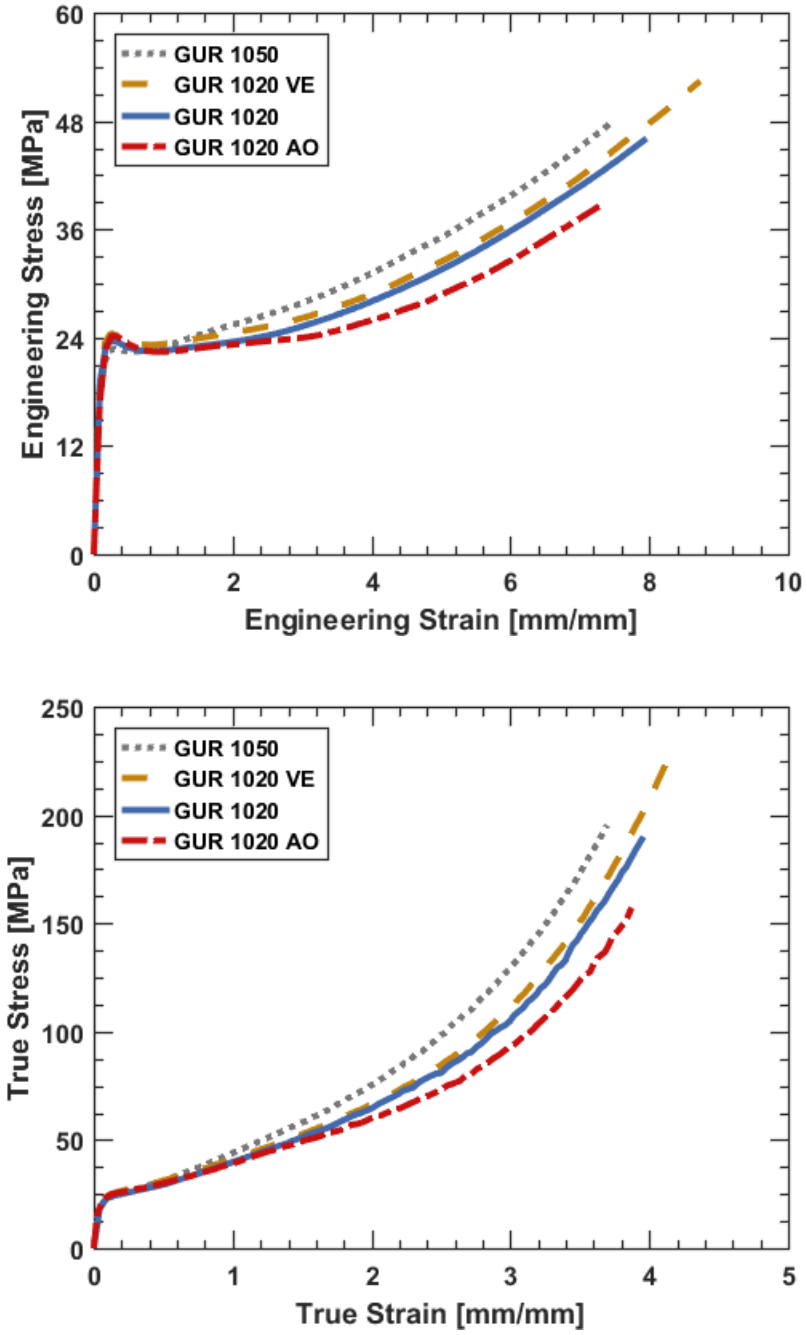

Figure 2. 4 – (A**)** Representative tensile behavior for the four base UHMWPE material groups engineering stress-strain curves. **(**B**)** Representative true stress-strain curves for the four base UHMWPE material groups. The stress-strain plots follow the color format for the different material formulations established in **Table 2.1**.

Table 2. 3 - Engineering and true tensile stress-strain data for all UHMWPE formulations (mean ± standard deviation).

Mechanical properties	UHMWPE material formulation					
	GUR 1020	GUR 1020 35 kGy	GUR 1020 75 kGy RM	GUR 1020 AO	GUR 1020 AO 80 kGy	GUR 1020 VE
Tensile true elastic modulus [MPa]	799.5 ± 26.2	758.2 ± 39.4	655.1 ± 42.7	925.9 ± 64.5	1076.8 ± 53.6	921.2 ± 13.6
Poisson's ratio	0.459 ± 0.015	0.483 ± 0.046	0.493 ± 0.034	0.544 ± 0.056	0.532 ± 0.013	0.633 ± 0.042
Engineering yield stress [MPa]	23.8 ± 0.2	23.6 ± 0.2	21.7 ± 0.2	24.3 ± 0.1	26.2 ± 0.1	24.5 ± 0.3
Tensile true 0.002 offset yield stress [MPa]	10.8 ± 1.2	12.0 ± 0.8	10.7 ± 0.5	12.5 ± 1.0	15.3 ± 0.5	13.5 ± 0.4
Tensile true 0.002 offset yield strain [mm/mm]	0.016 ± 0.002	0.018 ± 0.002	0.018 ± 0.002	0.016 ± 0.002	0.015 ± 0.002	0.017 ± 0.001
β [MPa]	− 19.8 ± 0.7	− 19.0 ± 1.3	− 18.3 ± 0.5	− 19.2 ± 1.2	− 20.5 ± 0.5	− 19.6 ± 0.4
γ	− 29.3 ± 0.8	− 28.2 ± 0.6	− 28.0 ± 1.4	− 29.9 ± 0.9	− 34.9 ± 0.9	− 28.9 ± 0.2
Engineering ultimate stress [MPa]	45.2 ± 2.7	46.2 ± 2.9	44.4 ± 4.3	39.7 ± 2.4	46.5 ± 1.8	52.9 ± 1.4
True ultimate stress [MPa]	188.2 ± 17	184.3 ± 16.1	156.3 ± 20.4	156.4 ± 15.2	152 ± 10.8	229.1 ± 9.7
True ultimate strain [mm/mm]	4.0 ± 0.1	4.0 ± 0.2	3.2 ± 0.1	3.8 ± 0.1	2.9 ± 0.1	4.2 ± 0.05
Energetic toughness [MJ/mm^3]	297.9 ± 24.7	301.3 ± 28.7	193.9 ± 20.9	253.6 ± 22.8	190.9 ± 14.5	361.5 ± 14.7

Mechanical properties	UHMWPE material formulation					
	GUR 1020 VE 50 kGy	GUR 1020 VE 75 kGy	GUR 1020 VE 100 kGy	GUR 1020 VE 125 kGy	GUR 1050	GUR 1050 75 kGy RM
Tensile true elastic modulus [MPa]	885.0 ± 31.5	1060.6 ± 37.4	1008.5 ± 36.6	865.4 ± 56.3	810.6 ± 26.2	762.3 ± 32.0
Poisson's ratio	0.499 ± 0.017	0.421 ± 0.027	0.464 ± 0.025	0.461 ± 0.040	0.540 ± 0.076	0.521 ± 0.043
Engineering yield stress [MPa]	24.9 ± 0.1	26.0 ± 0.1	25.2 ± 0.2	25.8 ± 0.1	22.9 ± 0.2	24.2 ± 0.2
Tensile true 0.002 offset yield stress [MPa]	14.1 ± 1.7	14.8 ± 0.3	14.7 ± 0.7	14.1 ± 1.1	13.2 ± 0.7	11.7 ± 0.4
Tensile true 0.002 offset yield strain [mm/mm]	0.018 ± 0.002	0.016 ± 0.001	0.017 ± 0.001	0.018 ± 0.0005	0.018 ± 0.001	0.017 ± 0.001
β [MPa]	− 18.5 ± 2.3	− 20.3 ± 0.7	− 19.7 ± 0.8	− 19.3 ± 1.5	− 18.0 ± 0.6	− 19.7 ± 0.9
γ	− 29.6 ± 1.6	− 33.2 ± 0.8	− 31.7 ± 1.1	− 31.7 ± 1.1	− 27.6 ± 0.7	− 31.5 ± 1.1
Engineering ultimate stress [MPa]	45.1 ± 1.5	50.7 ± 1.7	44.4 ± 2.8	49.1 ± 1.7	50.5 ± 5.7	45.7 ± 3.0
True ultimate stress [MPa]	167.1 ± 7.1	178.9 ± 10.1	146.4 ± 13.6	158.8 ± 9.7	202.8 ± 29.9	127.9 ± 12.8
True ultimate strain [mm/mm]	3.6 ± 0.1	3.3 ± 0.1	2.9 ± 0.1	2.9 ± 0.1	3.7 ± 0.3	2.4 ± 0.1
Energetic toughness [MJ/mm^3]	246.1 ± 11	241.8 ± 16.4	183.0 ± 16.7	187.9 ± 13.6	311.1 ± 50.4	137.4 ± 16

2.4.3 Poisson's Ratio

Poisson's ratio was calculated for the range of UHMWPE formulations using a linear regression from true axial strains of 0.0005 to the true tensile yield strain taken from the 0.002 offset line. This method yielded a Poisson's ratio for GUR 1020 that matched previously reported values of 0.46 (Kurtz, 2009). **Figure 2.5** depicts a representative graph of axial and transverse true strains versus load. The plot reveals that there is non-linear behavior and highlights the complexities of calculating the Poisson's ratio in polymers such as UHMWPE. The Poisson's ratio values across the UHMWPE material groups are summarized in **Table 2.3.** As the radiation cross-linking dosage increased for GUR 1020, Poisson's ratio values approached 0.50. GUR 1020 AO, GUR 1020 AO 80kGy, GUR 1020 VE, and all GUR 1050 formulations exhibited Poisson's Ratios higher than 0.50 suggesting orientation effects from the consolidation process in the material. The orientation effect could also come from the process of antioxidant addition and higher molecular weight locking in the polymer network structure. As the cross-linking dosage was increased for GUR 1020 VE, the Poisson's ratio decreased and leveled off at roughly 0.46 (**Figure 2.6**) potentially suggesting that chain scission might unlock the network from consolidation and antioxidant addition.

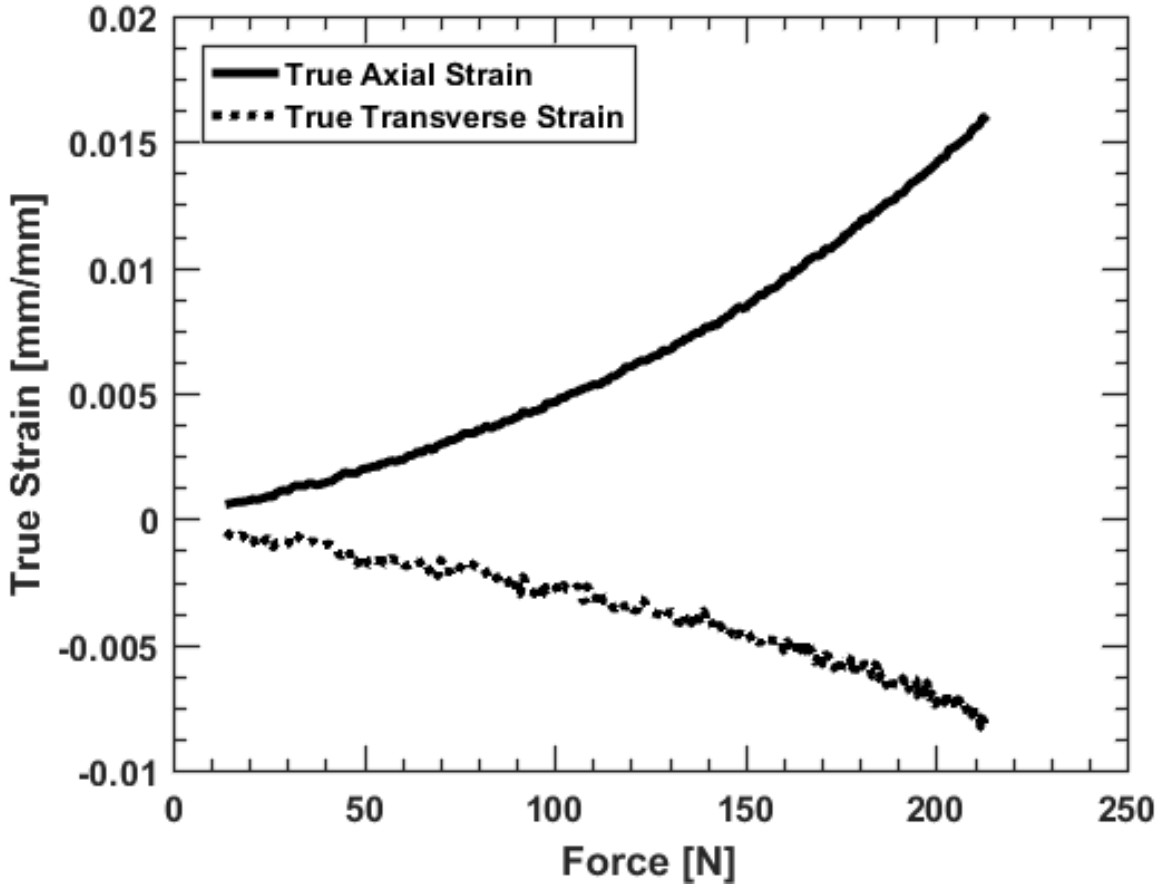

Figure 2. 5 – Representative true axial and transverse strains versus load for GUR 1020 used in the calculation of Poisson's ratio.

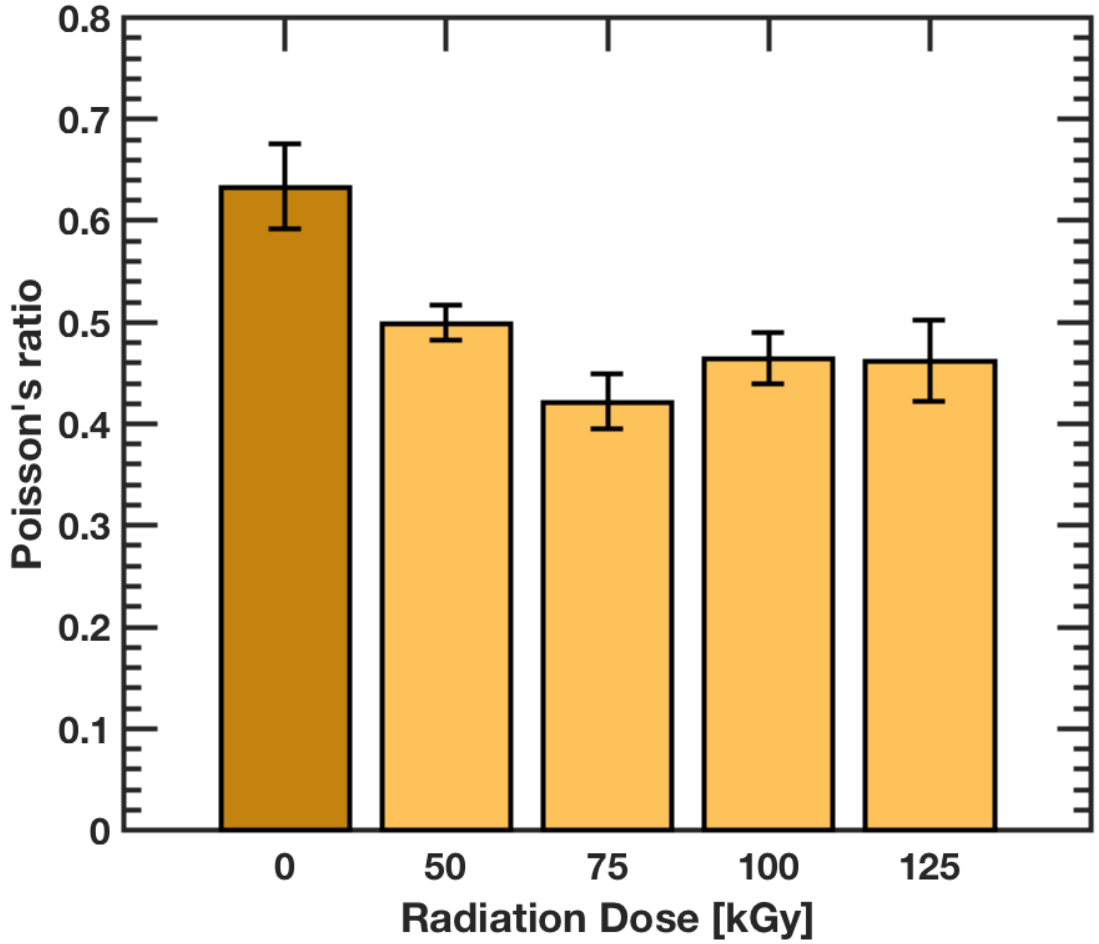

Figure 2. 6 – Poisson's ratio as a function of radiation dose [kGy] for the GUR 1020 VE formulations (mean ± standard deviation).

2.4.4 Compression Properties

The compressive elastic modulus, true yield stress, and true yield strain across all UHMWPE material formulations are provided in **Table 2.4**. The elastic modulus in compression ranged from 521MPa to 1130MPa. True 0.002 offset yield stress ranged from 10.9 MPa to 15.3 MPa with 0.002 offset yield strain ranging from 0.015 to 0.029. Overall the moduli and yield values measured in compression were not exactly the same as those found in tension however, the same trends that were present in tension were present in compression. For instance, GUR 1020 AO 80kGy exhibited the highest modulus and yield values in tension and compression while GUR 1020 75kGy RM exhibited the lowest. The majority of true offset yield strain values in compression were below 0.02 strain in accordance with previous work (Kurtz et al., 2002; Kurtz et al., 1998). Additionally, the compressive modulus and yield stress of GUR 1050 matched results found earlier from Kurtz and colleagues (Kurtz et al., 2002).

2.4.5 Nanoindentation Properties

Reduced elastic modulus and hardness values for all the UHMWPE formulations are provided in **Table 2.4**. Local moduli calculated from nanoindentation were lower on average compared to tension and compression. Additionally the relative standard deviations for modulus from nanoindentation were higher owing to the non-linearity in the unloading portion of the force versus displacement curves. GUR 1020 AO 80kGy exhibited the highest nanoindentation modulus and hardness across the UHMWPE formulations which was consistent with results from tension and compression. GUR 1020 75kGy RM was not consistent with exhibiting the lowest modulus and hardness out of the material formulations as would be inferred from the tension and compression results.

Table 2. 4 – Compression and nanoindentation properties (mean ± standard deviation).

Mechanical properties	UHMWPE Material Formulation					
	GUR 1020	GUR 1020 35 kGy	GUR 1020 75 kGy RM	GUR 1020 AO	GUR 1020 AO 80 kGy	GUR 1020 VE
Compressive true elastic modulus [MPa]	900 ± 49.4	539 ± 68.2	521 ± 23.4	925 ± 114	1130 ± 23.1	870 ± 35.5
Compressive 0.002 true offset yield stress [MPa]	12.0 ± 0.28	14.0 ± 4.1	10.9 ± 1.1	12.8 ± 0.8	15.3 ± 0.4	13.1 ± 0.7
Compressive 0.002 true offset yield strain [mm/mm]	0.015 ± 0.001	0.029 ± 0.014	0.023 ± 0.003	0.016 ± 0.003	0.016 ± 0.001	0.018 ± 0.001
Nanoindentation modulus [MPa]	728.5 ± 110.7	787.0 ± 184.3	660.6 ± 137.2	745.3 ± 187.5	918.4 ± 240.1	611.2 ± 205.4
Nanoindentation hardness [MPa]	37.0 ± 9.0	37.6 ± 10.0	35.8 ± 9.5	35.0 ± 9.3	43.8 ± 13.5	29.6 ± 9.9

Mechanical properties	UHMWPE Material Formulation					
	GUR 1020 VE 50 kGy	GUR 1020 VE 75 kGy	GUR 1020 VE 100 kGy	GUR 1020 VE 125 kGy	GUR 1050	GUR 1050 75 kGy RM
Compressive true elastic modulus [MPa]	982 ± 28.2	1090 ± 14.2	953 ± 36.2	1040 ± 61.6	851 ± 71.8	591 ± 31.0
Compressive 0.002 true offset yield stress [MPa]	13.2 ± 0.8	14.4 ± 0.3	12.4 ± 0.6	14.0 ± 0.8	13.8 ± 1.5	12.6 ± 1.3
Compressive 0.002 true offset yield strain [mm/mm]	0.017 ± 0.001	0.017 ± 0.001	0.019 ± 0.001	0.017 ± 0.003	0.019 ± 0.002	0.023 ± 0.003
Nanoindentation modulus [MPa]	815.1 ± 141.6	912.8 ± 147.4	717.1 ± 96.0	880.7 ± 129.7	776.35 ± 118.2	837.98 ± 152.2
Nanoindentation hardness [MPa]	33.5 ± 5.3	41.1 ± 9.7	32.6 ± 5.0	36.2 ± 7.8	40.4 ± 8.65	30.8 ± 6.19

2.4.6 Statistical Analysis

2.4.6.1 Mechanical Property Statistical Analysis

Non-parametric statistical analysis demonstrated that several bulk mechanical properties were well correlated across different testing and measurement conditions. Elastic modulus and yield strength were well correlated in tension and compression (**Table 2.5,2.6**). Additionally engineering yield stress was well correlated with both tensile and compressive true offset yield stress suggesting that bulk mechanical property measurements produce the same trends across analysis methods. Nanoindentation hardness was not correlated with any bulk mechanical measurement of yield strength however compressive modulus and nanoindentation modulus were weakly correlated. This lack of correlation between bulk properties and nanoindentation can possibly be attributed to the size scale differences in analysis methods. No correlation was found between engineering and true ultimate stress.

Table 2. 5 – Spearman rank correlation coefficient matrix between the different elastic modulus properties of all UHMWPE formulations**.**

	Tensile true elastic modulus ρ	**Compressive true elastic modulus ρ**	**Nanoindentation elastic modulus ρ**
Tensile true elastic modulus ρ	1		
Compressive true elastic modulus ρ	0.839*	1	
Nanoindentation elastic modulus ρ	N/A	0.587	1

N/A, did not show statistical significance between two variables.

* $p \leq 0.01$.

Table 2. 6 – Spearman rank correlation coefficient matrix between the different yield properties of all UHMWPE formulations.

	Engineering Yield Stress ρ	Tensile true 0.002 offset yield stress ρ	Compressive true 0.002 offset yield stress ρ	Nanoindentation hardness ρ
Engineering yield stress ρ	1			
Tensile true 0.002 offset yield stress ρ	0.860*	1		
Compressive true 0.002 offset yield stress ρ	0.802*	0.711*	1	
Nanoindentation hardness ρ	N/A	N/A	N/A	1

N/A, did not show statistical significance between two variables.

* $p \leq 0.01$.

Spearman rank correlation coefficients were also performed between the tensile true offset yield strength and the non-linear model parameters in an effort to understand plastic hardening behavior in UHMWPE. There was a relationship between yield strength and non-linear plastic models parameter β (ρ = -0.860, p = 0.0006) and γ (ρ = -0.685, p = 0.02) showing that as yield strength increased β and γ would decrease. Essentially as yield strength in UHMWPE material formulations is increased, the rate at which the material plastically deforms increases as well. A lower β in **equation 3** translates to a higher rate the material approaches the asymptotic yield stress limit which can be seen in **figure 2.2B** comparing the hardening behavior of the highest and lowest strength material formulations. These observations are only valid when looking at UHMWPE up to true strains of 0.12 where these model parameters are valid.

2.4.6.2 Microstructural Statistical Analysis

Non-parametric statistical analysis showed that elastic modulus in tension and compression correlated with crystallinity (**Table 2.7**). Poisson's ratio was found not to correlate with any microstructural properties most likely due to our microstructural analysis focusing on lamellar size and not orientation. Engineering and true yield stress values from tension and compression correlated well with both crystallinity and lamellar thickness. Tensile modulus correlated with lamellar thickness. Non-linear hardening parameters, β and γ, also demonstrated correlation with crystallinity. Finally tensile elastic modulus and engineering ultimate stress showed correlation with lamellar thickness.

Table 2. 7 – Spearman rank correlation coefficients for microstructural and mechanical properties across all UHMWPE formulations.

Microstructural property	Tensile true elastic modulus ρ	Compressive true elastic modulus ρ	Poisson's ratio ρ	Engineering yield stress ρ	Tensile true 0.002 offset yield stress ρ	Compressive true 0.002 offset yield stress ρ	β ρ	γ ρ	Engineering ultimate stress ρ
Crystallinity, Xc	0.718*	0.704	N/A	0.806*	0.739*	0.661	0.739*	− 0.669	N/A
Lamellar thickness, D	0.636	N/A	N/A	0.678	0.615	0.631	N/A	N/A	0.748*

N/A, did not show statistical significance between two variables.

* $p \leq 0.01$.

2.5 Discussion

Material properties of UHMWPE depends upon resin type, consolidation process, degree of cross-linking, post-irradiation thermal treatment as well as antioxidant chemistry. Understanding the constitutive behavior of UHMWPE is requisite for optimizing long-term performance of these polymers in TJRs. Moreover, quasi-static properties such as ultimate strength, strain to failure and energetic toughness provide insight into clinical performance of these polymers in orthopedic bearing applications. To the authors' knowledge, this is the first comprehensive study that characterizes microstructure, tension and compression constitutive behavior, as well as nano-mechanical surface properties across a spectrum of clinical UHMWPE formulations. The expansive mechanical analysis conducted within this study is an attempt to accomplish two primary goals 1.) Thoroughly describe methods in the analysis of basic mechanical properties and provide justifications for why these methods are important and should be used moving forward 2.) Cohesively link mechanical properties, through multiple deformation schemes and microstructure, all in an attempt to provide insight to engineers and designers to improve implant performance and longevity.

Engineering tensile stress-strain tests are commonly used to characterize the mechanical behavior of UHMWPE and to compare resins for use in total joint replacements. The constitutive behavior of UHMWPE is complicated by its extensive plastic deformation facilitated through fibrillation of its microstructure and thus the polymer is more accurately characterized by the use of true stress-strain relationships (Kurtz et al., 2002; Kurtz et al., 1998). **Figure 2.4** shows a clear distinction between the engineering and true tensile behavior for the four base UHMWPE formulations. Notably, the engineering stress-strain curve (**Figure 2.4A**) exhibits a local maximum that is generally used as the yield point of UHMWPE. In comparison, the true stress-strain curve does not show this maximum but rather it captures the large deformations observed in UHMWPE (**Figure 2.4B**).

For this study, we used a 0.002 offset line to analyze yielding for the true tensile behavior across the UHMWPE formulations in order to directly compare tension and compression properties as well as build upon a previously established elastic-plastic material model (Kurtz et al., 2002; Kurtz et al., 1998; Kurtz et al., 2006). We found that the tensile true offset yield stress values ranged from 10.2MPa to 15.3MPa (true offset yield strain values ranged between 0.015 to 0.018)**.** In comparison, the compressive true offset yield stress spanned 10.9MPa to 15.3MPa (true offset yield strain values ranged between 0.015 to 0.029). It is notable that the measured tensile and compressive yield values were extremely close across material formulations. The similarities between tension and compression were further corroborated with our Spearman rank correlation coefficients demonstrating that the same yield trends exist across loading scenarios and material formulations. The yield values only differed for a particular formulation by at most 2.3MPa and 0.011 strain for GUR 1020 VE 100kGy and GUR 1020 75kGy RM respectively. Additionally the range of our yield values were consistent with previous work published by Kurtz and colleagues using the 0.002 offset method (Kurtz et al., 2002; Kurtz et al. 2006). The offset method however is not traditionally the accepted yield point in a polymer despite the current and previous usage of this to determine yield in UHMWPE.

The yield point of a material traditionally represents the onset of plastic (permanent deformation); however there is microstructural evidence that non-recoverable deformation occurs in UHMWPE before reaching the macroscopic yield point or onset of stable necking. Earlier compression studies with simultaneous microstructure characterization have revealed non-reversible microstructure evolution at small deformations (Bartczak et al., 1992; Lin & Argon, 1994). Similarly, Kurtz and colleagues demonstrated that there was non-recoverability at compressive strains below the 0.002 offset yield strain and that the offset method was a valid way to determine when those non-recoverable strains increased sharply (Kurtz et al., 1998). Such findings have important implications for designing against and understanding plastic deformation of UHMWPE in TJRs. The 0.002 offset method with true stress-strain data serves to conservatively predict yield and aid in formulating a more accurate plastic flow model. As a result, we strongly urge that *true* stress-strain data should be used as a more accurate constitutive model for determining fundamental material behavior such as modulus, yield and ultimate properties. We further suggest moving away from the traditional definition of the local maximum on the engineering stress-strain curve as the yield point in UHMWPE as it may overestimate yield strength especially for a material used in a safety critical application like that of TJRs.

Poisson ratio is another important material property that is essential for constitutive modeling and analysis of mechanical behavior. The value of Poisson's ratio of UHMWPE is commonly assumed as 0.46; yet little is known about the effects of processing, cross-linking, thermal treatments and use of antioxidants on this parameter. The R^2 values for the calculation of elastic modulus from the true stress-strain data ranged from 0.95 to 0.99 for strains between 0.0005 and 0.009 demonstrating reasonable linearity to the stress-strain relationship of UHMWPE at low strains. According to ASTM D638 (Annex A3), if a polymer exhibits a non-linear stress-strain relationship then the Poisson's ratio should be determined within the true axial strain range of 0.0005 to 0.0025. The true axial strain limit in our study was chosen as the tensile true offset yield strain. This method was employed to determine if the true axial and transverse strain response was linear up to that point as well as to compare our values with those reported in the literature previously. To the authors' knowledge, only one modern study, Kurtz et al., 2006, has looked at Poisson's ratio changes due to orientation and radiation cross-linking. For this study, Kurtz et al. found Poisson's ratio within the elastic regime but did not mention any more specifics (Kurtz et al., 2006). **Figure 2.5** shows that the true axial and transverse strain versus load responses of UHMWPE up to the true axial offset yield strain deviate from ideal linearity. Despite this non-linearity our calculation of Poisson's ratio produced results consistent with values cited in the literature for GUR 1020 (Kurtz, 2009). This method is further corroborated by the low standard deviations for our measured Poisson's ratio values across the UHMWPE formulations.

It is remarkable that some of the measured values of Poisson's ratio for various UHMWPE formulations exceeded 0.50. This finding suggests some aspect of anisotropy in the polymer and is likely attributed to microstructure changes owed to process formulation specifically chain alignment in the polymer from compression molding (Bailey, 2012; Chang et al., 1999; Elliott et al., 2002; Kempson, 1982). Previously it was thought that compression molding would produce material that was more isotropic in morphology however with higher molecular weight resins (GUR 1050) and antioxidant additions this is not the case based on our Poisson's ratio findings (Bellare and Cohen, 1996; Kurtz et al., 1999a; Pruitt and Bailey, 1998). As a result, further characterization of the Poisson's ratio and orientation effects on basic mechanical properties

(elastic modulus, yield strength, etc.) for various clinical formulations and material processing conditions of UHMWPE is highly warranted.

UHMWPE anisotropy was previously investigated by Kurtz using GUR 1050 50kGy cross-linked material that was ram extruded after cross-linking (ArCom XL) to knowingly impart directionality into the material (Kurtz et al., 2006). Kurtz found mixed conclusions with some mechanical properties being affected by orientation while other properties were not. For instance there was basically no change in Poisson's ratio when measured in compression with different orientations to the long axis of the ArCom XL rod stock. At the same time, Poisson's ratio was not investigated for orientation effects in tension. Elastic modulus was another mechanical property missing a tensile pairing for orientation effects. Overall from Kurtz et al., 2006 there are still unanswered questions regarding anisotropy that warrant further investigation to cohesively understand how anisotropic behavior might exist across different loading scenarios, processing conditions, resin types and antioxidant additions.

Anisotropic behavior in UHMPWE is important to understand since implants experiencing wear and fatigue can be affected by orientation with drastically different consequences. Ohta determined increased wear resistance with preferential crystal alignment to the contact surface (Ohta et al., 2003). Pruitt found decreases in fatigue fracture performance when extruded material was fatigued perpendicular to the extrusion direction where crystallographic deformation was restricted (Pruitt and Bailey, 1998). Our microstructural analysis dealt mainly in the size of crystalline and amorphous features in pre-deformed as processed material. Correlations have been made with crystallographic orientation throughout the deformation process in UHMWPE and HDPE (Bartczak et al., 1992; Bellare and Cohen, 1996; Cohen et al., 1992). It is possible that investigations into the crystal alignment pre and post deformation might have explained our anisotropic results with Poisson's ratio. It is recommended that additional SAXS and transmission electron microscopy (TEM) studies be performed on antioxidant and high molecular weight resins of UHMWPE, across consolidation methods, to better understand these previously unknown crystallographic orientation effects. Ultimately microstructural mechanisms, as our study and others have shown, are linked to basic mechanical properties like modulus, yield strength, and ultimate strength, which are the fundamental requisite material properties for stress analysis of orthopedic implants (Atwood et al., 2011; Medel et al., 2009; Simis et al., 2006; Turell and Bellare, 2004).

Basic mechanical properties derived from true stress-strain relations and constitutive behavior are paramount in simulating accurate material deformation in UHMWPE implants. Bergström has developed several comprehensive constitutive models based on limited physical experimental true stress-strain datasets (Bergström et al., 2003, 2002). He even mentions the need for a more comprehensive mechanical property database to validate his overarching model (Bergström et al., 2002). Our study moves toward building that necessary database however introducing the need to incorporate potential anisotropic behavior. The prospect of having significant differences in modulus, Poisson's ratio, yield strength, hardening parameters, and ultimate strength in different loading scenarios adds complexity to Bergström's unified model. However, part of what a large mechanical property database means for a unified constitutive model is culling where anisotropic or other effects might be more or less important to incorporate.

Our study was able to show a wide range in properties with different material formulations while also demonstrating agreement between deformation schemes providing a much needed push

to understand which mechanical parameters are the most important for a constitutive model. We were able to show agreement between tensile and compressive deformation schemes across UHMWPE formulations with correlations to microstructure. These agreements along with past studies, justify some validity in the assumption that tension and compression follow almost the same behavior up to 0.12 strain in some UHMWPE formulations (Kurtz et al., 1998). At the same time, our results show a wide range in elastic-plastic behavior (**Figure 2.2**) between different material treatments highlighting the need to further gather experimental data when UHMWPE is altered in some way. The only way to understand material property effects and material anisotropy is to conduct additional mechanical testing to provide the necessary modeling parameters. Mechanical and constitutive properties for UHMWPE implants however can change during *in vivo* loading and capturing these changes is important for modeling. Often there is insufficient retrieved implant material to conduct a bulk tension or compression test of the material. Nanoindentation can provide the necessary insights into mechanical property alterations in this scenario.

Nanoindentation is another characterization tool that offers a viable method for analyzing the surface mechanical properties of UHMWPE. Nanoindentation makes use of indenter tips that span from nanometer to micron length scales and for this reason the method offers insight into local mechanical properties as well variations in surface hardness owed to microstructure. The method differs from bulk mechanical testing not only in size scale sampled but also in its use of unloading curves as a metric for determining a reduced modulus and hardness (Oliver and Pharr, 1992). For these reasons nanoindentation is not expected to provide identical elastic modulus values to those measured with bulk tests but rather the method offers correlating trends in modulus or hardness across UHMWPE formulations and is useful for retrievals or where material is limited (Ebenstein & Pruitt, 2006; Klapperich et al., 2002). Hardness determined from nanoindentation correlated with some compressive and tensile yield stress trends across the UHMWPE formulations. For GUR 1020 and 1050 resins, the hardness decreased with increased cross-linking with the same trend observed in yield stress measured in tension and compression. Similarly, the GUR 1020 AO 80kGy and GUR 1020 VE 75kGy exhibited the highest modulus and yield stress values in tension and compression which were corroborated in the nanoindentation properties.

As with the other material characterization techniques, a standardized method is needed for nanomechanical characterization of UHMWPE. Nanoindentation is affected not only by changes in local microstructure and variations in Poisson's ratio (as discussed above) but also the inherent viscoplastic nature of UHMWPE. Despite these limitations, nanoindentation offers general insight into surface mechanical properties. The method may be useful in implant design as it can be utilized to assess surface property changes owed to clinical use (Medel et al., 2009).

The microstructure evaluation of UHMWPE is equally important in assessing clinical outcomes for the polymer. It is well known that lamellar size (thickness and spacing) can have a significant effect on crack propagation mechanisms and can directly impact the fatigue fracture resistance of the polymer (Atwood et al., 2011; Baker et al., 2003; Simis et al., 2006). SAXS is an established method for quantifying lamellar architecture in UHMWPE and provides superior sampling statistics compared with other microstructural assessment methods (Turell and Bellare, 2004). In this study, a number of fundamental mechanical properties were found to positively correlate with crystallinity and lamellar thickness, **Table 2.8,** suggesting that morphological changes to UHMWPE can influence mechanical properties. This finding suggests that tailoring the microstructure can be an important pathway for achieving optimized mechanical properties of UHMWPE across different loading scenarios.

2.6. Conclusions

Our work evaluates methods for measuring elastic modulus, Poisson's ratio, yield conditions in stress and strain, ultimate true stress and strain, and energetic toughness across tensile and compressive behavior. Through our methods, this study shows that variations in clinical formulations of UHMWPE that span resin type, degree of cross-linking, thermal treatment and antioxidant chemistry result in differences in microstructure, crystallinity and mechanical properties. This wealth of data provides the necessary insight to orthopedic implant designers and engineers. Microstructure measured with DSC and SAXS correlates with mechanical properties that are requisite for structural function of this polymer in TJRs. Additionally our methods and analysis demonstrate the anisotropic effects in material formulations and consolidation methods previously not thought possible requiring future mechanical testing and microstructural evalution. Finally, nanoindentation is shown to be a useful metric for determining reduced modulus and hardness across UHMWPE formulations. This is the first study to simultaneously capture mechanical and microstructural properties across an extensive cohort of UHMWPE formulations for use in modern orthopedic implants.

Acknowledgments—We are grateful to Quadrant, Orthoplastics, and DePuy for providing UHMWPE materials for this study. Funding for this study has been provided by the endowment from the Lawrence Talbot Endowed Professorship, a National Science Foundation Graduate Research Fellowship and the Ian Finnie graduate research fellowship at UC Berkeley.

Chapter 3 – The fracture of ultra-high molecular weight polyethylene

Abstract

This chapter presents a cohesive methodology for quantifying the fracture behavior of structural polymers. We accomplish this task by reviewing the complexities of polymer fracture mechanics and associated *J*-integral fracture toughness testing as well as by conducting appropriate nonlinear-elastic fracture mechanics measurements with comprehensive analysis. *J*-based crack-initiation and crack-growth fracture toughness testing is performed on ten clinically relevant formulations of ultra-high molecular weight polyethylene (UHMWPE). This polymer is chosen for its extensive literature base in terms of its mechanical properties and fracture toughness behavior, as well as its safety-critical importance and broad use in total joint replacements. One of the current limitations in polymer fracture characterization is the use of "engineering" constitutive behavior to determine initiation fracture toughness compared with "true" constitutive properties. UHMWPE offers a plethora of true tensile stress-strain data that serves as a template and predicate base for fracture analysis. This chapter aims to demonstrate why using true constitutive behavior for polymer fracture mechanics is so important and why a justified comprehensive analysis method is needed in order to reliably measure the fracture toughness of polymeric materials.

3.1 Introduction

Ultra-high molecular weight polyethylene (UHMWPE) remains the polymer of choice for use in total joint replacements (TJRs). Its clinical use spans sixty years and accordingly there is an abundance of research literature available that provides insight into the mechanical behavior of this polymer (Kurtz, 2015). UHMWPE is a semi-crystalline polymer with crystalline lamellae embedded in an amorphous matrix that is well above its glass transition (-80°C) temperature (Sara A Atwood et al., 2011; Bistolfi et al., 2009; Turell and Bellare, 2004). This polymer is defined by its very high molecular weight (2-6 million g/mol) where these long chains facilitate high entanglement density that limit the crystallinity to about 50% yet afford the polymer exceptional energetic toughness (Kurtz, 2009; Pruitt, 2005). Despite its excellent energetic toughness and inherent biocompatibility, UHMWPE in its untailored form is susceptible to wear when articulating against the hard bearings typically used in TJRs (Kurtz, 2015, 2009). Modern formulations of UHMWPE make use of irradiation cross-linking to improve wear resistance, as well as thermal and antioxidant treatments to improve its *in vivo* oxidative resistance (Kurtz, 2015). The improvements to wear and oxidation resistance come though at the expense of mechanical properties (Kurtz, 2015) and the detriment of fatigue fracture resistance (Ansari et al., 2016; Sara A Atwood et al., 2011; Baker et al., 2003b; Crowninshield and Muratoglu, 2008; Gencur et al., 2006; Rimnac and Pruitt, 2008; Simis et al., 2006).

Despite its long and storied use in such a safety critical environment, there has been little consensus on how to assess the constitutive behavior and the crack initiation fracture toughness of UHMWPE. One major incongruity lays its foundation in the discrepancy in using *engineering* versus *true stress-strain* data to determine its mechanical properties. This problem is not unique to UHMWPE and includes a number of engineering polymers. Unlike metallic materials, semi-crystalline polymers when stressed above glass transition temperature undergo stable necking throughout their extensive deformation. This has profound effects when analyzing plastic flow properties such as yield strength and ultimate strength that are important parameters for determining *J*-integral based J_{Ic} fracture toughness values.

The nonlinear plane-strain initiation fracture toughness value, J_{Ic}, is classically defined as the end of "apparent" crack extension due to crack-tip blunting, often identified as a stretch zone on the fracture surface, at the onset of crack initiation due to material tearing (Clarke et al., 1979; Landes and Begley, 1974; Paris et al., 1979). This parameter is determined experimentally using a single or multi-specimen test (as defined in the ASTM Standards ASTM E1820 for metals; ASTM D6068 for polymers) to create a *J*-integral versus crack extension $J_R(\Delta a)$ crack-resistance (R-) curve (**Figure 3.1**). A theoretical blunting line is drawn to intersect the J_R curve to determine J_{Ic} (Clarke et al., 1979; ASTM E1820). The intersection of the blunting line and the *R*-curve should then correlate with crack initiation (at the end of crack extension due to blunting), which in turn should be represented by the stretch zone width (SZW) on the fracture surface. In this methodology, the SZW can be used directly with the material flow properties to determine J_{Ic} since the blunting line and stretch zone are directly related to the crack-tip opening displacement (CTOD) (Amouzouvi and Bassim, 1982; Liu and Kobayashi, 1980).

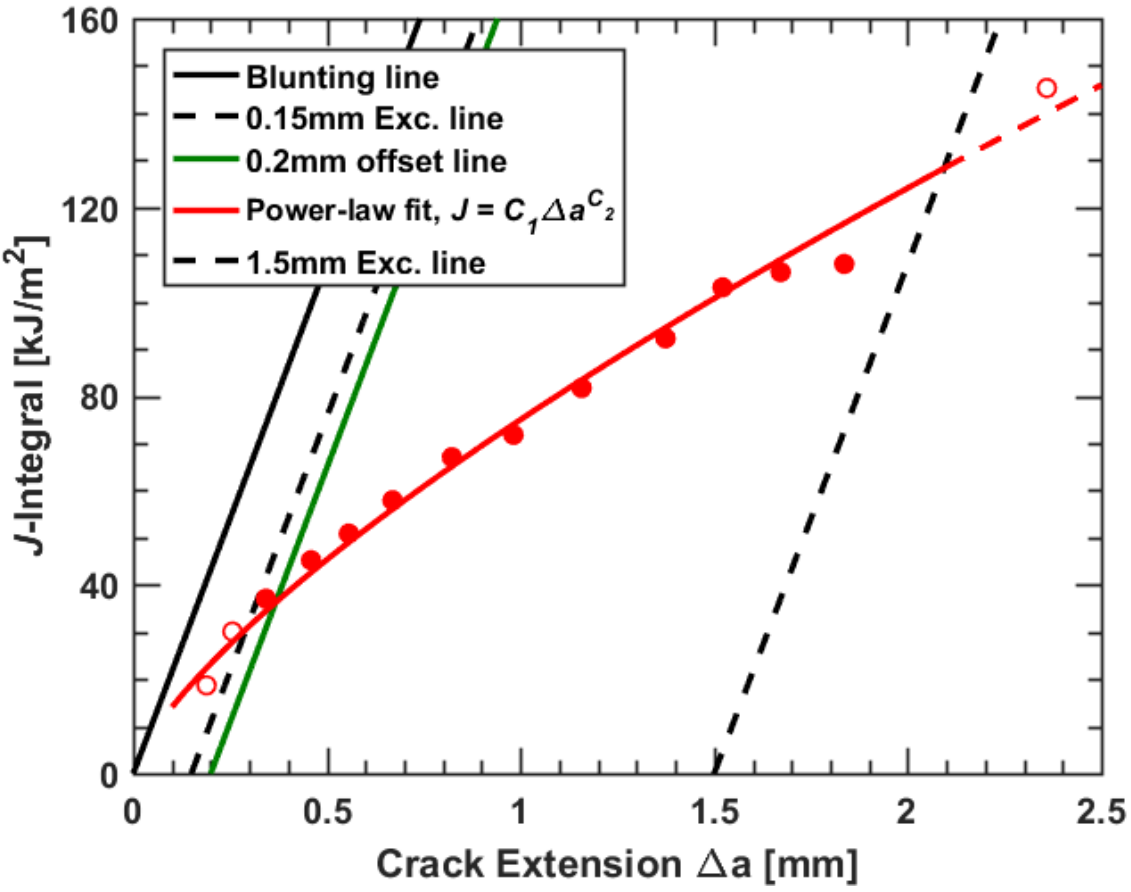

Figure 3. 1 – Exemplar $J_R(\Delta a)$ crack-resistance curve based on the ASTM E1820 standard and adapted from data gathered within this study. The theoretical blunting lines and exclusion lines are depicted in the figure. Data within the 0.15 mm and 1.5 mm exclusion lines are deemed acceptable data since it meets the criteria for J-dominance. Valid data are depicted in closed circles while non-valid data as depicted as open circles. A power-law curve is fit to the valid data. The point where the 0.2 mm offset line intersects the J_R is considered to be J_Q and can be deemed J_{Ic} so long as size requirements are met.

The challenge in polymers is the difficulty in observation and existence of a stretch zone that shows the extent of crack extension due to blunting that is a result of crazing and/or crack tip stretching (Chan and Williams, 1983; Huang and Williams, 1990; Narisawa, 1987; Pascaud et al., 1997a). As a result, there is currently no accepted definition of J_{Ic} for polymers[1], whereas a 0.2 mm offset line parallel to the blunting line and its intersection with a power-law J_R curve is used

[1] Polymers have historically adopted the use of a blunting line to define initiation toughness but due to the inherited complexities in polymer fracture, ASTM has stayed away from implementing an initiation toughness method for these materials.

to define J_{Ic} in metals (ASTM E1820). J_{Ic} measurements for metals by this ASTM method are a practical definition of initiation toughness since, akin to polymers, there are complexities in identifying the actual point of crack initiation (Huang and Williams, 1990), yet this technique is deemed to produce reliable and repeatable results (Heerens et al., 1988; Schwalbe and Heerens, 1985). However, in contrast, the methodology for determining a practical definition of initiation toughness within the polymer community is still under debate stemming primarily from the complexity of polymeric constitutive behavior.

The blunting line approach to determine crack initiation in polymers can lead to severe overestimates due to the fact that *engineering* stress-strain constitutive properties have been historically used in polymer fracture mechanics (Chan and Williams, 1983; Hashemi and Williams, 1991, 1986a, 1986b; Huang and Williams, 1987; Narisawa, 1987; Narisawa and Takemori, 1989; Pascaud et al., 1997a, 1997b; Rimnac et al., 1988; Varadarajan and Rimnac, 2008). The flow stress used in J_{Ic} testing per ASTM E1820 makes use of an engineering definition of yield (σ_Y) and ultimate tensile (σ_U) stresses and accordingly the flow stress, $\sigma_{flow} = ½ (\sigma_Y + \sigma_U)$. This has been well suited for many high strength, low strain-hardening metals as differences between true and engineering stress-strain properties are minor (**Figure 3.2A**) (Heerens et al., 1988; Landes, 1995; Landes and Begley, 1974; Mills, 1981; Schwalbe and Heerens, 1985). This approach can cause problems in polymers capable of extensive plastic deformation, or low-strength high strain-hardening behavior, as it can result in a severe underestimate of the flow stress and an overly shallow blunting line that intersects the J_R curve at larger crack extensions not representative of the *J*-integral values close to the onset of crack initiation (Chan and Williams, 1983; Hashemi and Williams, 1991, 1986a, 1986b; Huang and Williams, 1987; Narisawa, 1987; Narisawa and Takemori, 1989; Pascaud et al., 1997a, 1997b; Rimnac et al., 1988; Varadarajan and Rimnac, 2008).

The marked differences in engineering versus true constitutive behavior for a polymer such as UHMWPE can be seen in **Figure 3.2B** where true ultimate stress is nearly four times larger than engineering ultimate stress. This difference in material properties has significant importance in defining the flow properties of a polymer material for use in a *J*-based fracture toughness assessment and, as such, the current use of such engineering stress-strain properties is clearly distorts the measurement of the crack-initiation in these materials. Despite this, to our knowledge, no study has as yet employed the true stress form of σ_{flow} when measuring the J_{Ic} fracture toughness of UHMWPE or similar polymers. Owing to its widespread use in TJR, UHMWPE serves as an ideal polymer to explore these questions as the extensive literature offers a framework for both constitutive and fracture properties (Ansari et al., 2016; Bellare et al., 2016; Gomoll et al., 2002; Steven M. Kurtz et al., 2006; Kurtz et al., 2002, 1998, Pascaud et al., 1997a, 1997b; Rimnac et al., 1988; Sobieraj et al., 2008, 2005; Varadarajan and Rimnac, 2008).

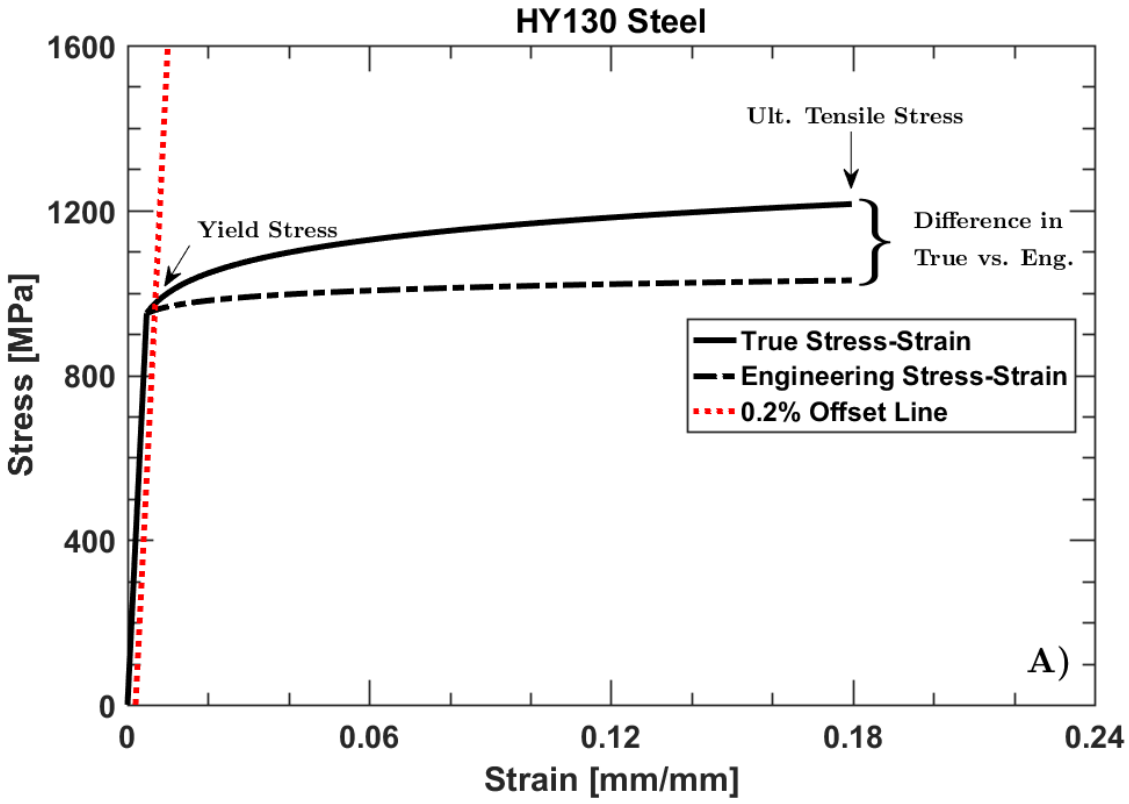
HY130 Steel
Ult. Tensile Stress
Yield Stress
Difference in
True vs. Eng.
True Stress-Strain
Engineering Stress-Strain
0.2% Offset Line
A)
Stress [MPa]
Strain [mm/mm]
1600
1200
800
400
0
0
0.06
0.12
0.18
0.24

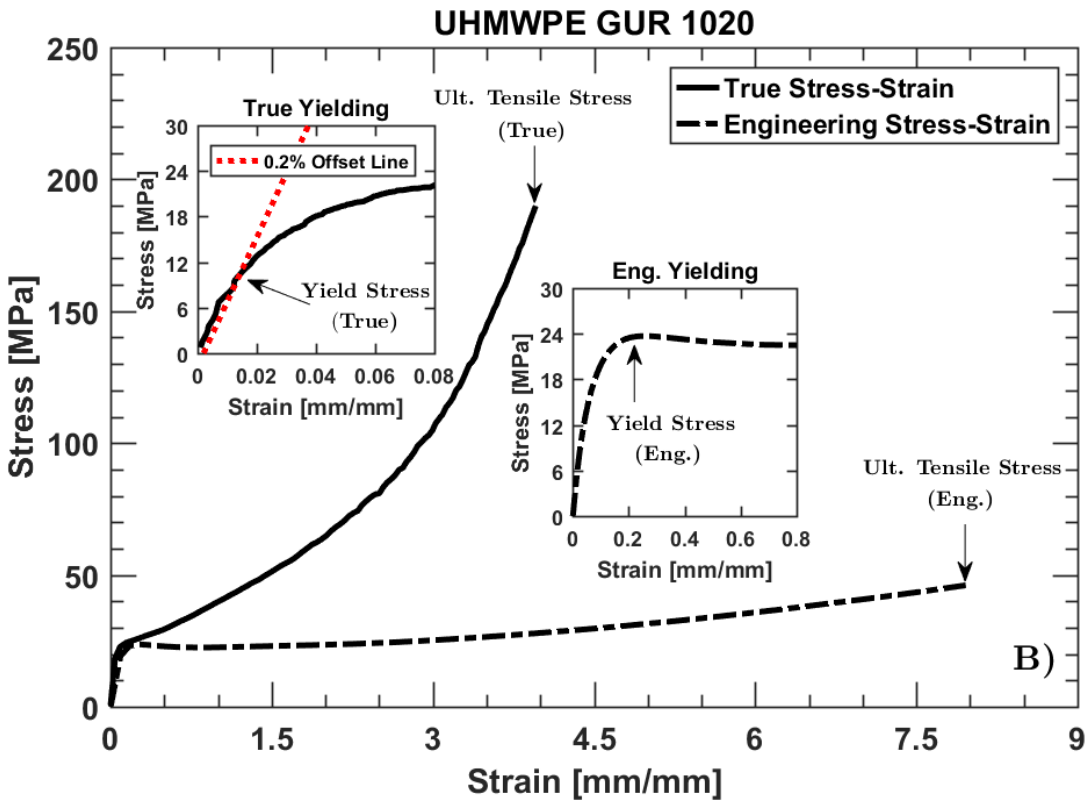
UHMWPE GUR 1020
True Stress-Strain
Engineering Stress-Strain
Ult. Tensile Stress
(True)
True Yielding
0.2% Offset Line
Yield Stress
(True)
Eng. Yielding
Yield Stress
(Eng.)
Ult. Tensile Stress
(Eng.)
B)
Stress [MPa]
Strain [mm/mm]
250
200
150
100
50
0
0
1.5
3
4.5
6
7.5
9

Figure 3. 2 – Engineering versus true stress-strain curves for typical metals and semi-crystalline polymers. **(A)** A comparison of both engineering and true stress-strain data of HY130 steel adapted from Clarke et al., 1980 (Clarke et al., 1980). The plot highlights the minimal differences between engineering and true properties for a high strength low-strain hardening material that the initial *J*-integral testing standards for metals were based on. **(B)** The same comparison for UHMWPE adapted from the data supplied for this study. The inserts are zoomed in portions of the true and engineering stress-strain curves at the beginning of deformations and up until yielding. The inserts demonstrate the differences in determining yield stress in true versus engineering stress-strain for a semi-crystalline polymer. The local maximum on the engineering stress-strain curve is classically determined as the yield stress in a semi-crystalline polymer. Note the absence of a local maximum in the true stress-strain curve compared to the engineering stress strain and the use of a 0.2% offset line to determine yield. Finally note the large differences, nearly a factor of four, in true versus engineering ultimate stress.

The purpose of this study is to evaluate the fracture toughness behavior of clinically relevant UHMWPE formulations to serve as a basis for developing a consistent and appropriate test methodology for determining the fracture toughness behavior of structural polymers. Moreover, fracture of UHMWPE poses a relevant clinical concern in implant designs with stress risers such as locking mechanisms and notches or where impingement overloads the polymer component Furmanski et al., 2009; Ansari et al., 2016). We evaluate the fracture toughness behavior of UHMWPE using the procedures outlined in ASTM E1820, ASTM D6068, as well as the earlier work of Paris et al. (1979); yet we employ the constitutive behavior evaluated in terms of true stresses and strains. Moreover, we seek to address a structure-property correlation in UHMWPE across these polymer resins. Specifically, our study assesses whether our methodology yields the same decrease in fracture toughness concomitant with increased cross-linking that is known to occur with fatigue fracture resistance of UHMWPE (Ansari et al., 2016; Sara A Atwood et al., 2011; Baker et al., 2003b; Gencur et al., 2006; Simis et al., 2006).

3.2 Background

J-integral fracture testing of polymers is an adaptation of the original multi-specimen *J*-integral resistance curve procedure developed by Landes and Begley for use on metals (Landes and Begley, 1974). There have been some procedural changes over the years; however, at its core the testing method for polymers remains the same. The multi-specimen procedure requires several identical test specimens to be loaded to varying displacements to elicit different corresponding amounts of crack growth. The specimens are then unloaded and broken to expose the fracture surface for crack growth measurement. Chan and Williams were the first to successfully apply this procedure to polymers; it was finally adapted to ASTM Standard D6068 with some small variations to the original Landes and Begley method (Chan and Williams, 1983; Landes and Begley, 1974).

Ultimately the metals community moved away from the multi-specimen procedure in favor of using a single-specimen to generate a J_R curve measuring crack growth through elastic (unloading) compliance. In the single-specimen procedure, a sample is loaded and then partially unloaded, repeating these steps several times to generate a J_R curve. Crack extension is determined from the unloading steps by measuring elastic compliance which is related to normalized crack length, a/W. However, normalized elastic compliance cannot be readily applied to polymers owing to their viscoelastic nature.

The single-specimen procedure is challenging for polymers as the normalized elastic compliance equations are specific for each polymer and its associated displacement rates. Another technical challenge is that many polymers demonstrate hysteresis in their unloading curves and it is difficult to pinpoint the range of the elastic region upon unloading to determine elastic compliance. (Chung and Williams, 1991; Hashemi and Williams, 1991). For these reasons, the polymer fracture community primarily uses the multi-specimen approach due to the complexities of applying the single-specimen procedure to these materials. The multi-specimen procedure offers a more conservative approach to creating a J_R curve since each data point comes from a separate specimen and crack extension is physically measured on the fracture surface.

For the multi-specimen procedure, J is calculated according to the following equation:

$$J = \frac{\eta U}{B b_0} \quad (20),$$

where U is the energy required to extend the crack, or the total area under the load versus load-line displacement curve, b_0 is the initial uncracked ligament, and η is known as the eta-factor which depends on specimen geometry. This J-integral solution was first developed by Rice and colleagues for deeply cracked bend specimens and was the basis for the multi-specimens J_R curve procedure introduced by Landes and Begley (Landes and Begley, 1974; Rice et al., 1973). Equation 1 is the fundamental J solution used in polymer fracture within ASTM D6068. The equation is utilized when plastic displacement outweighs elastic contributions and as a result can be directly used on the raw load versus load-line displacement data. An eta-factor of $\eta = 2$ was found to be sufficient for the original bend specimens and for C(T) specimens was later found to be given by $\eta = 2 + 0.522(b_0/W)$ (Clarke and Landes, 1979). To create the J_R curve, J is calculated at different load versus load-line displacements and married to the corresponding amount of crack growth measured on the fracture surface of the specimen. After the construction of a J_R curve, the data must fall within a validity window to satisfy the Hutchinson-Rice-Rosengren (HRR) field verifying that J-dominance is maintained. Currently there are discrepancies between the two J-integral standards of metals and polymers when it comes to determining a region of valid J data on the J_R curve.

ASTM E1820 requires 0.15 mm and 1.5 mm exclusion lines in order to determine the window of valid J-integral to crack growth data for analysis (Figure 1) and sets a hard limit for crack growth to $0.25b_0$. ASTM D6068 currently does not provide an exclusion window apart from setting a minimum of subcritical crack growth at 0.05 mm and a maximum at $0.1b_0$. The maximum crack growth limits for J-integral were originally set according to experimental evidence by Shih which showed J was accurately predicted when crack extension was limited to $0.06b_0$ (Clarke et al., 1979; Huang, 1991; Huang and others, 1996; Huang and Williams, 1990; Shih et al., 1978). This limit was further justified by Hutchinson and Paris through the non-dimensional parameter, ω, was required to be much greater than 1:

$$\omega = \frac{b_0}{J} \cdot \frac{dJ}{da} \gg 1, \quad (21)$$

where dJ/da is the slope of the J-integral versus crack growth (Δa) curve (Hutchinson and Paris, 1979). Hutchinson and Paris essentially validated Shih's data using Equation 2 (Hutchinson and Paris, 1979; Shih et al., 1978). As a result, Shih's work became the basis for the 1.5 mm exclusion line. Clarke and colleagues performed a multi-facility round robin study to create the first standardized J_{Ic} standardized testing procedure using HY130 steel specimens with an approximate B of 25.4mm (1 in). Using this as a model along with a starting $a/W = 0.5$ and applying Shih's criteria of limiting crack growth to $0.06b_0$, the 1.5 mm (0.06 in) exclusion line was created. The 0.15 mm (0.006 in) exclusion line was then produced as a corollary to the 1.5 mm exclusion line. The point of eliminating crack growth below $0.006b_0$ was to exclude points where it is difficult to distinguish between crack extension due to blunting and actual crack growth (Clarke et al., 1980).

The 0.15 mm and 1.5 mm exclusion lines have existed since despite the fact they were based on one particular specimen's dimensions and do not adapt to changes in size.

As it was thought that limiting crack growth to $0.06b_0$ might be too stringent. Gordon and Jones conducted *J*-integral testing of a titanium alloy to explore these specimen size effects and found that crack extensions up to $0.1b_0$ still exhibited size-independence (Gordon and Jones, 1989). Accordingly, ASTM then adopted a maximum crack growth limit of $0.1b_0$ for both metals and polymers. Later ASTM E1820 relaxed the maximum crack growth limit to $0.25b_0$ for metals, while ASTM D6068 retained a maximum growth limit of $0.1b_0$ for polymers. Wallin analyzed the growth limit of $0.25b_0$ in metals from a range of *J*-based toughness data in high and low toughness steels to calculate ω and found that the maximum crack growth limit of $0.25b_0$ was acceptable (Wallin, 2009). However, corresponding increases to the crack growth limit have yet to be justified or accepted for polymers and requires some examination. The question then becomes what is the appropriate lower limit for crack growth in polymers?

The 0.05 mm lower crack growth limit in ASTM D6068 was created from a single study from Narisawa and Takemori (Narisawa and Takemori, 1989). Huang and Williams have raised several issues in regards to their study including recommending using a lower exclusion line based on $0.006b_0$ instead of a 0.05 mm lower limit that would not accommodate changes in specimen size. (Huang and Williams, 1990). From the work of Shih and Clarke, a lower growth limit of $0.006b_0$ should be used for both polymers and metals since that limit accommodates changes in specimen dimensions (Clarke et al., 1980; Shih et al., 1978). Now that it is understood how a J_R curve can be produced and the region of valid data identified, what is the proper way to determine initiation toughness in a material?

Currently both ASTM E1820 and D6068 construct a power law through the valid data points according to the equation:

$$J = C_1 \Delta a^{C_2}, \tag{22}$$

where C_1 and C_2 are the power-law fit constants. A 0.2 mm offset blunting line is then constructed to determine size-dependent fracture toughness values, J_Q from the intersection of the 0.2 mm offset blunting line and the power-law J_R curve. The 0.2-mm offset blunting line is given by the following equation:

$$J = 2\sigma_{\text{flow}}(\Delta a - 0.2mm). \tag{23}$$

The 0.2 mm offset blunting line was implemented to be close enough to actual initiation to produce size- and geometry-independent values while increasing reproducibility and reliability in measurement (Heerens et al., 1988; Schwalbe and Heerens, 1985). It is a well-defined approximation of the crack-initiation toughness, and has been the gold standard ever since. However, only ASTM E1820 currently uses this 0.2 mm offset blunting line to determine initiation toughness in metals.

The 0.2 mm offset blunting line has been used to analyze initiation toughness in several polymers but has not been widely adopted for a number of reasons (Chung and Williams, 1991;

Hashemi and Williams, 1991; Pascaud et al., 1997a, 1997b; Rimnac et al., 1988; Varadarajan and Rimnac, 2008). First, the blunting and crack growth processes in polymer fracture are not the same as in metals. For example, some polymers undergo crazing ahead of the crack tip or undergo viscoelastic crack tip stretching (Chung and Williams, 1991). Chung and Williams argued that as a result of these two processes the blunting line in polymers is difficult to ultimately establish and warrants further investigation if such a line is to be used to define initiation toughness (Chung and Williams, 1991). The difficulties in the establishment of a proper blunting line is not a unique phenomenon to polymers; it has been present in the metals community as well.

J-integral fracture methods were originally established using high strength low-strain hardening metals and engineering flow properties. For example the round robin study that established the first *J*-integral testing standard used HY130 steel (Clarke et al., 1980). **Figure 2a** illustrates the plastic flow properties of HY130 steel and it is clear there is little difference between true flow and engineering properties. Using the engineering definition of σ_u, which is customary, rather than a more accurate true stress definition, would make little difference to the calculated flow stress, σ_{flow}, and therefore would have very little effect on the determination of initiation toughness. When *J*-based fracture toughness measurements are applied to low-strength, high-strain hardening metals, true versus engineering flow properties matter. Several authors have found that using engineering flow properties in these metals overestimate J_{Ic} and have tried to incorporate true stress-strain properties in the use of a blunting line to solve this problem (Heerens et al., 1988; Landes, 1995; Mills, 1981; Schwalbe and Heerens, 1985). Ultimately this idea was never incorporated into the *J*-based fracture toughness standard for metals. However, although the problem is far more acute for metals, the effect of utilizing true stress-strain flow properties in the procedures for measuring the *J*-based crack-initiation toughness in polymers has yet to be explored.

To circumvent the complicated deformation process and use of a blunting line, the polymer community has suggested creating a definition for crack-initiation toughness as the *J* value at 0.2 mm of crack growth from the power law curve fit:

$$J_{0.2} = C_1(0.2mm)^{C_2}, \tag{24}$$

(Hale, 1990; Huang, 1996). Also, the community has suggested using the Tearing Modulus, *T*, given by:

$$T = \frac{dJ}{d\Delta a}\frac{E}{\sigma_{flow}^2}, \tag{25}$$

where $\frac{dJ}{d\Delta a}$ is the linear slope of the J_R curve, and *E* is the Young's modulus, as an easier and more accurate description of polymer fracture behavior (Narisawa, 1987; Paris et al., 1979). These suggestions have also not been adopted by the *J*-based fracture toughness testing standard for polymers. The current standard, ASTM D6068, simply requires that one report the power law fit constants as the only properties of the $J_R(\Delta a)$ curve since it is believed the only way to compare fracture behavior of different polymers is through direct comparisons of $J_R(\Delta a)$ curves (Huang, 1996). Overall the polymer fracture community needs a thorough experimental assessment of

historical methods against using proper true stress-strain constitutive behavior in order to finally establish a proper procedure for determining the fracture properties of these materials. This is the basis of the current work and provides our rationale for seeking an accurate and reproducible means for determining the crack-initiation fracture toughness of polymers.

3.3 Methods

3.3.1 Materials

Ten clinically relevant UHMWPE formulations were investigated (**Table 3.1**). UHMWPE was sourced from three different consolidators: Orthoplastics (Lancashire, UK), DePuy (Warsaw, IN), and Quadrant EPP (Fort Wayne, IN). Variations to two base resins, GUR 1020 and GUR 1050, were investigated across a range of cross-link density and antioxidant chemistry. The antioxidants were comprised of 0.1 wt.% Vitamin E (VE) and COVERNOX™ (AO) (medical grade version of Irganox™ 1010) which were blended into GUR 1020 resin before consolidation. Lastly, irradiation cross-linking dosages at 75 kGy in base resin materials were re-melted (RM) to alleviate free radicals and served as cross-linked samples without antioxidants. Four distinct material categories (Table 1) were explored: 1020 resin (0 kGy, 75 kGy RM); 1020 resin with AO antioxidant (AO 80 kGy); 1020 resin with 0.1 wt.% vitamin E (VE 0 kGy, VE 50 kGy, VE 75 kGy, VE 100 kGy, VE 125 kGy); and 1050 resin (0 kGy, 75 kGy RM). All UHMWPE materials were compression molded except for GUR 1050 75kGy RM which was ram extruded.

Table 3. 1 – UHMWPE material formulations and consolidators. Darker colors at the top of the table denote base formulations in that group. The following lighter colors denote irradiation cross-link treatments to that material formulation group.

UHMWPE Material Formulation and Manufacturer			
GUR 1020 (Orthoplastics)	GUR 1020 AO 80kGy (Depuy)	GUR 1020 VE (Orthoplastics)	GUR 1050 (Orthoplastics)
GUR 1020 75kGy RM (Orthoplastics)		GUR 1020 VE 50 kGy (Orthoplastics)	GUR 1050 75kGy RM (Quadrant)
		GUR 1020 VE 75kGy (Orthoplastics)	
		GUR 1020 VE 100 kGy (Orthoplastics)	
		GUR 1020 VE 125kGy (Orthoplastics)	

3.3.2. Mechanical test methods

3.3.2.1. Tensile constitutive behavior

The Young's modulus, Poisson's ratio, yield stress, yield strain, ultimate tensile stress, ultimate tensile strain, and energetic toughness were determined in accordance with ASTM Standard D638; values were calculated, however, in terms of both engineering and true stresses and strains. Type IV tensile bar specimens, measuring ~3.2 mm in thickness and ~6 mm in width, were computer numerical control (CNC) machined with 10 specimens per UHMWPE material group, 5 specimens for uniaxial tensile testing and 5 specimens for Poisson's ratio testing. Gauge lengths of 26 and 5 mm were used to measure axial and transverse strains, respectively. All specimens were conditioned at 25°C with 50% relative humidity in a Caron 6010 environmental chamber (Marietta, OH) for at least 40 h prior to testing. Tension testing was performed on a Shimadzu AGS-X electromechanical load frame (Kyoto, Japan) with a 1 kN load cell at a displacement rate of 50 mm/min with test temperature maintained at 23 ± 2°C. Poisson's ratio testing was performed using an MTS Mini-Bionix II load frame (Eden Prairie, MN) using a 5 kN load cell.

Material deformation for tensile testing and Poisson's ratio testing was measured by a non-contact dual video extensometer (based on a Point Grey FL3-U3-88S2C-C camera) setup capable of meeting the outlined demands to track true material deformation. Custom developed software tracked optical targets marked on the sample to measure true axial strain, true transverse strain, and instantaneous cross-sectional area at the gauge length through the deformation process. The video extensometer was calibrated before use to an Edmund Optics 0.5-mm pitch optical calibration grid, correcting for perspective and non-linear distortion. In addition, crosshead displacement was also tracked during testing to record engineering tensile properties. All data were analyzed using a custom MATLAB script (Natick, MA).

Young's modulus was determined by a linear least-squares regression from 0.0005 strain to 0.009 strain on the true stress-strain curve. Machine stiffness was accounted for during test setup. Dynamic mechanical analysis (DMA) is perhaps a better way to calculate elastic modulus in polymers; however, it was felt that determining elastic modulus from tensile stress-strain was better suited for our study since tensile data would be coupled with tensile fracture data for analysis. The true yield stress (σ_Y (true)) was calculated from the intersection of a 0.2% strain offset line from the elastic region of the true stress-strain curve (Kurtz et al., 2002, 1998, 2006). True energetic toughness was calculated as the area under the true stress-strain curve and the true ultimate tensile stress (σ_U (true)) was determined from the maximum load divided by the instantaneous cross-sectional area of the test specimen at that point (**Figure 3.2B**) determined using three-dimensional digital image correlation. Engineering yield stress (σ_Y (eng)) was taken as the local maximum on the engineering stress-strain curve, while engineering ultimate tensile stress (σ_U (eng)) was taken as the maximum point on the engineering stress-strain curve, or the maximum load divided by initial cross-sectional area (**Figure 3.2B**). The Poisson's ratio was determined based on measured true axial and transverse strain, as defined by ASTM D638 Appendix A3:

$$\nu = \frac{\frac{d\varepsilon_t}{dP}}{\frac{d\varepsilon_a}{dP}} \ , \tag{26}$$

where $d\varepsilon_t$ is the absolute change in transverse strain, $d\varepsilon_a$ is the absolute change in axial strain, and dP is the change in the applied load. The slopes of $d\varepsilon_t/dP$ and $d\varepsilon_a/dP$ were found from a linear regression of the data from 0.0005 true axial strain to yield strain determined from a 0.002 strain offset using a custom MATLAB script. A more detailed discussion of this analysis can be found in **Chapter 2**.

3.3.2.2. Fracture toughness testing

Fracture toughness testing was conducted to determine the crack-initiation toughness and stable tearing fracture properties using the nonlinear-elastic fracture-mechanics *J*-integral approach outlined in ASTM Standards D6068 and E1820. Compact-tension C(T) specimens were CNC machined from stock material to a width *W* of 31.8 mm and thickness *B* of 15.9 mm, according to the specifications outlined in ASTM D6068. C(T) specimens designated in ASTM E1820 require input from a clip gauge to measure crack length during testing through elastic unloading compliance. Since ASTM D6068 is a multi-specimen fracture procedure, there was no need to machine specimens for use with a clip-gauge. Specimens were initially machined notched to a crack length to an $a/W \sim 0.5$, and then pre-cracked with pristine razor blades to an a/W between 0.50 to 0.65, as outlined in ASTM D6068. Razor micro-notching was performed due to the extreme difficulty in generating a sharp crack via fatigue loading in UHMWPE and other tough polymers (Sara A Atwood et al., 2011; Hale, 1990). Producing a razor pre-crack has been shown to produce more conservative initiation toughness values (Hale, 1990). Testing for the construction of multi-specimen polymeric J_R curves was conducted on an MTS 831 load frame (Eden Prairie, MN) outfitted with an Instron 8800 Fastrack controller (Norwood, MA).

For each *J*-based *R*-curve, a minimum of 8 identical C(T) specimens was used to generate individual points on the curve, with more specimens being used when available from stock material. Specimens were loaded at a displacement rate of 1 mm/min to different displacements to elicit corresponding amounts of crack growth and then immediately freeze fractured in liquid nitrogen to expose the fracture surface for crack-growth measurement. Crack extension, Δa, was measured on an Olympus microscope stage (Tokyo, Japan) according to the five-point average method outlined in ASTM D6068. *J* was then calculated according to Eq. 1. The lower limit for crack extension, where data can be considered, was restricted to $0.006b_0$ or ~0.1mm based on our b_0 values. The corresponding upper limit for crack extension, however, was not limited to the suggested $0.1b_0$ in an effort to explore higher crack growth limits in polymers. The upper limits of crack extension were tested for *J*-dominance by modifying Eq. 2 for use with a power-law fit to give:

$$\omega = \frac{b_0 C_2}{\Delta a}, \tag{27}$$

(Wallin, 2009). A 0.2 mm offset blunting line (Eq. 3) was constructed to determine size-dependent fracture toughness values, J_Q.

The 0.2 mm offset blunting line was constructed in two ways. One was constructed using a σ_{flow} that was the average of σ_Y (True) and σ_U (True). The other way was using a σ_{flow} that was the σ_U (Eng.) that has been used previously with *J*-based toughness measurements on UHMWPE (Pascaud et al., 1997a, 1997b; Rimnac et al., 1988; Varadarajan and Rimnac, 2008). Qualification for size-independent fracture toughness values, J_{Ic}, was determined by satisfying the conditions for crack-tip *J*-dominance and for plane-strain conditions, as per ASTM Standard E1820:

$$B, b_0 \geq \alpha \frac{J_Q}{\sigma_{\text{flow}}}. \tag{28}$$

This produced two sets of comparative results, J_Q/J_{Ic} using engineering σ_{flow} properties, J_Q/J_{Ic}(eng.), and J_Q/J_{Ic} using the true σ_{flow} properties, J_Q/J_{Ic}(True).

Under ASTM E1820, $\alpha = 10$; however, originally Landes and Begley proposed that $\alpha=25$ to meet size-independent toughness requirements (Landes and Begley, 1974). For our study a more conservative $\alpha = 25$ was used to determine if specimen dimensions met the criteria for a valid J_{Ic}. Size-independence has not been thoroughly studied for *J*-based toughness measurements for the fracture of polymers. It is unknown at this point if $\alpha = 25$ is too conservative or not conservative enough in determining size independence in these materials. As it stands, further testing for size independence should be performed but for the purposes of this study we chose to use the more historical conservative estimate of $\alpha = 25$. The *J*-integral value at 0.2 mm crack extension ($J_{0.2}$), using Eq. 6**,** was also tabulated as a third comparison result against J_Q/J_{Ic}(Eng.) and J_Q/J_{Ic}(True).

Once J_{Ic}(Eng.) or J_{Ic}(True) was determined, the plane-strain mode I fracture toughness was back-calculated from the J_{Ic} values using the standard mode I *J*-*K* equivalence relationship:

$$K_{\text{JIc}} = \sqrt{E J_{\text{Ic}} / (1 - \nu^2)}. \tag{29}$$

Again, we are unsure if size-independence is accurately met from Eq. 10. As a result, it is entirely possible that the K_{JIc} values from Eq. 11 could indeed be size-dependent fracture toughness, K_Q, values. We hope that through future investigation, our conservative choice of $\alpha = 25$ produces size- intendent values. Finally, the tearing modulus, *T*, was calculated according to Eq. 7 using the true σ_{flow} and $\frac{dJ}{d\Delta a}$ calculated as a linear least squares regression through the qualified data points, as outlined by Clarke (Clarke et al., 1980).

3.3.2.3. Fractography

The fracture surfaces of the C(T) specimens were examined using a JEOL scanning electron microscope (SEM) (Akishima, Tokyo) to identify the absence or presence of stretch zones in fractured samples. These samples were first sputter-coated with gold to make the fracture surfaces visible in the SEM, and were viewed from the top down to compare with previous studies which investigated stretch zone widths in structural polymers (Chan and Williams, 1983; Narisawa, 1987; Pascaud et al., 1997a, 1997b).

3.3.2.4. Statistical analysis

Determination of relationships between microstructural properties and fracture toughness properties were performed using a nonparametric Spearman rank correlation coefficient (MATLAB) (Sara A Atwood et al., 2011). Microstructural properties were taken for the material formulations from **Chapter 2**. The same statistical analysis was conducted between σ_{flow} calculated from true and engineering properties with $dJ/d\Delta a$. It is our hypothesis that cross-linking dosage should affect the tensile flow properties and the J_R curve, represented through $dJ/d\Delta a$, in the same manner, increasing cross-linking dosage will reduce tensile flow properties and resistance to fracture. If true flow properties demonstrate the same trend with the $dJ/d\Delta a$ while engineering properties do not, this reinforces our argument that using true versus engineering properties is the best way to characterize deformation and fracture in polymers.

3.4 Results

3.4.1. Tensile constitutive behavior

A summary of tensile true and engineering stress-strain constitutive properties is shown in Table 2. The σ_U (True), is 2.7 to 4.3 times higher than σ_U (Eng.) across all the UHMWPE material formulations. Radiation cross-linking decreases the true ultimate stress, strain, and energetic toughness for these materials. GUR 1020 VE has the highest ultimate stress, strain, and energetic toughness due to the antioxidant additions. Antioxidant chemistry and cross-linking also affect Poisson's ratio across the material formulations. Notable is that GUR 1050 formulations and GUR 1020 VE display Poisson's ratio values higher than 0.5. Cross-linking in the GUR 1020 VE decreases Poisson's ratio with increasing cross-linking dosage where a limit at 0.46 is reached, the established literature value for Poisson's ratio of UHMWPE (Kurtz, 2009). Further discussion on the constitutive properties of these materials can be found in **Chapter 2**.

Table 3. 2 – Summary of the true tensile properties used for facture analysis (mean ± standard deviation).

	Tensile mechanical properties							
UHMWPE material formulation	**True elastic modulus [MPa]**	**Poisson's ratio**	**True 0.2% offset yield stress [MPa]**	**True ultimate stress [MPa]**	**True ultimate strain [mm/mm]**	**True energetic toughness [MJ/mm^3]**	**Engineering yield stress [MPa]**	**Engineering ultimate stress [MPa]**
GUR 1020	799.5 ± 26.2	0.459 ± 0.015	10.8 ± 1.2	188.2 ± 17	4.0 ± 0.1	297.9 ± 24.7	23.8 ± 0.2	45.2 ± 2.7
GUR 1020 75kGy RM	655.1 ± 42.7	0.493 ± 0.034	10.7 ± 0.5	156.3 ± 20.4	3.2 ± 0.1	193.9 ± 20.9	21.7 ± 0.2	44.4 ± 4.3
GUR 1020 AO 80kGy	1076.8 ± 53.6	0.532 ± 0.013	15.3 ± 0.5	152 ± 10.8	2.9 ± 0.1	190.9 ± 14.5	26.2 ± 0.1	50.5 ± 2.4
GUR 1020 VE	921.2 ± 13.6	0.633 ± 0.042	13.5 ± 0.4	229.1 ± 9.7	4.2 ± 0.05	361.5 ± 14.7	24.5 ± 0.3	52.9 ± 1.4
GUR 1020 VE 50kGy	885.0 ± 31.5	0.499 ± 0.017	14.1 ± 1.7	167.1 ± 7.1	3.6 ± 0.1	246.1 ± 11	24.9 ± 0.1	45.1 ± 1.5
GUR 1020 VE 75kGy	1060.6 ± 37.4	0.421 ± 0.027	14.8 ± 0.3	178.9 ± 10.1	3.3 ± 0.1	241.8 ± 16.4	26.0 ± 0.1	50.7 ± 1.7
GUR 1020 VE 100kGy	1008.5 ± 36.6	0.464 ± 0.025	14.7 ± 0.7	146.4 ± 13.6	2.9 ± 0.1	183 ± 16.7	25.2 ± 0.2	44.4 ± 2.8
GUR 1020 VE 125kGy	865.4 ± 56.3	0.461 ± 0.040	14.1 ± 1.1	158.8 ± 9.7	2.9 ± 0.1	187.9 ± 13.6	25.8 ± 0.1	49.1 ± 1.7
GUR 1050	810.6 ± 26.2	0.540 ± 0.076	13.2 ± 0.7	202.8 ± 29.9	3.7 ± 0.3	311.1 ± 50.4	22.9 ± 0.2	50.5 ± 5.7
GUR 1050 75kGy RM	762.3 ± 32.0	0.521 ± 0.043	11.7 ± 0.4	127.9 ± 12.8	2.4 ± 0.1	137.4 ± 16	24.2 ± 0.2	45.7 ± 3.0

3.4.2. Fracture toughness results

Table 3.3 shows a summary of the fracture toughness values determined using the multi-specimen approach from $J_R(\Delta a)$ curves for all UHMWPE material formulations. **Figures 3.3-3.4** show the vast differences in blunting lines using true or engineering flow properties, respectively. Experimental J_Q values calculated from true and engineering σ_{flow} properties differed by 17.6% to 72.8%.

Table 3. 3 – Summary of fracture toughness properties.

	***J*-Integral fracture property**								
UHMWPE material formulation	**C_1**	**C_2**	**$J_{0.2}$ [kJ/m^2]**	**J_{Ic} (True) [kJ/m^2]**	**J_Q (Eng.) [kJ/m^2]**	**K_{JIC} (True) [MPa$\sqrt{m}$]**	**dJ/dΔa [MPa]**	**T**	**ω**
GUR 1020	77.4	0.71	24.7	40.6	87.1	6.41	52.5	4.24	4.3
GUR 1020 75kGy RM	45.5	0.65	16.0	22.2	30.4	4.38	30.2	2.84	5.3
GUR 1020 AO 80kGy	49.9	0.66	17.3	24.9	34.4	6.12	30.1	4.63	4.0
GUR 1020 VE	69.1	0.69	22.9	32.5	66.8	7.07	50.4	3.15	5.7
GUR 1020 VE 50kGy	59.1	0.67	20.1	30.1	48.7	5.85	39.2	4.10	4.9
GUR 1020 VE 75kGy	53.1	0.67	18.1	25.4	35.1	5.72	37.1	4.19	4.9
GUR 1020 VE 100kGy	46.5	0.76	13.7	19.7	27.4	5.03	34.7	5.40	4.9
GUR 1020 VE 125kGy	42.8	0.67	14.5	19.5	25.2	4.63	30.7	3.55	4.5
GUR 1050	75.0	0.73	23.3	36.1	81.2	6.42	49.2	3.42	3.8
GUR 1050 75kGy RM	39.0	0.61	14.6	20.2	24.1	4.60	23.4	3.67	5.0

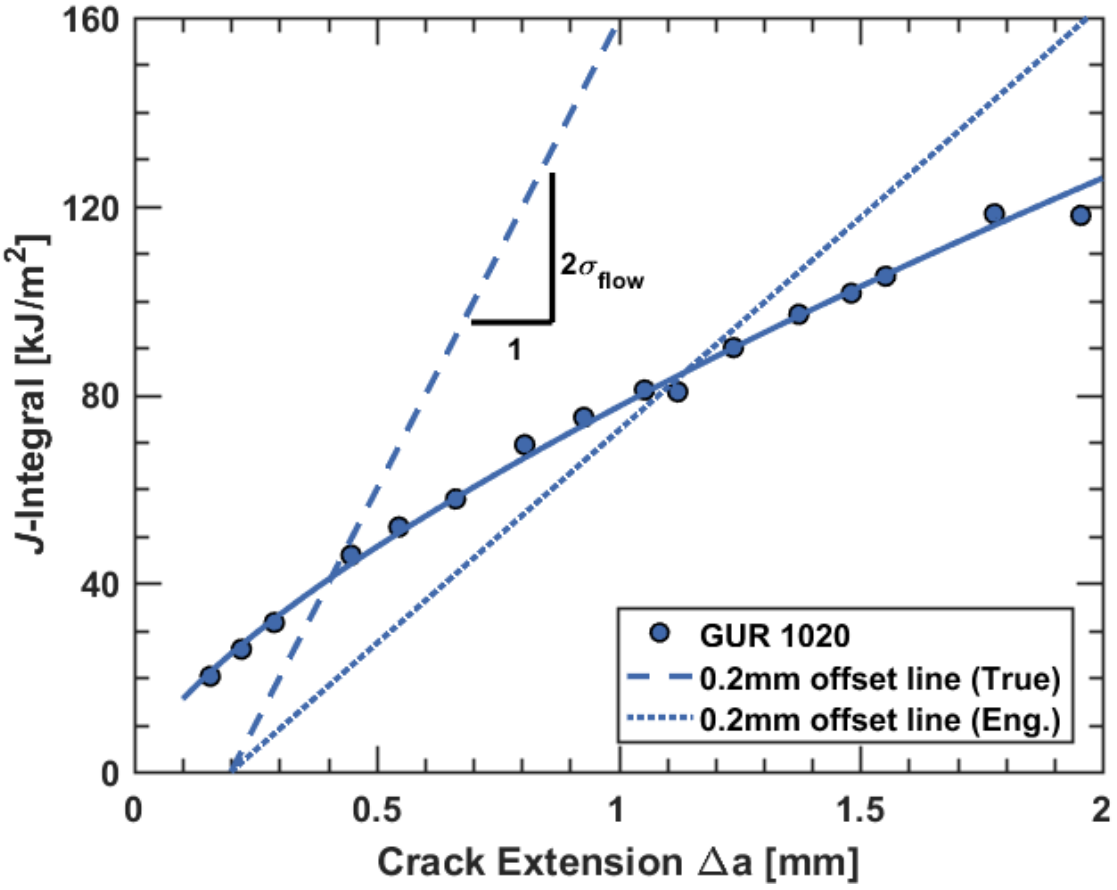

Figure 3. 3 – J_R curve of GUR 1020 with 0.2mm offset blunting lines from true and engineering flow properties. J_Q is determined at the intersection of the 0.2mm offset blunting line and the J_R curve. The two different blunting lines illustrate the extreme differences when using true versus engineering flow properties especially in tough polymers like untreated GUR 1020 UHMWPE. The J_R plot follows the color format of the different material formulations established in **Table 3.1**.

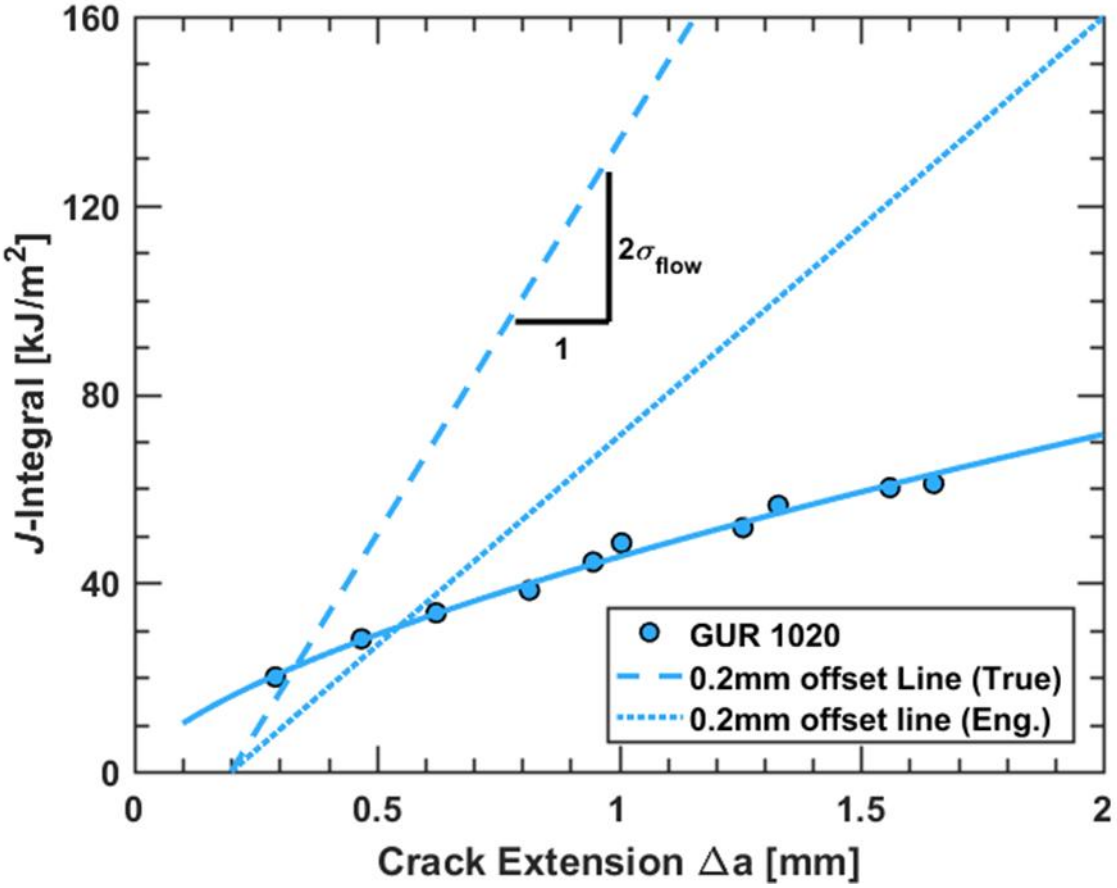

Figure 3. 4– J_R curve of GUR 1020 75kGy RM with 0.2mm offset blunting lines from true and engineering flow properties. J_Q is determined at the intersection of the 0.2mm offset blunting line and the J_R curve. The two different blunting lines illustrate the differences when using true versus engineering flow properties. The differences in blunting lines for GUR 1020 VE 125kGy are less pronounced than in **Figure 3.3** with GUR 1020 given the high cross-link dosage for this material. The J_R plot follows the color format of the different material formulations established in **Table 3.1**.

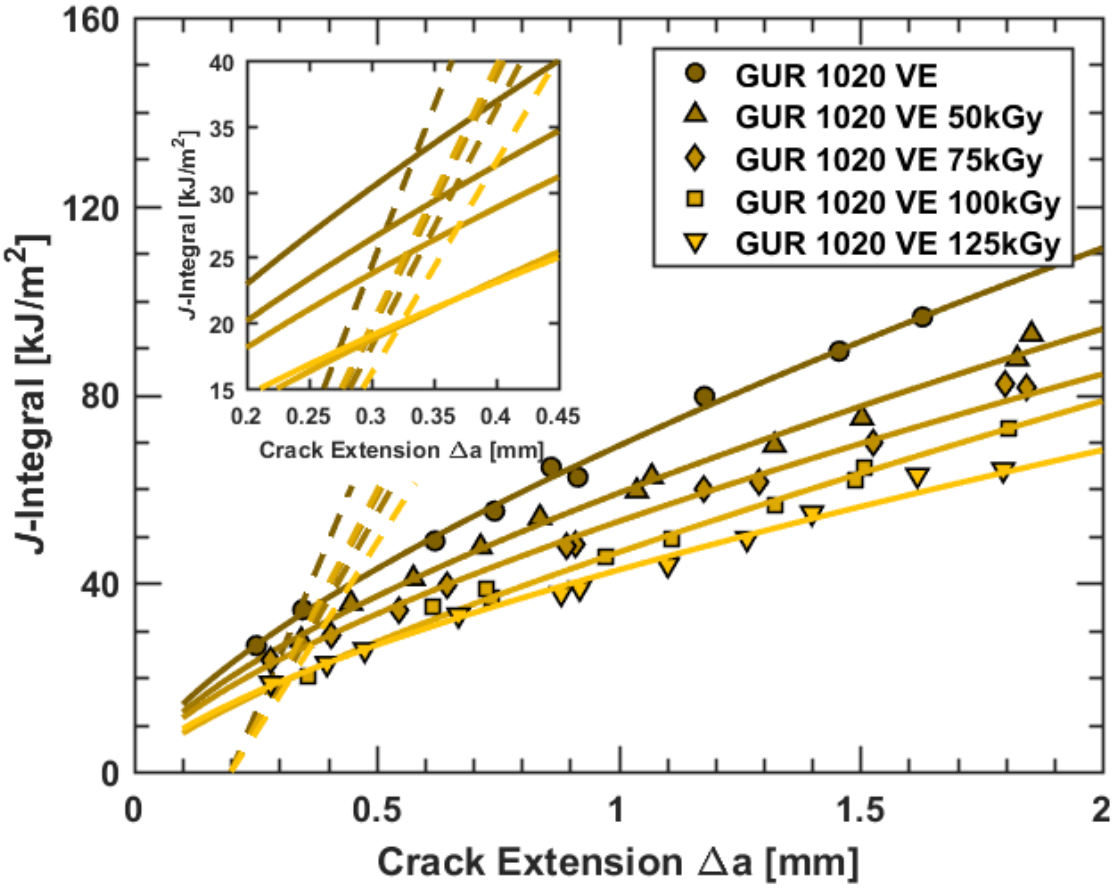

Figure 3. 5 – J_R curves with 0.2-mm offset blunting lines from true flow properties for GUR 1020 VE antioxidant UHMWPE material formulations. The insert is a close-up where the 0.2mm offset blunting lines intersect the various J_R curves. The J_R plot modifies the color format for the material formulations established in **Table 3.1** giving the different GUR 1020 VE formulations a variation in color gradient to distinguish them from one another.

The power-law fit for all J_R curves produced statistical R^2 values greater than 0.99 and the linear fit for $\frac{dJ}{d\Delta a}$ produced R^2 values greater than 0.97. The largest crack extension seen in testing was 2.2 mm with ω values ranging from 4.0-5.7. According to Wallin, an ω in excess of 2 is required for *J*-dominance for a maximum crack extension up to $0.25b_0$ (Wallin, 2009). We maintained this criterion up to $0.14b_0$ demonstrating valid crack extensions in excess of the ASTM D6068 standard which prescribes $0.1b_0$. The lowest crack-initiation toughness values were those from $J_{0.2}$ with the highest toughness values from J_Q measured using an engineering σ_{flow}.

3.4.3. Fractography

SEM images of representative UHMWPE fracture surfaces are pictured in Figure 4.6. No clearly identifiable stretch zone across the representative surface can be seen at higher magnification in Figure 4.6C. These results are in contradiction to Pascaud et al. (1997a) but are in agreement with the results of Narisawa (1987). UHMWPE is known to produce a cohesive zone ahead of the crack tip (Medel and Furmanski, 2015). It is not the same as a craze zone since there are no apparant voids that form; however, this cohesive zone could well be the explanation for why no visible stretch zones could be seen on the fracture surfaces (Medel and Furmanski, 2015). Clearly, the use of a measured stretch zone is not a practical means to assess the extent of crack-tip blunting prior to crack initiation in all polymers.

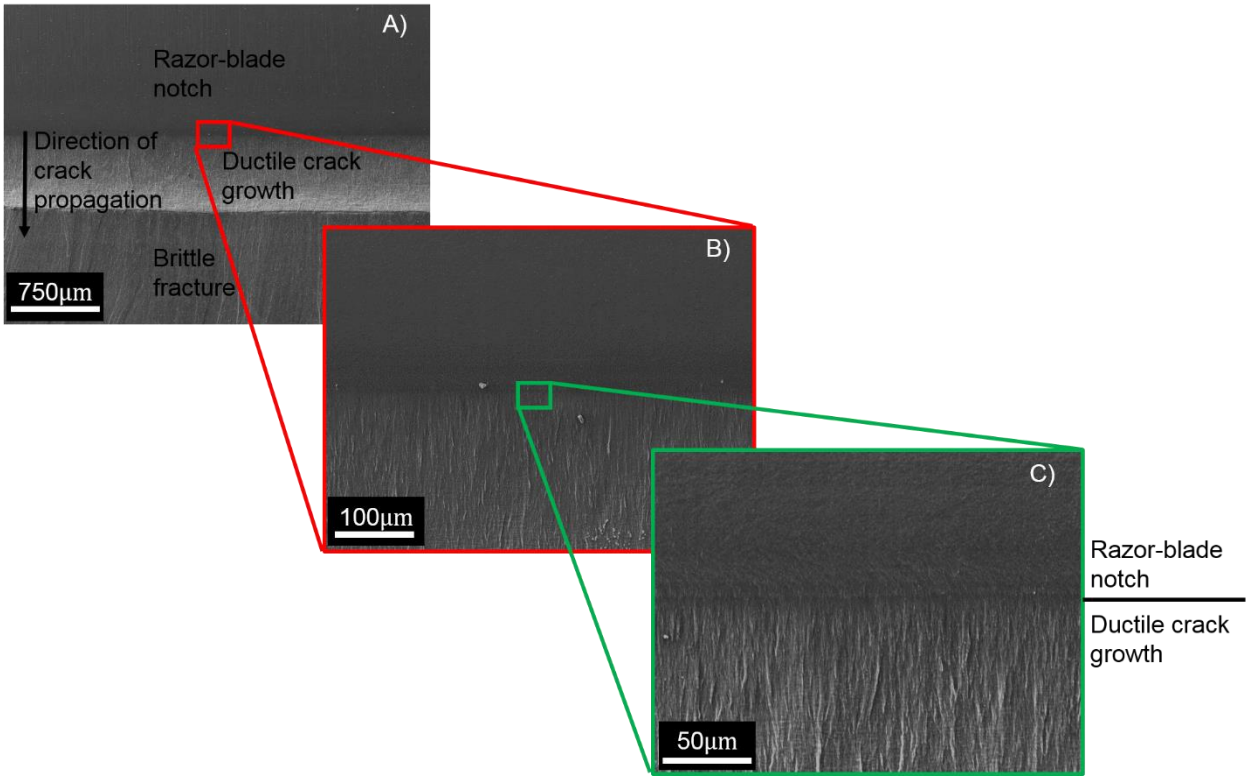

Figure 3. 6 – Fracture surface of a GUR 1020 VE 50kGy specimen. The black arrow indicates crack growth direction. (A) Fractograph with top third of image being initial razor blade notch, middle third being ductile crack growth, and the bottom third being brittle growth from freeze fracture in liquid nitrogen. (B) Fractograph showing top half of image is the razor blade notch and bottom half is ductile growth. (C) Higher magnification fractograph of the transition area between razor blade notch and ductile crack growth highlighting the absence of a SZW. The texture of ductile crack growth is a result of the cohesive zone that forms in from of the crack tip in UHMWPE, similar to a craze zone but without void formation (Kurtz, 2015).

3.4.4 Statistical Analysis Results

Fracture toughness behavior was compared for trends against microstructural parameters such as crystallinity, derived from differential scanning calorimetry (DSC), and lamellar level properties derived from small-angle x-ray scattering (SAXS) analysis. Analysis showed no statistically significant trends between any microstructural properties and fracture toughness properties. Despite this result, there were statistically significant findings between σ_{flow} properties and dJ/dΔa.

Statistical significance (p=0.001) was found between the true σ_{flow} and dJ/dΔa while no statistically significant trends were found between engineering values of σ_Y, σ_U, and dJ/dΔa. The true σ_{flow} was then plotted against dJ/dΔa in order to determine a more exact relationship between the two properties (**Figure 3.7**). This figure demonstrates a potential linear relationship between true σ_{flow} and dJ/dΔa; accordingly, a linear regression was performed producing an R^2 of 0.82, indicating that there is proportionality between the true σ_{flow} and dJ/dΔa. What this means is that cross-linking affects true flow properties and the $J_R(\Delta a)$ curve in the same expected manner. As this is simply not the case for the engineering flow properties, this adds further justification for requiring the adoption of the true stress-strain properties for the procedures to reliably measure J-based crack-initiation toughness in polymeric materials.

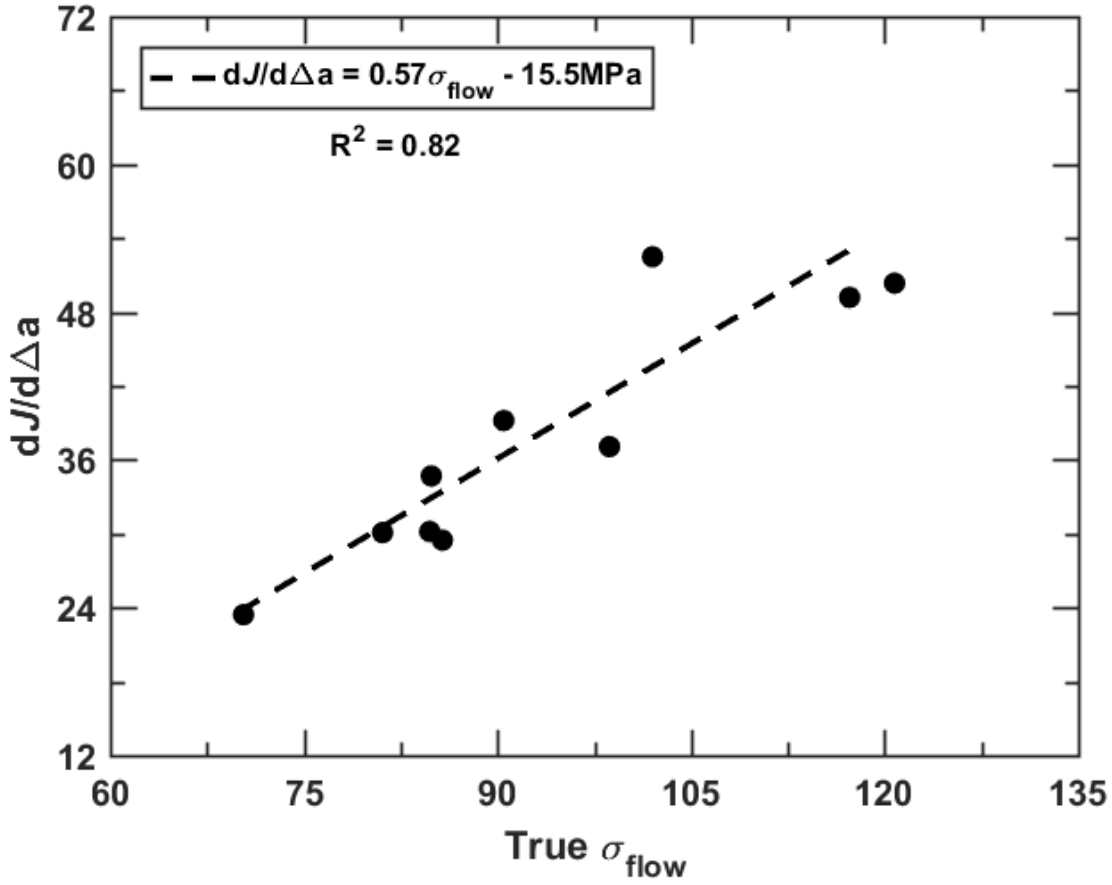

Figure 3. 7 – Linear correlation between median true flow properties and the linear slope of the J_R curve, $dJ/d\Delta a$. Flow properties derived from true tensile stress-strain constitutive properties are shown to correlated well with $dJ/d\Delta a$ providing some justification for the use of true constitutive properties in *J*-based polymer fracture analysis.

3.5 Discussion

This study successfully employs true tensile constitutive behavior to reliably define the onset of crack initiation in the determination of the *J*-based fracture toughness in a structural polymer. This work discerns itself from the traditional methodology that employs a non-conservative engineering basis of the flow stress to determine J_{Ic} fracture toughness (Chan and Williams, 1983; Hashemi and Williams, 1991, 1986a, 1986b; Huang and Williams, 1987; Narisawa, 1987; Narisawa and Takemori, 1989; Pascaud et al., 1997a, 1997b; Rimnac et al., 1988; Varadarajan and Rimnac, 2008). Our study offers a methodology that facilitates relative rankings of fracture toughness values of a well-known safety-critical medical polymer as the predictive material (Huang and others, 1996). This methodology successfully captures the decreases in fracture properties resulting from an increasing cross-linking dosage across several clinical formulations of UHMWPE; it is further consistent with the known reduction in fatigue fracture resistance following such cross-linking (Ansari et al., 2016; Sara A Atwood et al., 2011; Baker et al., 2003b; Crowninshield and Muratoglu, 2008; Gencur et al., 2006; Rimnac and Pruitt, 2008; Simis et al., 2006). Our results demonstrate that we are able to obtain a relative ranking of crack-initiation toughness values using a σ_{flow}, based on the average of σ_Y (True) and σ_U (True) while also demonstrating, through our SEM images, the complexities in identifying a true site of fracture initiation.

$J_{0.2}$ has been proposed as a measure of initiation toughness in polymers so long as it can provide a correct relative ranking or prediction of material performance (Hale, 1990; Huang, 1996). The primary concern with $J_{0.2}$ as a practical crack-initiation toughness value is that it is an arbitrary point on the J_R curve and does not take into account the material flow properties (Huang, 1996). In our study $J_{0.2}$, J_Q(Eng.) and J_{Ic}(True) produced nearly identical relative rankings between UHMWPE formulations with the exception of GUR 1020 VE 125kGy. Our hypothesis was that the material with the highest cross-link density would exhibit the lowest fracture properties. If $J_{0.2}$, J_Q(Eng.) and J_{Ic}(true) all produce correct ranking according to our hypothesis, then what should be the preferred method of measuring initiation toughness in structural polymers?

J_Q(Eng.) values appear to grossly exaggerate the crack-initiation toughness. The fundamental point to using an offset blunting line to predict J_Q/J_{Ic} is to make the measurement repeatable and reliable compared to the actual point of initiation seen through the stretch zone (Heerens et al., 1988; Schwalbe and Heerens, 1985). As a result, the intent of the 0.2 mm offset blunting line is to be as close to crack initiation as possible while still allowing for a small amount of crack growth to reduce error. Extrapolating Δa from the three highest J_Q(Eng.) values (GUR 1020, GUR 1050, and GUR 1020 VE) produced crack growths from 0.97 to 1.10 mm. However, it is not possible that the SZW would be on the order of 1 mm in these tough polymers. Fracture surfaces on specimens with crack growths below 1 mm, as pictured in Figure 4.6, demonstrate rippling and crisscrossing, which is evidence of lamellar tearing in UHMWPE, possibly due to the cohesive zone (Medel and Furmanski, 2015; Rimnac et al., 1988). Pascaud observed a stretch zone in

UHMWPE of ~300μm and noted that the 0.2 mm offset blunting line overestimates J_Q/J_{Ic} when using σ_{flow} based on the engineering σ_U (Pascaud et al., 1997a). Additionally, Varadarajan and Rimnac found that J_Q values for cross-linked UHMWPE were much smaller when measured from the crack-tip opening displacements (CTOD), as compared to a 0.2 mm offset blunting line determination from the engineering σ_{flow}. Our assessment here is that measuring J_Q/J_{Ic} for polymers according to a 0.2 mm offset blunting line based on an engineering definition of the flow stress should be avoided.

We then ask whether alternatively a $J_{0.2}$ or J_Q/J_{Ic}(True) definition of the crack-initiation toughness should be measured. In **Figure 3.5**, the J_R curves for the GUR 1020 VE 100kGy and 125kGy materials can be seen to overlap near 0.35 mm of crack extension. There are issues defining crack initiation as $J_{0.2}$ when J_R curves overlap. The arbitrary point definition can be misleading since the GUR 1020 VE 125kGy material is tougher at crack extensions less than 0.35 mm compared to the GUR VE 100kGy material while the opposite is true at crack extensions exceeding 0.35 mm. Higher cross-linking dosages should reduce fracture toughness; however, using $J_{0.2}$ at small crack extensions in this case implies otherwise. Huang suggested that the only way to compare crack growth resistance in polymers is through direct comparison of the entire J_R curve (Huang, 1996). While we agree that the data presented by the entire J_R curve itself is important, it does not mean that a practical definition of J_Q/J_{Ic} should be ignored. If anything, defining initiation toughness through an arbitrary point with $J_{0.2}$ should be avoided.

Historically speaking, the σ_{flow} has always been defined in terms of engineering stresses when used in *J*-integral testing of metals (Mills, 1981). Many tough polymers, like UHMWPE, can be categorized as low-strength high strain-hardening materials given their low yield strength and extensive ductility. The major differences come from how close the engineering properties are to the true material properties. Under tensile deformation, many semi-crystalline polymers form a stable neck that draws and strain hardens after yielding. Hence, a simple conversion between true and engineering stresses, that is typically employed in metals, is not possible in polymers. As a result, more sophisticated methods of tracking deformation are required to produce true stress-strain relationships (G'sell and Jonas, 1979). There are striking differences between engineering and true properties in semi-crystalline polymers, such as the UHMWPE materials depicted in **Figure 3.2B**. There is an absence of a local maximum on the true stress-strain curve and the ultimate stress is roughly four times higher on the true stress-strain curve, as compared to the engineering curve. This has an even larger impact on σ_{flow} than compared to low-strength high strain-hardening metals and highlights the importance of using true material properties for standard tensile behavior and fracture in such polymers. Even though a more accurate description of flow properties should be used for fracture in polymers, flow properties should approximately correlate with a stretch zone in the material since that is the truest measurement of crack initiation in materials.

Our SEM images highlight the complexity of trying to identify true initiation toughness in structural polymers. Chan and Williams demonstrated that they were able to produce nearly identical values of SZW and interpolated crack-extension at J_{Ic} in high-density polyethylene (HDPE) using σ_Y (Eng.) as σ_{flow} (Chan and Williams, 1983). Narisawa (1987) failed to see a stretch zone when testing HDPE whereas Pascaud et al. (1997a) observed a stretch zone in UHMWPE and created a correlating blunting line based on his observations. Alternatively, we did not observe

stretch zones in any of the clinical formulations of UHMWPE. It is possible that the rupture of a cohesive or craze zone in UHMWPE can remove crack extension due to crack-tip blunting. This highlights the unique complexities in polymer fracture, justifying SZW and interpolated crack extension with very different flow stresses in related polymers and the overall uncertainty in the interpretation of subcritical crack growth (Chan and Williams, 1983; Narisawa, 1987; Pascaud et al., 1997a). As a result, more work is needed to elucidate why an absence of a stretch zone might exist in polymer materials. Overall, this justifies the use of an offset blunting line in the ASTM E1820 standard to allow for some amount of crack growth to predict initiation toughness and why this can also work for polymers so long as true flow properties are used.

One way we can accurately justify our use of a blunting line that uses true σ_{flow} is if it corresponds to how the overall J_R curve behaves with cross-linking since that is our primary method of material ranking. This means that less cross-linking should produce higher crack-growth resistance, through a higher $dJ/d\Delta a$, and will have a higher σ_{flow} producing a steeper blunting line. Our study found a strong correlation with true σ_{flow} and $dJ/d\Delta a$ such that the lowest cross-linked materials produced the highest true σ_{flow} and $dJ/d\Delta a$ (Figure 7). No correlations were found with engineering σ_{flow} and $dJ/d\Delta a$. This is important for two reasons. The first is that engineering σ_{flow} does not behave in the same ranked manner as $dJ/d\Delta a$ with cross-linking. In fact, engineering σ_{flow} (engineering σ_u) ranges between 40 to 52 MPa for all material showing no real significant changes when cross-linked when it is very clear that material performance should be affected. Secondly, the true σ_{flow} does rank with cross-linking in the same manner as $dJ/d\Delta a$. Values of the true σ_{flow} range between 70 to 121 MPa showing a much greater spread in properties which is expected when comparing cross-linked and non-cross-linked materials. Fundamentally all of this stems from the very significant differences in the engineering versus true stress-strain properties for polymer materials that exhibit low-strength and high strain-hardening characteristics; indeed, our statistical correlations reinforce why using true properties is paramount for the characterization of the *J*-based fracture toughness of polymers.

Finally, critical updates need to be added to both ASTM D6068 and ASTM E1820 standards. These updates include elimination of the outdated 0.05mm, 0.15mm, and 1.5mm exclusions lines in ASTM D6068 and ASTM E1820. Upper and lower exclusion limits should be based on specimen size, specifically b_0 and not on absolute dimensions. Finally, ASTM Standard D6068 for polymers should incorporate a 0.2 mm offset blunting line to enable a reliable determination of the *J*-based crack-initiation fracture toughness, but the flow stress used in the determination of this blunting line must be based on the true σ_y and σ_U and not, as is currently employed, on the engineering stress calculation.

3.6. Conclusions

Our methodology demonstrates that practical definition of J_Q/J_{Ic} is possible in polymers provided that the true stress-strain relationships are utilized for determining flow stress. True σ_U can be up to four times higher compared to engineering σ_U in tough polymers such as UHMWPE. This has a significant impact on the flow stress when calculated as the average of σ_y and σ_U. There still exists some discrepancies with regard to a correlation of a correct blunting line with a stretch zone in polymer materials and additional mechanistic work should be performed to elucidate these relationships. Furthermore, it is recommended that the current *J*-integral standards are updated for

several reasons: the ASTM D6068 can include a 0.2 mm offset blunting line to determine J_Q/J_{Ic} as long as true stress-strain properties are used to determine flow stress, and both standards should be revised such that the minimum and maximum crack-extension exclusion limits are based on a percentage of the initial uncracked ligament, rather than in terms of absolute numbers.

In summary, we have the following specific recommendations for the measurement of the *J*-based crack-initiation fracture toughness of low-strength high strain-hardening polymers:

1. Use of a lower crack-extension exclusion limit of $0.006b_0$ and an upper exclusion limit greater than $0.1b_0$, where b_0 is the initial uncracked ligament.
2. Use of a 0.2 mm offset blunting line for determining the crack-initiation fracture toughness in polymers with the true stress-strain material properties measured in order to calculate the flow stress. For strain-hardening polymers, the true constitutive behavior would need to be determined by *in situ* methods, such as video extensometers, that track the long stable neck to the point of failure.
3. Mechanistic work should be performed to solidify the blunting line in polymers and understand why there might be an absence or discrepancy in seeing a stretch zone in these materials.
4. Update of the exclusion line protocols in the ASTM E1820 standard. The current upper limit of crack growth, $0.25b_0$, is acceptable.

Acknowledgments

This work was supported by the endowment from the Lawrence Talbot Endowed Professorship and the Ian Finnie graduate research fellowship at the University of California, Berkeley (for LGM and LAP). The fracture toughness testing facilities was provided by the Mechanical Behavior of Materials Program (KC-13) at the Lawrence Berkeley National Laboratory, funded by the U.S. Department of Energy, Office of Science, Office of Basic Energy Sciences, Materials Sciences and Engineering Division, under contract no. DE-AC02-05CH11231.

Chapter 4 – Fracture mechanisms in ultra-high molecular weight polyethylene

Abstract

This chapter presents mechanistic observations on miniature fracture specimens of ultra-high molecular weight polyethylene (UHMWPE) in order to understand the crack growth process in this polymer. These observations are performed to elucidate and rationalize procedural methods for *J*-integral fracture toughness testing of polymers. Small-scale single edge notched bend specimens are deformed in a scanning electron microscope (SEM) in order to witness real-time crack growth processes. This chapter aims to provide qualitative mechanistic evidence for changes to how *J*-integral fracture toughness is conducted.

4.1 Introduction

Micromechanisms of crack inception and advancement are key to understanding fracture toughness properties in structural materials. Intrinsic toughening mechanisms generally take place ahead of the crack in a process zone while extrinsic mechanisms occur in the wake of crack advance (Launey and Ritchie, 2009). There are two primary fracture mechanisms that occur intrinsically in polymers; shear yielding or plastic flow where molecular chains slide past one another when a critical shear stress is activated or crazing which occurs in glassy or amorphous polymers (Kramer, 1983). When a tensile stress is applied to a glassy polymer, localized void formation takes place ahead of the crack tip creating fibrils that carry the load (Kramer, 1983; Trassaert and Schirrer, 1983). The crack advances with the rupture of individual fibrils. Many semi-crystalline polymers, like high-density polyethylene (HDPE), under tensile load can form craze structures (Friedrich, 1983). Crazing in HDPE has been extensively studied as the material plays an important role in the safety critical gas pipe industry (Bhattacharya and Brown, 1985; Brown et al., 1987; Brown and Bhattacharya, 1985; Friedrich, 1983; Huang and Brown, 1992, 1991, 1988; Lu et al., 1988; Lu and Brown, 1986; Ward et al., 1991). Ultra-high molecular weight polyethylene (UHMWPE) is perhaps an even more safety critical relative of HDPE that is used as a counter bearing in orthopedic implants.

UHMWPE is a semi-crystalline homopolymer with a molecular weight of 2-6 million g/mol where these long chains facilitate high entanglement density that afford the polymer exceptional energetic toughness (Kurtz, 2009; Pruitt, 2005). Both HDPE and UHMWPE are made up of the same homopolymer (polyethylene) but differ drastically in terms of molecular weight. Despite superior energetic toughness and a sixty year use in orthopedic implants, the material can fail *in vivo* due to the generation of wear debris from the formation of micro cracks underneath the bearing surface (Pascaud et al., 1997b). As a result, understanding fracture behavior and mechanisms in UHMWPE is important. There have been numerous fracture studies on UHMPWE applying the elastic-plastic fracture mechanics or *J*-integral approach (Bellare et al., 2016; Gomoll et al., 2002; Pascaud et al., 1997a, 1997b; Rimnac et al., 1988; Varadarajan and Rimnac, 2008). These studies have explored some mechanistic characterization through scanning electron microscopy (SEM) of the fracture surface to understand material behavior (Pascaud et al., 1997a, 1997b; Rimnac et al., 1988). However, there has been no comprehensive study to examine ductile fracture mechanisms in UHMWPE as the crack advances in real-time. Looking at real-time crack advance in UHMWPE would solve many unanswered questions in the polymer community as a whole.

First there has been a longstanding debate in defining a *J*-based crack-initiation toughness or J_{Ic} in polymers. The reason for this is the disagreement in observing a stretch zone on the fracture surface that marks the end of crack extension due to blunting and the onset of crack growth due to material tearing, the classic definition of J_{Ic} (Chan and Williams, 1983; Narisawa, 1987; Pascaud et al., 1997a, 1997b; Varadarajan and Rimnac, 2008). Observing real-time shear banding or craze mechanisms could provide the necessary information as to why there is an apparent lack of stretch zone on the fracture surface in some polymers. Secondly, observing real-time crack growth mechanisms could provide the necessary justification for the use of a proper blunting line to define J_{Ic} in polymers. The blunting line is a theoretical line based on a materials flow stress, σ_{flow}, the average of the yield and ultimate stress, where its intersection with the *J*-integral versus crack

growth (Δa) curve defines J_{Ic} experimentally. Chung and Williams have commented on the importance of understanding crack growth mechanisms in different polymers in order to use an appropriate blunting line to determine J_{Ic} (Chung and Williams, 1991). They commented on how depending if the material exhibits crazing or crack-tip stretching, the blunting line slope could be drastically different based on those mechanistic cases (Chung and Williams, 1991).

Accordingly, the purpose of this study is to investigate real-time crack growth in different clinically relevant UHMWPE formulations to understand how crack growth mechanisms influence procedural methods in polymer fracture mechanics analysis. It is done in an effort to build upon a comprehensive *J*-integral fracture study on UHMWPE performed by these authors. The previous study was performed to define a standardized method for evaluation of *J*-integral fracture in polymers using UHMWPE as the test material. Unlike crazing in HDPE, UHMWPE has been seen in limited studies to produce a cohesive zone ahead of the crack tip (Medel and Furmanski, 2015). The cohesive zone looks like a craze or process zone in front of the crack tip but with no void formation (Medel and Furmanski, 2015). It has been suggested that the formation and rupture of the cohesive zone forms a characteristic rippling and crisscross pattern on the fracture surface but has not been observed in real-time (Medel and Furmanski, 2015). Additionally understanding cohesive zone rupture might elucidate why difficulties in stretch zone characterization exist in UHMWPE, HDPE, and other crazing polymers.

4.2 Methods

Real-time crack growth observation was performed on miniature single edge notched bend (SENB) specimens in a Hitachi S4300SE/N SEM (Tokyo, Japan). SENB specimens were machined from stock UHMWPE material formulations to a 5x5mm square cross section and a length of 20mm. Specimens were pre-cracked using fresh razor blades to a normalized crack length, *a/W*, between 0.5 and 0.65. Testing for real-time crack growth observation was conducted inside the SEM on a Deben in-situ tensile, compression, and horizontal bend stage (Suffolk, UK) using a 200N load cell at a rate of 0.4mm/min. Prior to testing, samples were sputter coated in gold for imaging inside the SEM. Pictures were captured throughout the deformation process in an effort to observe crack growth mechanisms in the material. Based on earlier testing, miniature SENB specimen dimensions did not meet criteria for *J*-controlled crack growth. As a result, determination of elastic plastic initiation toughness values was not considered in this study. The real-time crack growth observation from this study was meant as a qualitative mechanistic pairing to our earlier work.

Six clinically relevant UHMWPE material formulations were observed out of the original ten materials from our previous study. The materials were sourced from two different UHMWPE consolidators, Orthoplastics (Lancashire, UK) and DePuy (Warsaw, IN). Variations to a single base resin, GUR 1020, were investigated across a range of radiation cross-linking dosage and antioxidant chemistry. The antioxidants were comprised of 0.1 wt.% Vitamin E (VE) and COVERNOX™ (AO) (medical grade version of Irganox™ 1010) which were blended into GUR 1020 resin before consolidation. Three distinct material categories explored were 1020 resin (0kGy, 75 kGy RM); 1020 resin with AO antioxidant (AO 80 kGy); 1020 resin with 0.1 wt.% vitamin E (VE 0 kGy, VE 50 kGy VE 125 kGy). GUR 1020 75kGy was re-melted (RM) to alleviate free radicals.

4.3 Results

All UHMWPE materials investigated, regardless of antioxidant addition or radiation cross-linking dosage, exhibited a cohesive zone ahead of the crack tip (**Figure 4.1**). The cohesive zone, from our magnifications, was absent of void formation across all materials as had been previous observed in UHMWPE (Medel and Furmanski, 2015). During the deformation process, the cohesive zone would begin to form and then stretch out eventually reaching a critical point where tearing would occur within the zone. Tearing of the cohesive zone for crack extensions was witnessed in all samples (**Figure 4.2** and **4.3**). Tearing of the cohesive zone produced the characteristic rippling and crisscross fracture patterns seen on previous top down fractographs of UHMWPE fracture specimens (**Figure 4.2** and **4.3**). The cohesive zone would typically begin to tear closest to the blunted crack tip where the zone was stretched out the most (Figure 2). As the material continued to deform, more material would tear within the cohesive zone moving to the zone tip (Figure 3). Eventually the cohesive zone would begin to tear beyond its current tip extending into non-deformed material (**Figure 4.4**). The only difference seen across materials was with GUR 1020 VE 125kGy which exhibited the longest cohesive zone at the start of deformation compared to all the other material formulations tested (**Figure 4.5**).

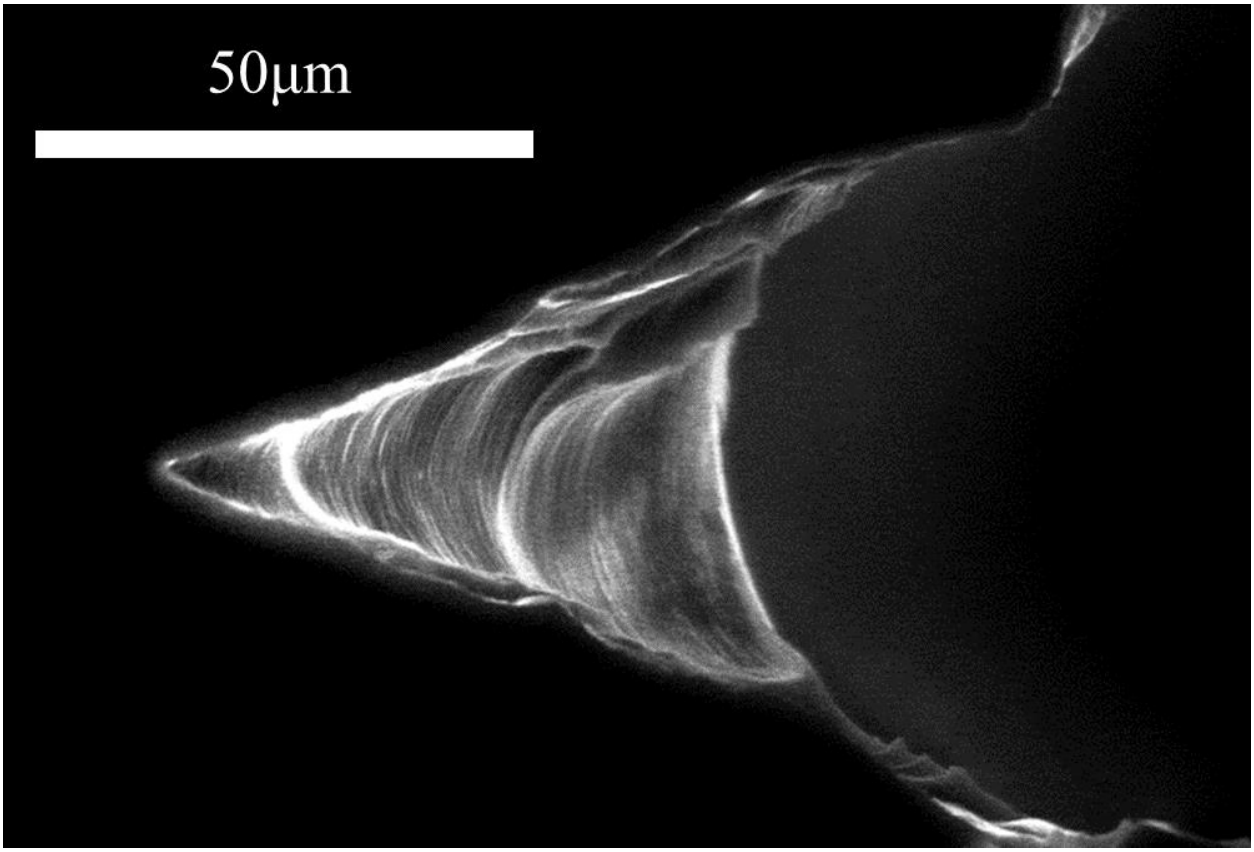

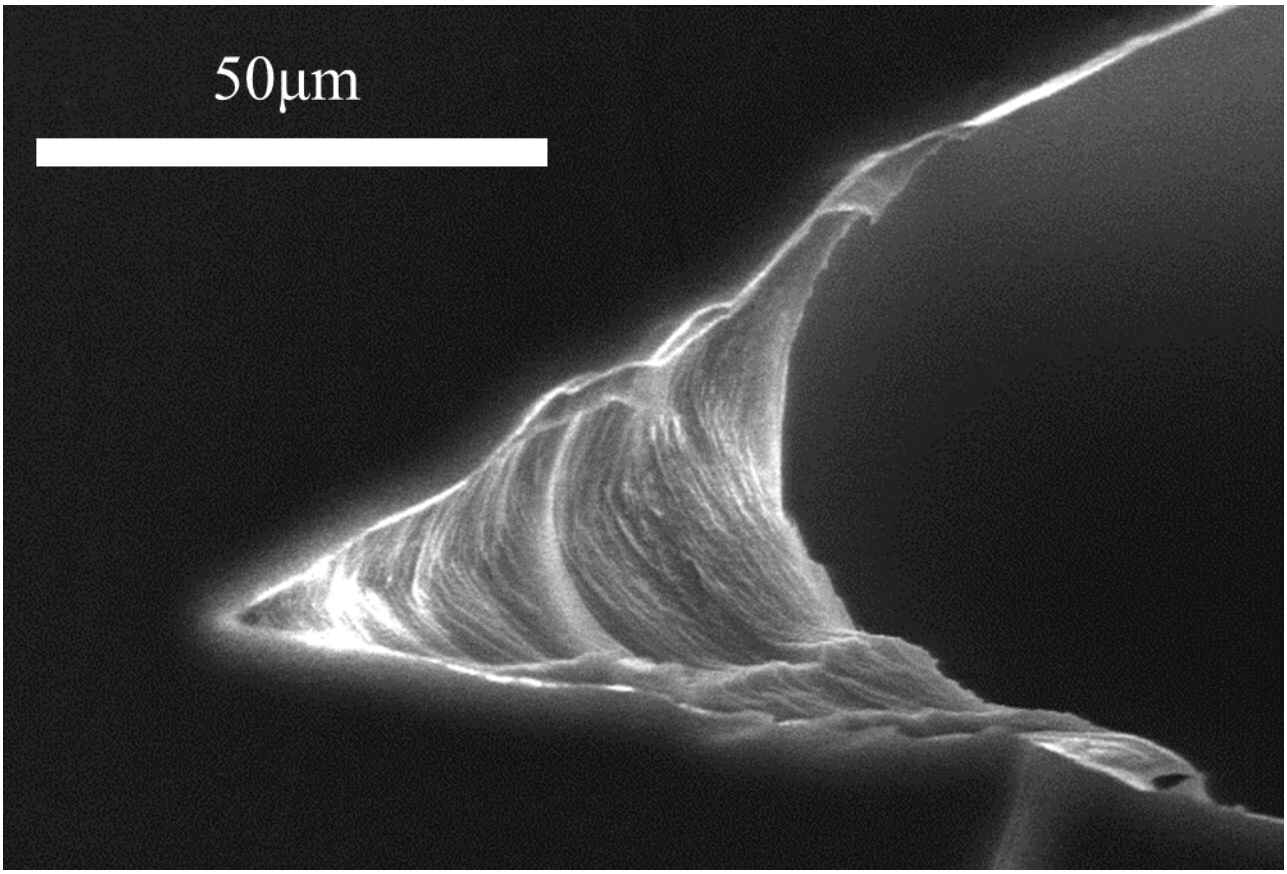

Figure 4. 1 – SEM images of the crack tip from SENB specimens demonstrating the existence of a cohesive zone in front of the frack tip. Voids are absent within the cohesive zone. It appears regardless of radiation cross-linking dosage or antioxidant chemistry that all material formulations experience a cohesive zone during deformation. (A) Cohesive zone formation in base GUR 1020 material. (B) Cohesive zone formation in GUR 1020 75kGy RM material.

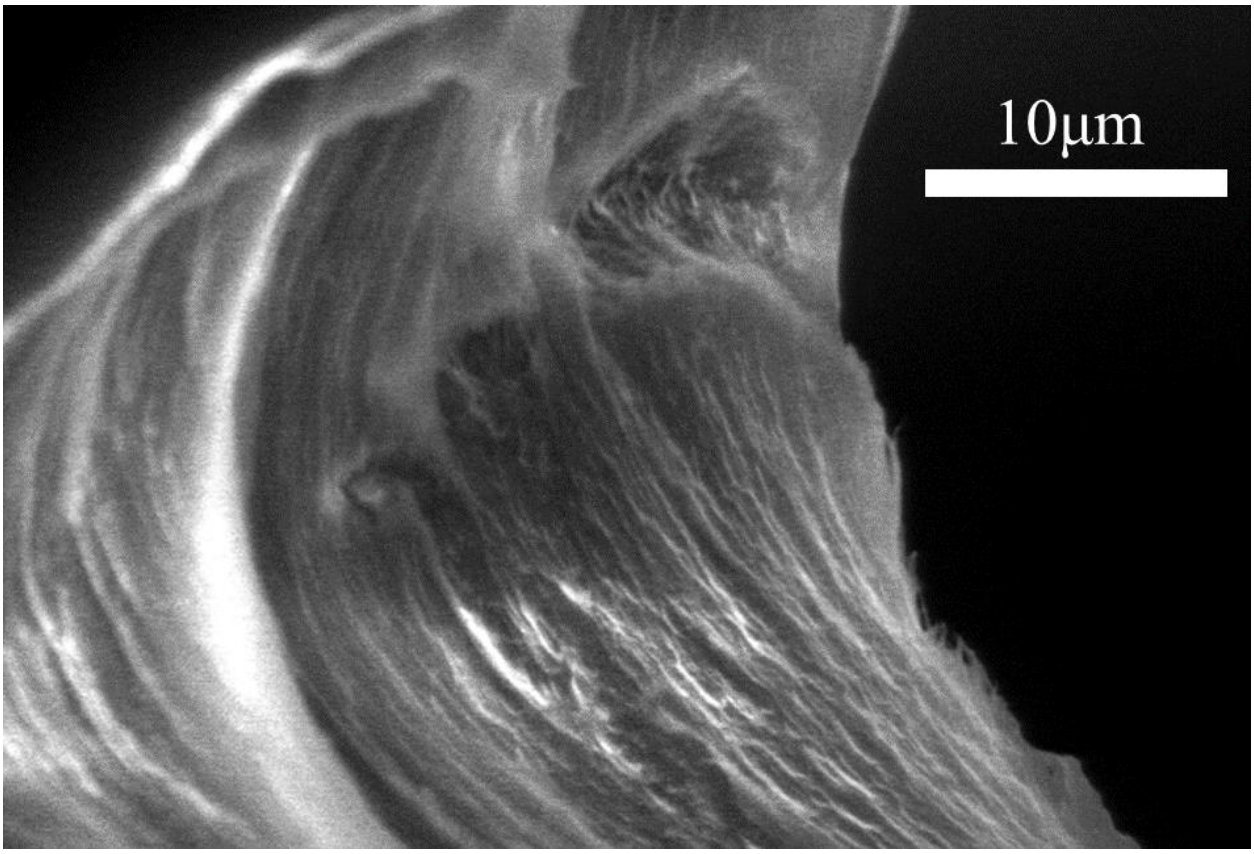

Figure 4. 2 – Close up SEM image of tearing within the edge of the cohesive zone and the blunted crack tip for GUR 1020 75kGy RM material.

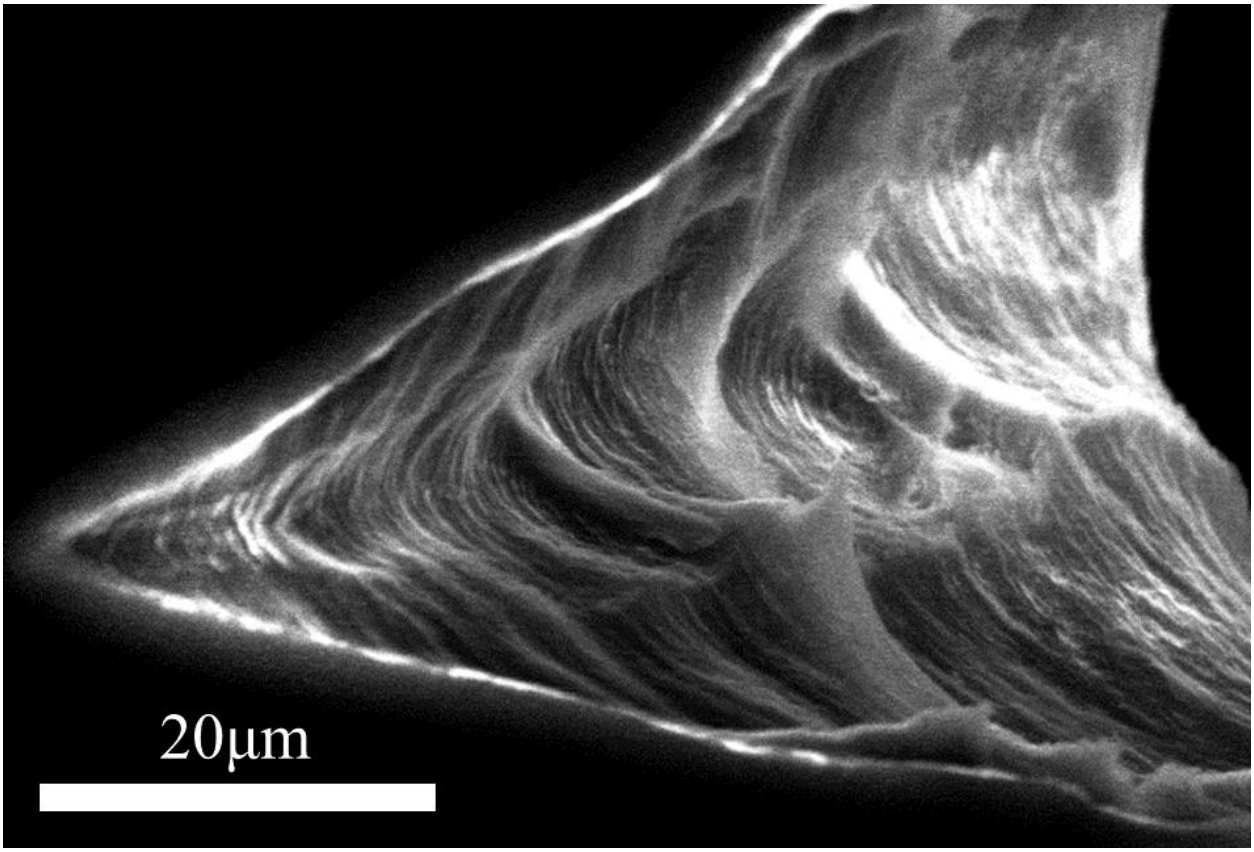

Figure 4. 3 – Close up SEM image showing multiple tear regions within the cohesive zone for GUR 1020 75kGy RM material. The multiple cohesive zone tears create the same texture that has been seen on top down SEM fractographs from previous UHMWPE fracture studies.

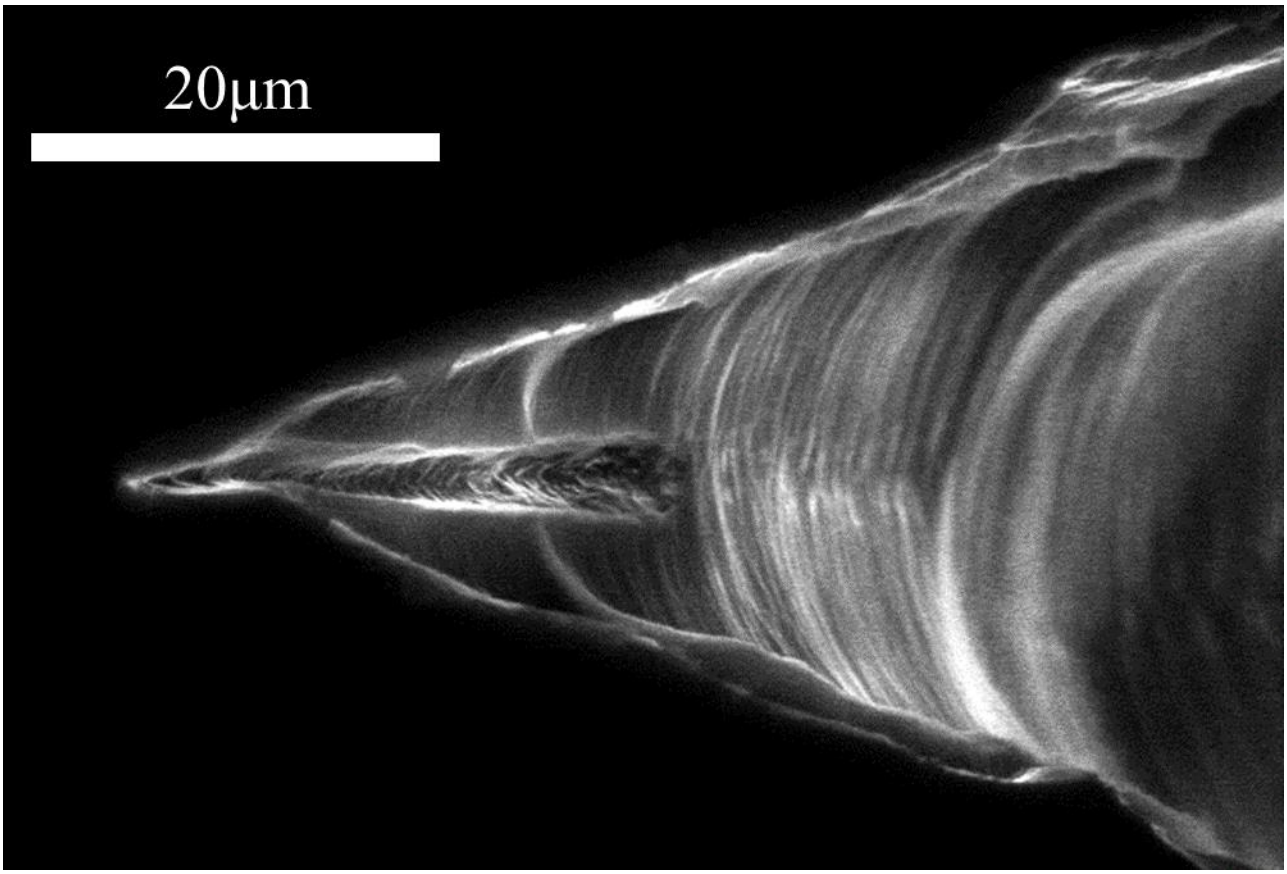

Figure 4. 4 – SEM image of the formation of a new part of the cohesive zone in GUR 1020. The new part of the cohesive zone can be towards the far left in the image as new material begins to tear.

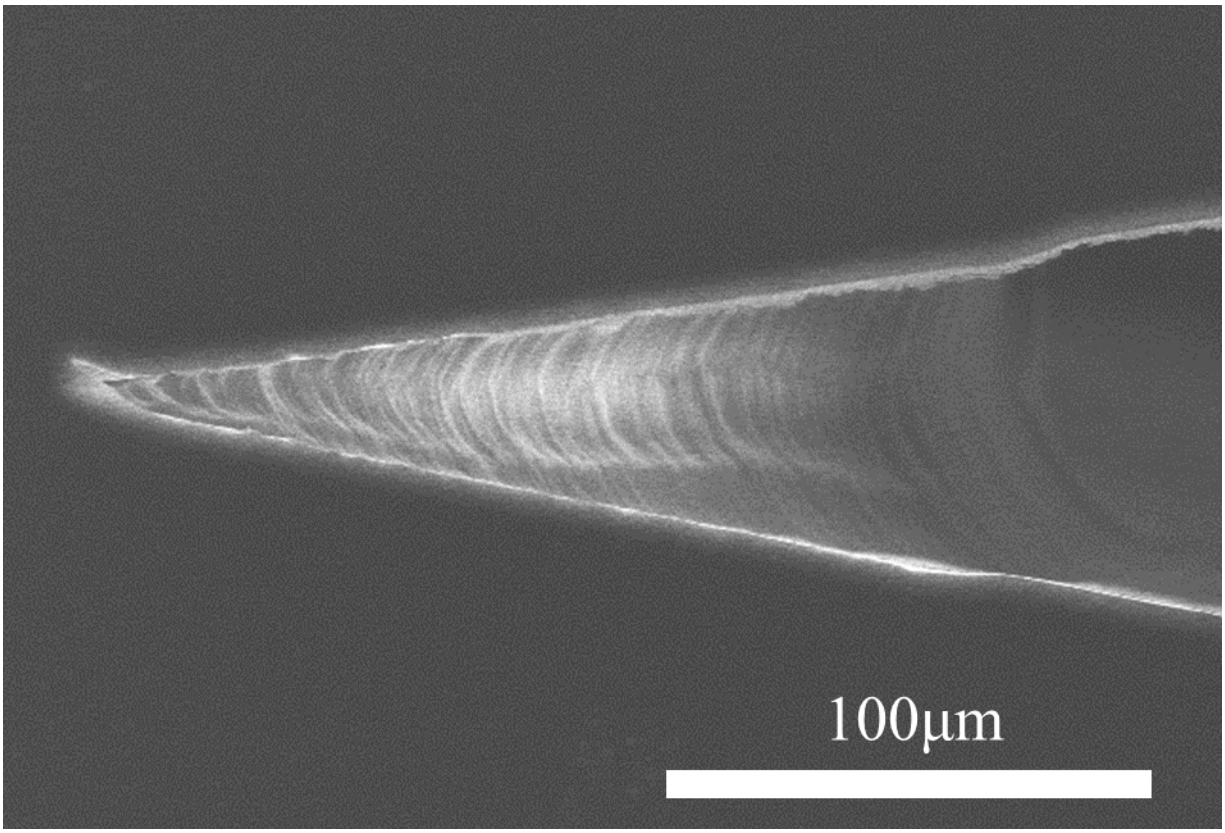

Figure 4. 5 – SEM image of the cohesive zone in GUR 1020 VE 125kGy. This material compared to the others investigated experienced the longest cohesive zone at the start of the deformation process.

Viscoelastic fracture mechanisms were also observed during testing. In many occasions as specimens were held under load to take pictures, the cohesive zone would begin to tear under the static load. Overall based on our observations it would seem crack growth in UHMWPE begins with the formation of a cohesive zone during the blunting process, tearing of the cohesive zone at certain critical loads, and finally extension of the cohesive zone into previously non-deformed material.

4.4 Discussion

Slow time dependent crack growth has been investigated by many authors for various polyethylene polymers used in the gas pipe industry. These studies have all demonstrated the formation of a craze structure ahead of the crack tip with crack advance through the rupture of craze fibrils (Bhattacharya and Brown, 1985; Brown et al., 1987; Brown and Bhattacharya, 1985; Friedrich, 1983; Huang and Brown, 1992, 1991, 1988; Lu et al., 1988; Lu and Brown, 1986; Ward et al., 1991). Our study showed that UHMWPE experiences ductile crack growth in a similar manner. A cohesive zone, in place of crazing, would appear in front of the crack-tip where crack advance would occur through rupture of the cohesive zone. Microstructural deformation ahead of

the crack tip in semi-crystalline polymers has been postulated to follow the deformation seen during tensile testing, 1.) Stretching of the amorphous region, 2.) Crystal slip 3.) Fibrillation of the crystalline domains 4.) Disentanglement of crystal segments 5.) Finally snapping of bonds between elongated chains (Friedrich, 1983). First determined in amorphous polymers, it was found that there was a critical molecular weight to be able to form craze structures as chain entanglements played an important role in stabilizing craze fibrils. UHMWPE, due it's extremely high molecular weight, is known to have high entanglement density where the molecular chains do not disentangle under 220°C compared to other polyethylene counterparts (Huang and Brown, 1992). Therefore UHMWPE should experience significant stable crazing. It is possible that the cohesive zone is actually a craze zone where the voids are extremely small. Kurtz was able to see what appeared to be craze fibrils spaced 2μm on the fracture surfaces of UHMWPE bulk tensile specimens (Kurtz et al., 1998). We could not image the cohesive zone in our samples at much higher magnifications due to the charging effects from that part of the sample not being gold coated.

From our observations, tearing of the cohesive zone is directly responsible for producing the crisscross and rippled patterns on the surface of UHMWPE fracture specimens. The rippling and crisscross pattern is also seen on the fracture surface of UHMWPE tensile samples (Kurtz et al., 1998). In UHMWPE tensile testing, the long stable neck that forms will eventually rupture in a fast brittle manner dissipating a large amount of energy creating the rippled and crisscross patterns as a byproduct. Many authors have suggested using true stress-strain data compared to engineering stress-strain data as a result of the long necking process UHMWPE experiences since true stress-strain behavior more accurately accounts for material deformation (Kurtz et al., 2002, 1998, Sobieraj et al., 2008, 2005). This was a central argument for us in an earlier study applying true stress-strain data in the calculation of σ_{flow} for *J*-integral based fracture toughness testing. Our real-time crack growth observations in UHMWPE reinforce why true stress-strain properties are paramount for *J*-integral fracture methods in polymers that exhibit craze type regions.

Essentially craze fibrils or the cohesive zone, are micron size tensile specimens ahead of the crack tip that fracture when significantly drawn out to a critical load. Brown and Bhattacharya noticed that craze fibrils in HDPE would lengthen by thinning while at the same time, new fibrils would form at the end of the deformation zone (Brown and Bhattacharya, 1985). The elongation and simultaneous thinning of fibrils is akin to the deformation experienced in bulk tensile testing of polymers. Chung and Williams have argued that crazing polymers, like HDPE, will have a shallow blunting line compared to other polymer crack-growth schemes. From observing real-time crack-growth in UHMWPE and from the extensive work of other authors studying the phenomenon of crazing, we feel the opposite is true. The elongation, thinning, and rupture of craze fibrils and the cohesive zone elude to the use of constitutive properties that more accurately take this type of deformation process into account.

True stress-strain derived constitutive properties in polymers account for the long stable neck during deformation to more accurately describe material behavior compared to engineering stress-strain derived properties. In many semi-crystalline polymers, such as HDPE or UHMWPE, plastic flow properties, like ultimate tensile stress, can differ by a factor of 4X when comparing true and engineering constitutive values (**Chapter 2,3**). *J*-integral based fracture has long used engineering constitutive values to define blunting underestimating material behavior (Chan and Williams, 1983; Chung and Williams, 1991; Hashemi and Williams, 1991, 1986a, 1986b, Huang

and Williams, 1990, 1987, Pascaud et al., 1997a, 1997b; Rimnac et al., 1988; Varadarajan and Rimnac, 2008). Craze fibrils and the cohesive zone experience drawing in the same manner as their bulk tensile specimen counterparts producing similar fracture features and strength results. Friedrich studied the formation of craze fibrils in polypropylene (PP) and compared the strength of those fibrils to the strength of bulk PP tensile samples (Friedrich, 1983). He determined that the true stress in the fibrils was in the same order of magnitude as the true fracture stress (or true ultimate tensile stress in a polymer) of a bulk PP tensile sample (Friedrich, 1983). Therefore from a mechanistic perspective, it makes the most sense to use true constitutive values to define flow properties in *J*-integral polymer fracture.

Our crack growth observations also point to why there is a discrepancy in the observation of a stretch zone on the fracture surface of many polymers. Crazing polymers demonstrate blunting at the crack tip from elongation and drawing of the lead fibrils or cohesive zone. Any evidence of crack growth due to pure blunting can be eliminated once those lead fibrils or areas of the cohesive zone rupture. Depending on fibril size, spacing, orientation, and density, ruptured fibrils can present a surface texture where distinguishing between a stretch zone and initial rupture can become exceedingly difficult. Typically fibrils or the cohesive zone should rupture in the center of the fracture specimen where plane-strain conditions are the closest to being satisfied. Though depending on orientation and stress state, some fibrils can fracture anywhere within the craze zone making fracture initiation difficult to define from an experimental vantage. Sirimamilla demonstrated for time-dependent crack initiation tests in UHMWPE that initiation could occur at the side of the specimen with the intersection of the notch tip and machined side groove instead of in the center of the notch (Sirimamilla et al., 2013). Does fracture initiation occur with the rupture of the first fibril or section in the cohesive zone or does initiation have to cross a size threshold requirement? Can initiation be accepted if does not occur in the middle of the specimen where it typically is predicted to occur? These questions help explain why J_{Ic} has been experimentally defined to include a small amount of crack.

ASTM E1820, the *J*-integral fracture testing standard for metals, uses a blunting line that is offset by 0.2mm, to intersect with the *J*-integral versus Δa curve to define J_{Ic}. This is not an exact definition of initiation toughness but a practical definition. It can be very difficult in metals, just like polymers, to view the extent of a stretch zone on the fracture surface or distinguish between large crack growth and subcritical crack growth (Clarke et al., 1980). As a result this became the accepted standard for J_{Ic} testing conducted in metals. Polymers experience similar issues with metals given the complex nature of a craze or cohesive zone outlined earlier. Therefore there is no reason why polymer fracture testing cannot use an offset blunting line to establish a practical definition of J_{Ic} at an allowable amount of crack growth.

4.5 Conclusions

Due to UHMWPE's large molecular weight, high entanglement density, and propensity to not disentangle below 220°C are probable reasons why the polymer produces a cohesive zone, or craze-like region without identifiable voids, ahead of the crack tip (Huang and Brown, 1992). Further it is possible that the cohesive zone is actually a craze zone where the voids are difficult to visual due to their small size. All UHMWPE material formulations, regardless of cross-linking or antioxidant additions, produced a cohesive zone in advance of the crack tip. The rupture of the

cohesive zone, as with craze fibril rupture, is responsible for crack growth in the material producing similar crisscross and rippling patterns seen on the fracture surfaces of bulk tensile specimens of UHMWPE (Kurtz et al., 1998; Rimnac et al., 1988). Extensive drawing of craze fibrils and the cohesive zone point to using true stress-strain derived flow properties in *J*-integral fracture analysis of UHMWPE and other polymer materials. Finally craze fibril or cohesive zone rupture are mechanistic explanations for why viewing a stretch zone on the fracture surface of UHMWPE and other polymers proves difficult. This points to adopting a practical definition of imitation toughness in polymers where a small amount of crack growth is allowed to avoid ambiguity.

Acknowledgments

This work was supported by the endowment from the Lawrence Talbot Endowed Professorship and the Ian Finnie graduate research fellowship at the University of California, Berkeley. The involvement of Bernd Gludovatz and Robert O. Ritchie, together with the fracture toughness testing facilities at the Lawrence Berkeley National Laboratory (LBNL), was supported by the Mechanical Behavior of Materials Program (KC-13) at LBNL, funded by the U.S. Department of Energy, Office of Science, Office of Basic Energy Sciences, Materials Sciences and Engineering Division, under contract no. DE-AC02-05CH11231.

Chapter 5 – Concluding remarks

Polymeric materials present many unique and interesting challenges when trying to analyze their mechanical behavior. Deformation, yielding, and fracture don't have precise rules and definitions leading to a wide reporting of basic properties such as elastic modulus and ultimate strength. Nowhere is this more apparent than with ultra-high molecular weight polyethylene (UHMWPE) given its extensive use in the safety critical application of total joint replacements (TJRs). This dissertation was a small step forward to try and really argue procedurally how polymeric materials should be analyzed for their mechanical behavior using UHMWPE as the test material.

True stress-strain testing of polymers has been around since G'sell and Jonas however has found limited utility outside of the medical device world when analyzing material mechanical behavior (G'Sell and Jonas, 1979). From this dissertation, the differences between ultimate properties from true and engineering stress-strain methods can differ by a factor of four. The incompressibility assumption that is used in metals to convert between engineering and true properties cannot be applied to many polymers given long stable necking. Polymeric materials are only increasing in their use given the recent rise in additive manufacturing. More and more components that are load bearing will be manufactured out of polymers in this way making it even more critical to have correct procedural methods for the mechanical analysis in polymers.

There is one part of polymer fracture that needs to be more extensively explored which is applying the unloading compliance method to analyze crack growth. The fracture analysis presented in **Chapter 3** is tedious and time consuming. One needs a lot of material and specimens to generate a single crack-growth resistance curve. The metals fracture community has moved away from a multi-specimen fracture technique to use single-specimen unloading compliance method. Though there are more hurdles to adopt this type of a technique for polymers it can be done. Hashemi, Chung, and Williams have demonstrated the method is possible and the polymer community could benefit from further research into implementing such a technique. This would help polymer fracture analysis become better adopted by researchers and engineers ultimately providing the necessary data for design of structural components that is currently missing.

Overall this dissertation makes one small step forward to improving the mechanical analysis of engineering polymers especially one used in safety critical orthopedic implants to hopefully increase implant longevity and performance.

References

ASTM D6068-10, Standard Test Method for Determining J-R Curves of Plastic Materials, ASTM International, West Conshohocken, PA, 2010, www.astm.org

ASTM E1820-17a, Standard Test Method for Measurement of Fracture Toughness, ASTM International, West Conshohocken, PA, 2017, www.astm.org

Amouzouvi, K.F., Bassim, M.N., 1982. Determination of fracture toughness from stretch zone width measurement in predeformed AISI type 4340 steel. Mater. Sci. Eng. 55, 257–262.

Ansari, F., Gludovatz, B., Kozak, A., Ritchie, R.O., Pruitt, L.A., 2016. Notch fatigue of ultrahigh molecular weight polyethylene (UHMWPE) used in total joint replacements. J. Mech. Behav. Biomed. Mater. 60, 267–279.

Atwood, S.A., Van Citters, D.W., Patten, E.W., Furmanski, J., Ries, M.D., Pruitt, L.A., 2011. Tradeoffs amongst fatigue, wear, and oxidation resistance of cross-linked ultra-high molecular weight polyethylene. J. Mech. Behav. Biomed. Mater. 4, 1033–1045.

Atwood, S.A., Van Citters, D.W., Patten, E.W., Furmanski, J., Ries, M.D., Pruitt, L.A., 2011. Tradeoffs amongst fatigue, wear, and oxidation resistance of cross-linked ultra-high molecular weight polyethylene. J. Mech. Behav. Biomed. Mater. 4, 1033–1045. https://doi.org/10.1016/j.jmbbm.2011.03.012

Bailey, W.J., 2012. Contemporary Topics in Polymer Science. Springer Science & Business Media.

Baker, D.A., Bellare, A., Pruitt, L., 2003a. The effects of degree of crosslinking on the fatigue crack initiation and propagation resistance of orthopedic-grade polyethylene. J. Biomed. Mater. Res. Part A 66A, 146–154. https://doi.org/10.1002/jbm.a.10606

Baker, D.A., Bellare, A., Pruitt, L., 2003b. The effects of degree of crosslinking on the fatigue crack initiation and propagation resistance of orthopedic-grade polyethylene. J. Biomed. Mater. Res. Part A 66A, 146–154. https://doi.org/10.1002/jbm.a.10606

Bartczak, Z., Cohen, R.E., Argon, A.S., 1992. Evolution of the crystalline texture of high-density polyethylene during uniaxial compression. Macromolecules 25, 4692–4704.

Bartel, D.L., Rawlinson, J.J., Burstein, A.H., Ranawat, C.S., Flynn Jr, W.F., 1995. Stresses in polyethylene components of contemporary total knee replacements. Clin. Orthop. Relat. Res. 317, 76–82.

Bellare, A., Cohen, R.E., 1996. Morphology of rod stock and compression-moulded sheets of ultra-high-molecular-weight polyethylene used in orthopaedic implants. Biomaterials 17, 2325–2333.

Bellare, A., Dorfman, R., Samuel, A., Thornhill, T.S., 2016. J-integral fracture toughness, Tearing modulus and tensile properties of Vitamin E stabilized radiation crosslinked UHMWPE. J. Mech. Behav. Biomed. Mater. 61, 493–498.

Bergström, J.S., Kurtz, S.M., Rimnac, C.M., Edidin, A.A., 2002. Constitutive modeling of ultra-high molecular weight polyethylene under large-deformation and cyclic loading conditions. Biomaterials 23, 2329–2343.

Bergström, J.S., Rimnac, C.M., Kurtz, S.M., 2003. Prediction of multiaxial mechanical behavior for conventional and highly crosslinked UHMWPE using a hybrid constitutive model. Biomaterials 24, 1365–1380.

Bhattacharya, S.K., Brown, N., 1985. The initiation of crack growth in linear polyethylene. J. Mater. Sci. 20, 2767–2775.

Bistolfi, A., Turell, M.B., Lee, Y.-L., Bellare, A., 2009. Tensile and tribological properties of high-crystallinity radiation crosslinked UHMWPE. J. Biomed. Mater. Res. Part B Appl. Biomater. 90, 137–144.

Bozic, K.J., Kurtz, S., Lau, E., Ong, K., Chiu, V., Vail, T.P., Rubash, H.E., Berry, D.J., 2009. The epidemiology of bearing surface usage in total hip arthroplasty in the United States. JBJS 91, 1614–1620.

Brown, N., Bhattacharya, S.K., 1985. The initiation of slow crack growth in linear polyethylene under single edge notch tension and plane strain. J. Mater. Sci. 20, 4553–4560.

Brown, N., Donofrio, J., Lu, X., 1987. The transition between ductile and slow-crack-growth failure in polyethylene. Polymer (Guildf). 28, 1326–1330.

Chan, M.K. V, Williams, J.G., 1983. Slow stable crack growth in high density polyethylenes. Polymer (Guildf). 24, 234–244.

Chang, D.G., Lottman, L.M., Chen, A.C., Schinagl, R.M., Albrecht, D.R., Pedowitz, R.A., Brossman, J., Frank, L.R., Sah, R.L., 1999. The depth-dependent, multi-axial properties of aged human patellar cartilage in tension. Trans. Annu. Meet.-Orthop. Res. Soc 24, 644.

Chung, W.N., Williams, J.G., 1991. Determination of J IC for polymers using the single specimen method, in: Elastic-Plastic Fracture Test Methods: The User's Experience (Second Volume). ASTM International.

Clarke, G.A., Andrews, W.R., Begley, J.A., Donald, J.K., Embley, G.T., Landes, J.D., McCabe, D.E., Underwood, J.H., 1979. A procedure for the determination of ductile fracture toughness values using J integral techniques. J. Test. Eval. 7, 49–56.

Clarke, G.A., Landes, J.D., 1979. Evaluation of the J Integral for the Compact Specimen. J. Test. Eval. 7, 264–269.

Clarke, G.A., Landes, J.D., Begley, J.A., 1980. Results of an ASTM Cooperative Test Program on the J Ic Determination of HY130 Steel. J. Test. Eval. 8, 221–232.

Cohen, R.E., Bartczak, Z., Argon, A.S., 1992. Evolution of the Crystalline Texture of High-Density Polyethylene during Uniaxial Compression. Macromolecules 25, 4692–4704. https://doi.org/10.1021/ma00044a034

Costa, L., Luda, M.P., Trossarelli, L., Del Prever, E.M.B., Crova, M., Gallinaro, P., 1998. Oxidation in orthopaedic UHMWPE sterilized by gamma-radiation and ethylene oxide.

Biomaterials 19, 659–668.

Crowninshield, R.D., Muratoglu, O.K., 2008. How have new sterilization techniques and new forms of polyethylene influenced wear in total joint replacement? J. Am. Acad. Orthop. Surg. 16, S80--S85.

Ebenstein, D.M., Pruitt, L.A., 2006. Nanoindentation of biological materials. Nano Today 1, 26–33.

Edidin, A.A., Jewett, C.W., Kalinowski, A., Kwarteng, K., Kurtz, S.M., 2000. Degradation of mechanical behavior in UHMWPE after natural and accelerated aging. Biomaterials 21, 1451–1460.

Elliott, D.M., Narmoneva, D.A., Setton, L.A., 2002. Direct measurement of the Poisson's ratio of human patella cartilage in tension. Trans. Soc. Mech. Eng. J. Biomech. Eng. 124, 223–228.

Friedrich, K., 1983. Crazes and shear bands in semi-crystalline thermoplastics, in: Crazing in Polymers. Springer, pp. 225–274.

Furmanski, J., Anderson, M., Bal, S., Greenwald, A.S., Halley, D., Penenberg, B., Ries, M., Pruitt, L., 2009. Clinical fracture of cross-linked UHMWPE acetabular liners. Biomaterials 30, 5572–5582.

Furmanski, J., Pruitt, L.A., 2007. Peak stress intensity dictates fatigue crack propagation in UHMWPE. Polymer (Guildf). 48, 3512–3519.

G'sell, C., Jonas, J.J., 1979. Determination of the plastic behaviour of solid polymers at constant true strain rate. J. Mater. Sci. 14, 583–591.

Gencur, S.J., Rimnac, C.M., Kurtz, S.M., 2006. Fatigue crack propagation resistance of virgin and highly crosslinked, thermally treated ultra-high molecular weight polyethylene. Biomaterials 27, 1550–1557.

Gomoll, a., Wanich, T., Bellare, a., 2002. J-integral fracture toughness and tearing modulus measurement of radiation cross-linked UHMWPE. J. Orthop. Res. 20, 1152–1156. https://doi.org/10.1016/S0736-0266(02)00073-6

Gordon, J.R., Jones, R.L., 1989. THE EFFECT OF SPECIMEN SIZE ON THE JR-CURVE BEHAVIOUR OF A TITANIUM ALLOY. Fatigue Fract. Eng. Mater. Struct. 12, 295–308.

Hale, G.E., 1990. Crack growth resistance curves for polymers-Development of a multiple specimen testing protocol, in: ECF8, Torino 1990.

Hashemi, S., Williams, J.G., 1991. Single and multi-specimenR-curve methods forJIC determination of toughened nylons. J. Mater. Sci. 26, 621–630.

Hashemi, S., Williams, J.G., 1986a. A fracture toughness study on low density and linear low density polyethylenes. Polymer (Guildf). 27, 384–392.

Hashemi, S., Williams, J.G., 1986b. Fracture characterization of tough polymers using the J method. Polym. Eng. Sci. 26, 760–767.

Heerens, J., Schwalbe, K.-H., Cornec, A., 1988. Modifications of ASTM E 813-81 Standard Test

Method for an Improved Definition of J Ic Using New Blunting-Line Equation, in: Fracture Mechanics: Eighteenth Symposium.

Huang, D.D., 1991. The application of the multispecimen J-integral technique to toughened polymers, in: Elastic-Plastic Fracture Test Methods: The User's Experience (Second Volume). ASTM International.

Huang, D.D., others, 1996. Applying fracture mechanics to material selection. Plast. Eng. 52, 37–40.

Huang, D.D., Williams, J.G., 1990. Comments on "fracture toughness of impact modified polymers based on the J-integral". Polym. Eng. Sci. 30, 1341–1344.

Huang, D.D., Williams, J.G., 1987. J testing of toughened nylons. J. Mater. Sci. 22, 2503–2508.

Huang, Y.-L., Brown, N., 1992. Slow crack growth in blends of HDPE and UHMWPE. Polymer (Guildf). 33, 2989–2997.

Huang, Y.-L., Brown, N., 1991. Dependence of slow crack growth in polyethylene on butyl branch density: morphology and theory. J. Polym. Sci. Part B Polym. Phys. 29, 129–137.

Huang, Y.-L., Brown, N., 1988. The effect of molecular weight on slow crack growth in linear polyethylene homopolymers. J. Mater. Sci. 23, 3648–3655.

Hutchinson, J.W., Paris, P.C., 1979. Stability analysis of J-controlled crack growth, in: Elastic-Plastic Fracture. ASTM International.

Iijima, M., Strobl, G., 2000. Isothermal crystallization and melting of isotactic polypropylene analyzed by time-and temperature-dependent small-angle X-ray scattering experiments. Macromolecules 33, 5204–5214.

Kempson, G.E., 1982. Relationship between the tensile properties of articular cartilage from the human knee and age. Ann. Rheum. Dis. 41, 508–511.

Klapperich, C., Komvopoulos, K., Pruitt, L., 2001. Nanomechanical Properties of Polymers Determined From Nanoindentation Experiments. J. Tribol. 123, 624. https://doi.org/10.1115/1.1330736

Klapperich, C., Pruitt, L., Komvopoulos, K., 2002. Nanomechanical properties of energetically treated polyethylene surfaces. J. Mater. Res. 17, 423–430.

Kramer, E.J., 1983. Microscopic and molecular fundamentals of crazing, in: Crazing in Polymers. Springer, pp. 1–56.

Kurtz, S.M., 2015. UHMWPE Biomaterials Handbook: Ultra High Molecular Weight Polyethylene in Total Joint Replacement and Medical Devices: Third Edition.

Kurtz, S.M., 2009. UHMWPE biomaterials handbook: ultra high molecular weight polyethylene in total joint replacement and medical devices. Academic Press.

Kurtz, S.M., Jewett, C.W., Bergström, J.S., Foulds, J.R., Edidin, A.A., 2002. Miniature specimen shear punch test for UHMWPE used in total joint replacements. Biomaterials 23, 1907–1919.

Kurtz, S.M., Mazzucco, D., Rimnac, C.M., Schroeder, D., 2006. Anisotropy and oxidative resistance of highly crosslinked UHMWPE after deformation processing by solid-state ram extrusion. Biomaterials 27, 24–34. https://doi.org/10.1016/j.biomaterials.2005.05.102

Kurtz, S.M., Muratoglu, O.K., Evans, M., Edidin, A.A., 1999a. Advances in the processing, sterilization, and crosslinking of ultra-high molecular weight polyethylene for total joint arthroplasty. Biomaterials 20, 1659–1688.

Kurtz, S.M., Pruitt, L.A., Crane, D.J., Edidin, A.A., 1999b. Evolution of morphology in UHMWPE following accelerated aging: the effect of heating rates. J. Biomed. Mater. Res. Part A 46, 112–120.

Kurtz, S.M., Pruitt, L., Jewett, C.W., Crawford, R.P., Crane, D.J., Edidin, A.A., 1998. The yielding, plastic flow, and fracture behavior of ultra-high molecular weight polyethylene used in total joint replacements. Biomaterials 19, 1989–2003. https://doi.org/http://dx.doi.org/10.1016/S0142-9612(98)00112-4

Kurtz, S.M., Villarraga, M.L., Herr, M.P., Bergström, J.S., Rimnac, C.M., Edidin, A.A., 2002b. Thermomechanical behavior of virgin and highly crosslinked ultra-high molecular weight polyethylene used in total joint replacements. Biomaterials 23, 3681–3697.

Landes, J.D., 1995. THE BLUNTING LINE IN ELASTIC-PLASTIC FRACTURE. Fatigue Fract. Eng. Mater. Struct. 18, 1289–1297.

Landes, J.D., Begley, J.A., 1974. Test results from J-integral studies: an attempt to establish a J Ic testing procedure, in: Fracture Analysis: Proceedings of the 1973 National Symposium on Fracture Mechanics, Part II.

Launey, M.E., Ritchie, R.O., 2009. On the fracture toughness of advanced materials. Adv. Mater. 21, 2103–2110.

Lin, L., Argon, A.S., 1994. Structure and plastic deformation of polyethylene. J. Mater. Sci. 29, 294–323. https://doi.org/10.1007/BF01162485

Liu, H.W., Kobayashi, H., 1980. Stretch zone width and striation spacing—the comparison of theories and experiments. Scr. Metall. 14, 525–530.

Lu, X., Brown, N., 1986. Predicting failure from the initiation stage of slow crack growth in polyethylene. J. Mater. Sci. 21, 4081–4088.

Lu, X., Wang, X., Brown, N., 1988. Slow fracture in a homopolymer and copolymer of polyethylene. J. Mater. Sci. 23, 643–648.

Medel, F.J., Furmanski, J., 2015. Fatigue and fracture of UHMWPE, in: UHMWPE Biomaterials Handbook (Third Edition). Elsevier, pp. 693–720.

Medel, F.J., Rimnac, C.M., Kurtz, S.M., 2009. On the assessment of oxidative and microstructural changes after in vivo degradation of historical UHMWPE knee components by means of vibrational spectroscopies and nanoindentation. J. Biomed. Mater. Res. Part A 89, 530–538.

Mills, W.J., 1981. Effect of temperature on the fracture toughness behavior of Inconel X-750, in:

Fractography and Materials Science. ASTM International.

Morrison, M.L., Jani, S., 2009. Evaluation of sequentially crosslinked ultra-high molecular weight polyethylene. J. Biomed. Mater. Res. Part B Appl. Biomater. 90, 87–100.

Muratoglu, O.K., Bragdon, C.R., O'Connor, D.O., Jasty, M., Harris, W.H., Gul, R., McGarry, F., 1999. Unified wear model for highly crosslinked ultra-high molecular weight polyethylenes (UHMWPE). Biomaterials 20, 1463–1470.

Narisawa, I., 1987. Fracture and toughness of crystalline polymer solids. Polym. Eng. Sci. 27, 41–45.

Narisawa, I., Takemori, M.T., 1989. Fracture toughness of impact-modified polymers based on the J-integral. Polym. Eng. Sci. 29, 671–678.

Ohta, M., Hyon, S.-H., Tsutumi, S., 2003. Control of crystalline orientation to enhance the wear resistance of ultra-high molecular weight polyethylene crystallization cups for artificial joints. Wear 255, 1045–1050.

Oliver, W.C., Pharr, G.M., 1992. An improved technique for determining hardness and elastic modulus using load and displacement sensing indentation experiments. J. Mater. Res. 7, 1564–1583.

Oral, E., Malhi, A.S., Muratoglu, O.K., 2006. Mechanisms of decrease in fatigue crack propagation resistance in irradiated and melted UHMWPE. Biomaterials 27, 917–925.

Paris, P.C., Tada, H., Zahoor, A., Ernst, H., 1979. The theory of instability of the tearing mode of elastic-plastic crack growth, in: Elastic-Plastic Fracture. ASTM International.

Pascaud, R.S., Evans, W.T., McCullagh, P.J.J., Fitzpatrick, D., 1997a. Critical assessment of methods for evaluating JIC for a medical grade ultra high molecular weight polyethylene. Polym. Eng. Sci. 37, 11–17.

Pascaud, R.S., Evans, W.T., McCullagh, P.J.J., FitzPatrick, D.P., 1997b. Influence of gamma-irradiation sterilization and temperature on the fracture toughness of ultra-high-molecular-weight polyethylene. Biomaterials 18, 727–735.

Premnath, V., Harris, W.H., Jasty, M., Merrill, E.W., 1996. Gamma sterilization of UHMWPE articular implants: An analysis of the oxidation problem. Biomaterials 17, 1741–1753. https://doi.org/10.1016/0142-9612(95)00349-5

Premnath, V., Harris, W.H., Jasty, M., Merrill, E.W., 1996. Gamma sterilization of UHMWPE articular implants: an analysis of the oxidation problem. Biomaterials 17, 1741–1753.

Pruitt, L.A., 2005. Deformation, yielding, fracture and fatigue behavior of conventional and highly cross-linked ultra high molecular weight polyethylene. Biomaterials 26, 905–915.

Pruitt, L.A., 2005. Deformation, yielding, fracture and fatigue behavior of conventional and highly cross-linked ultra high molecular weight polyethylene. Biomaterials 26, 905–915. https://doi.org/10.1016/j.biomaterials.2004.03.022

Pruitt, L., Bailey, L., 1998. Factors affecting near-threshold fatigue crack propagation behavior of orthopedic grade ultra high molecular weight polyethylene. Polymer (Guildf). 39, 1545–

1553.

Pruitt, L., Rondinone, D., 1996. The effect of specimen thickness and stress ratio on the fatigue behavior of polycarbonate. Polym. Eng. Sci. 36, 1300–1305.

Rice, J., Paris, P., Merkle, J., 1973. Some further results of J-integral analysis and estimates, in: Progress in Flaw Growth and Fracture Toughness Testing. ASTM International.

Rimnac, C., Pruitt, L., 2008. How do material properties influence wear and fracture mechanisms? J. Am. Acad. Orthop. Surg. 16, S94--S100.

Rimnac, C.M., Wright, T.M., Klein, R.W., 1988. J integral measurements of ultra high molecular weight polyethylene. Polym. Eng. Sci. 28, 1586–1589.

Schwalbe, K.-H., Heerens, J., 1985. Proposed modifications of ASTM E813-81 standard test method for JIc. Nucl. Eng. Des. 87, 101–107.

Shih, C.F., Andrews, W.R., Delorenzi, H.G., Van Stone, R.H., Yukawa, S., Wilkinson, J.P.D., 1978. Crack initiation and growth under fully plastic conditions: a methodology for plastic fracture. EPRI Ductile Fract. Res. Rev. Doc. EPRI NP-701-SR.

Simis, K.S., Bistolfi, A., Bellare, A., Pruitt, L.A., 2006. The combined effects of crosslinking and high crystallinity on the microstructural and mechanical properties of ultra high molecular weight polyethylene. Biomaterials 27, 1688–1694. https://doi.org/10.1016/j.biomaterials.2005.09.033

Sirimamilla, P.A., Furmanski, J., Rimnac, C.M., 2013. Application of viscoelastic fracture model and non-uniform crack initiation at clinically relevant notches in crosslinked UHMWPE. J. Mech. Behav. Biomed. Mater. 17, 11–21.

Sobieraj, M.C., Kurtz, S.M., Rimnac, C.M., 2005. Notch strengthening and hardening behavior of conventional and highly crosslinked UHMWPE under applied tensile loading. Biomaterials 26, 3411–3426. https://doi.org/10.1016/j.biomaterials.2004.09.031

Sobieraj, M.C., Kurtz, S.M., Wang, A., Manley, M.M., Rimnac, C.M., 2008. Notched stress-strain behavior of a conventional and a sequentially annealed highly crosslinked UHMWPE. Biomaterials 29, 4575–4583. https://doi.org/10.1016/j.biomaterials.2008.08.010

Tanabe, Y., Strobl, G.R., Fischer, E.W., 1986. Surface melting in melt-crystallized linear polyethylene. Polymer (Guildf). 27, 1147–1153.

Trassaert, P., Schirrer, R., 1983. The disentanglement time of the craze fibrils in polymethylmethacrylate. J. Mater. Sci. 18, 3004–3010.

Turell, M.B., Bellare, A., 2004. A study of the nanostructure and tensile properties of ultra-high molecular weight polyethylene. Biomaterials 25, 3389–3398.

Varadarajan, R., Rimnac, C.M., 2008. Evaluation of J-initiation fracture toughness of ultra-high-molecular-weight polyethylene used in total joint replacements. Polym. Test. 27, 616–620.

Wallin, K., 2009. Specimen Size Limitations in JR Curve Testing—Standards versus Reality, in: Small Specimen Test Techniques: 5th Volume. ASTM International.

Ward, A.L., Lu, X., Huang, Y., Brown, N., 1991. The mechanism of slow crack growth in polyethylene by an environmental stress cracking agent. Polymer (Guildf). 32, 2172–2178.